UNITED NATIONS UNIVERSITY

GEOTHERMAL TRAINING PROGRAMME

ORKUSTOFNUN

Öskurhóll, Hveravellir at Kjölur

Hary Koestono

LAHENDONG GEOTHERMAL FIELD, INDONESIA: GEOTHERMAL MODEL BASED ON WELLS LHD-23 AND LHD-28

Report 3
December 2010

UNITED NATIONS UNIVERSITY
GEOTHERMAL TRAINING PROGRAMME
Orkustofnun, Grensásvegur 9,
IS-108 Reykjavík, Iceland

Reports 2010
Number 3

LAHENDONG GEOTHERMAL FIELD, INDONESIA: GEOTHERMAL MODEL BASED ON WELLS LHD-23 AND LHD-28

MSc thesis
School of Engineering and Natural Sciences
Faculty of Earth Science
University of Iceland

by

Hary Koestono
Pertamina Geothermal Energy
Menara Cakrawala 15th Floor
Jl. MH. Thamrin 9, Jakarta
INDONESIA
hary_ka@pgeindonesia.com

United Nations University
Geothermal Training Programme
Reykjavík, Iceland
Published in December 2010

ISBN 978-9979-68-285-1
ISSN 1670-7427

This MSc thesis has also been published in April 2010 by the
School of Engineering and Natural Sciences, Faculty of Earth Sciences
University of Iceland

INTRODUCTION

The Geothermal Training Programme of the United Nations University (UNU) has operated in Iceland since 1979 with six month annual courses for professionals from developing countries. The aim is to assist developing countries with significant geothermal potential to build up groups of specialists that cover most aspects of geothermal exploration and development. During 1979-2010, 452 scientists and engineers from 47 countries have completed the six month courses. They have come from Asia (42%), Africa (29%), Central America (15%), and Central and Eastern Europe (14%). There is a steady flow of requests from all over the world for the six month training and we can only meet a portion of the requests. Most of the trainees are awarded UNU Fellowships financed by the UNU and the Government of Iceland.

Candidates for the six month specialized training must have at least a BSc degree and a minimum of one year practical experience in geothermal work in their home countries prior to the training. Many of our trainees have already completed their MSc or PhD degrees when they come to Iceland, but several excellent students who have only BSc degrees have made requests to come again to Iceland for a higher academic degree. In 1999, it was decided to start admitting UNU Fellows to continue their studies and study for MSc degrees in geothermal science or engineering in co-operation with the University of Iceland. An agreement to this effect was signed with the University of Iceland. The six month studies at the UNU Geothermal Training Programme form a part of the graduate programme.

It is a pleasure to introduce the 23rd UNU Fellow to complete the MSc studies at the University of Iceland under the co-operation agreement. Mr. Hary Koestono, BSc in Geology, of Pertamina Geothermal Energy in Indonesia, completed the six month specialized training in Borehole Geology at the UNU Geothermal Training Programme in October 2007. His research report was entitled: "Borehole geology and hydrothermal alteration of well HE-24, Hellisheidi geothermal field, SW-Iceland". After one year of geothermal research work in Indonesia, he came back to Iceland for MSc studies at the Faculty of Earth Sciences of the University of Iceland in August 2008. In April 2010, he defended his MSc thesis presented here, entitled "Lahendong geothermal field, Indonesia: Geothermal model based on wells LHD-23 and LHD-28". His studies in Iceland were financed by the Government of Iceland through a UNU-GTP Fellowship from the UNU Geothermal Training Programme. We congratulate him on his achievements and wish him all the best for the future. We thank the Faculty of Earth Sciences at the School of Engineering and Natural Sciences of the University of Iceland for the co-operation, and his supervisors for the dedication.

Finally, I would like to mention that Hary´s MSc thesis with the figures in colour is available for downloading on our website *www.unugtp.is* under publications.

With warmest wishes from Iceland,

Ingvar B. Fridleifsson, director
United Nations University
Geothermal Training Programme

ACKNOWLEDGEMENT

- I would like to express my thanks to Dr. Ingvar B. Fridleifsson and Mr. Lúdvík S. Georgsson for giving me the opportunity to work towards in master's degree.
- My really special thanks go to my supervisor Dr. Hjalti Franzson, for his patient and excellent guidance during the completion of my master's thesis.
- Thanks to Prof. Stefán Arnórsson for his excellent lectures, discussion and helps.
- Dr. Thráinn Fridriksson, for his criticism and corrections.
- Ms. Anette K. Mortensen for discussion and helps in the fluid inclusion and binocular microscope.
- Thanks also go to Mr. Sigurdur Sveinn Jónsson in acknowledgedment of his kind help in the preparation of clay samples for XRD analysis and discussions.
- Thanks to Dr. Karl Grönvold and Mr. Níels Óskarsson for their patience in helping on prepare, analyse and discuss the samples for Microprobe and ICP analysis.
- Thanks to Ms. Thórhildur Ísberg, Ms. Dorthe H. Holm, and Mr. Markús A.G. Wilde for their assistance during the study.
- I extend my appreciation to Pertamina Geothermal Energy for supporting and allowing me to participate in this programme.
- Thanks to all the UNU fellows for their friendship and support.
- Thanks to all the geosciences group of ISOR for their friendship and discussions.
- Thanks to all friends in the Askja group for their helps and the friendship.
- My deepest thanks go to my wife Linda Astuti and my son, Daffa Rifqi Putratama for their patience and support during the more than one and half years master programme.
- And lastly, to Almighty God, who made all these things possible.

ABSTRACT

The Lahendong high-temperature geothermal field is tectonically located in the northern neck arm of Sulawesi Island. The field is within the depression of the Pangolombian caldera with clear fault structures in the eastern part but relatively open to the west. Permeability structures on surface are mostly fault controlled with a dominant NW-SE and NE-SW directions. The field is a liquid dominated system divided into two reservoirs, the hotter southern one and the colder Northern one. A total of twenty eight wells have been drilled into these reservoirs. A total 60 MWe are produced from nine wells. This study focuses on two wells in this system, LHD-23 and LHD-28. The main emphasis was on analysing the cuttings with binocular, petrographic and fluid inclusion microscopes, XRD, and then microprobe and chemical analysis with ICP equipment on selected samples.

The strata are divided into three main formations: Post Tondano is the youngest, then the Tondano unit which is the pyroclastics of a catastrophic eruption during the collapse of the large Tondano depression and lastly the Pre-Tondano succession. The strata are predominantly made up of basaltic andesite lavas, tuffs and breccias. Chemical analysis, however, shows that a considerable part of the Pre-Tondano series is rhyolitic in composition, indicating a different volcanic evolution. The depth of the Tondano unit in the Lahendong wells show irregularitites which may suggest a subsidence within the Pangolombian caldera structure.

The data on the 24 aquifers in both wells show a relationhip with the stratigraphy and fractures, but some relations are inconclusive due to limited data. Evidence of aquifers associated with secondary porosity is also present. The neutral pH hydrothermal alteration is dominant in the system with quartz, calcite, chalcedony, wairakite, epidote, wollastonite and actinolite and clays. These are divided into five alteration zones of smectite zone, smectite-chlorite, chlorite-illite, chlorite-illite-epidote, and epidote-actinolite. Fluid inclusions provided a good control on the likely formation temperatures in the wells, and showed the temperatures falling on the boiling point curve for both wells. Acidic fluid was encountered in well LHD-23. A specific search was made in order to find acid alteration and locate the source of acidic fluid entering the well. The acid alteration included kaolinite, pyrophyllite, diaspore and sulphur. The most likely location for the acid aquifer was at about 1000 m in the well, slightly below the production casing, and is possibly related to the fault structure F-6.

Depth to the first occurrence of epidote for all wells shows an N-S alignment of the geothermal system, and possibly also a NW-SE alignment in the northern part. This compares well with the geophysical MT-resistivity survey done in the area. These may indicate an effect of N-S structural control (e.g. F-6) and NW-SE (e.g. F-2 and F-9).

TABLE OF CONTENTS

LIST OF FIGURES

LIST OF TABLES

1. INTRODUCTION

1.1 General overview

Indonesia is located at the junction of three active plates; the India Australia in the south, Eurasia in the north and the Pacific plate in the east. The subduction of India-Australian plate beneath Eurasia plate triggers volcanism along Sumatera, Java, Bali, Nusa Tenggara, Maluku and Sulawesi Islands from west to east (Figure 1). Indonesia is located along the southern part of the Ring of Fire with a long subduction boundary due to which more than 200 volcanoes are active on its different islands extending from west to east. Its location along the ring of fire has made it to be endowed with geothermal resources ranking it with countries having top geothermal potential in the world. The geothermal potential in Indonesia is about 40% of the world total with an approximate potential of about 20.000 MW (Fauzi et al., 2000).

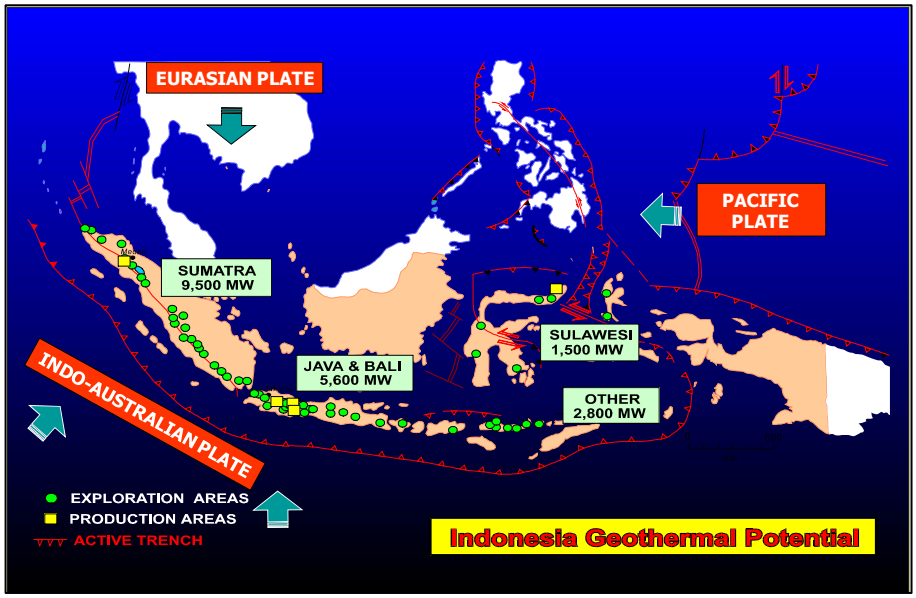

FIGURE 1: Tectonic setting and the geothermal potential of Indonesia (Pertamina geothermal database)

Exploration for a geothermal resource in Indonesia associated with active fumarole and solfatara fields was first proposed in 1918. Exploration drilling started in 1926 by Volcanological section (later Volcanological Survey of Indonesia, VSI) where several wells were drilled inside a large fumarole field at Kawah Kamojang. In 1928 exploration on the Dieng field was conducted after which no further attempts were made for exploration of geothermal fields until 1972. In the 1970s ten geothermal areas in Java and outside were explored in some detail and three high temperature reservoirs discovered at Java prospect. In the 1980s to mid 1990s 45 new prospects were explored and high temperature reservoirs were discovered in Java, Sulawasi and Sumatra islands. In the mid 1990s to 2000 another six prospects were tested by deep drilling which discovered again high temperature reservoirs at Sumatra, Java and Bali islands (Hochstein and Sudarman, 2008).

The geothermal activity in Indonesia is dominated by a high temperature geothermal system. Quaternary volcanism and active volcanoes along well defined volcanic arcs are dominant throughout the country and the geothermal system occurring in these areas of intense volcanic activity are associated with surface manifestations discharging fluids at boiling temperatures (Hochstein and Sudarman, 2008).

The electricity demand in Indonesia is very high as compared to the current supply. To overcome this high demand of electricity a project has been initiated with the aim of developing the different energy sectors. One of the renewable energy sectors currently started to be developed is the geothermal which is barely utilized with an installed capacity of 1159 MWe or about 4% from the total potential of geothermal energy in Indonesia (Ibrahim et al., 2005). The current project initiated by the government as a crash program aims at achieving 10000 MWe on the overall energy sectors. One of the sectors is geothermal energy where intense exploration and drilling activity has been conducted throughout the country in the different prospect areas with high temperature reservoirs.

Lahendong is one of these promising geothermal fields located in North Sulawesi in the eastern part of Indonesia. This field is currently operating at 60 Mwe and has an estimated resource potential of about 120 MW. To date, a total of 28 wells have been drilled in this field. Two wells, LHD-23 and LHD-28 will be discussed in this study.

1.2 Objective of the study

The objectives of the study are:

1. To identify the rocks penetrated in wells LHD-23 and LHD-28.
2. To identify the hydrothermal alteration minerals found in wells LHD-23 and LHD-28
3. To determine the mineral sequences in the wells and to understand the precipitation history of the secondary minerals in veins and vesicles.
4. To determine the location of the aquifers (feed points) in the wells based on the appropriate data such as circulation losses during drilling, rate of penetration, temperatures log, and correlation with geological structures.
5. To determine the source of the acid fluid in the Lahendong geothermal field based on the hydrothermal minerals and fluid chemistry data.
6. To visualize the conceptual models of the Lahendong geothermal field

2. GEOLOGY

2.1 Regional geology

Lahendong geothermal field is located at about 30 km south of Manado city, in the northern arm of Sulawesi Island. Sulawesi Island formed due to an active subduction in the south eastern part (Mollucca Sea) and northern part (Celebes Sea) (Figure 2).

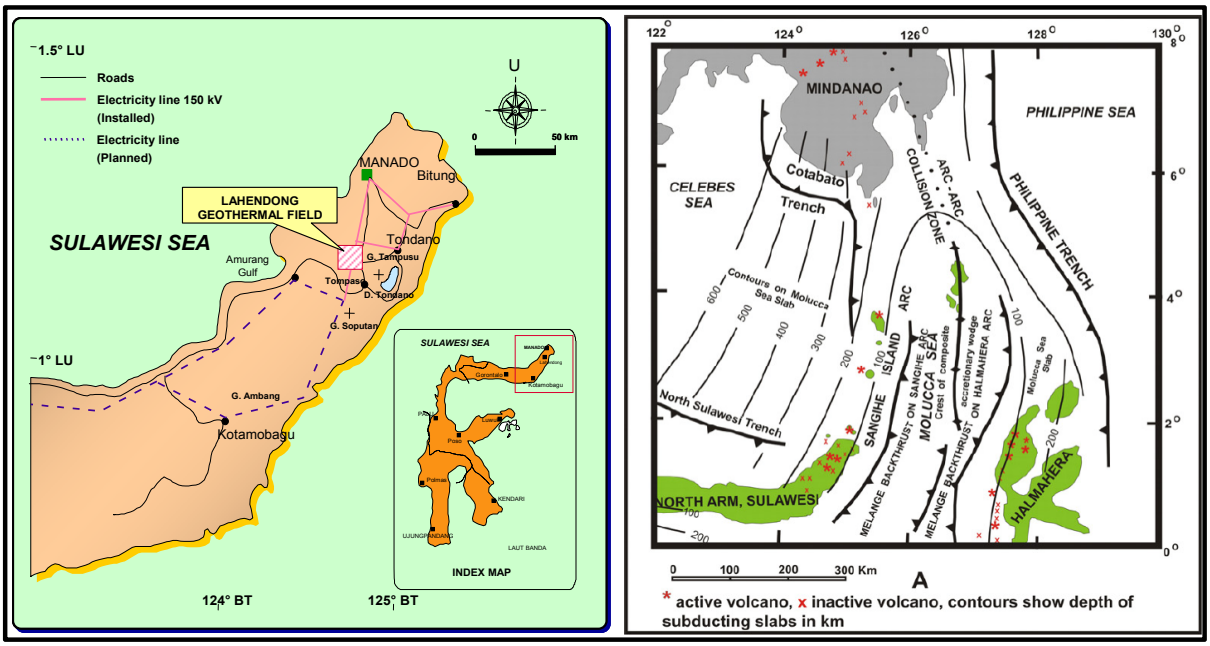

FIGURE 2: A map of North Sulawesi showing the location of the Lahendong geothermal field and the tectonic system (The tectonic system map is taken from Utami et al., 2005)

Regionally, this field is located in the west margin of the Tondano Depression which extends about 20 km in a north-south direction and opens to the west. Within this depression is the Pangolombian rim, circular in shape, and is an important structure in Lahendong geothermal system.

This geothermal field was discovered in 1982 and geological, geochemical and geophysical studies have been conducted since that time. Three shallow wells were drilled around Linau Lake in the same year. From 1982 to 1987, Pertamina drilled 7 exploration wells LHD-1 and LHD-5 in the northern reservoir system, LHD-4 in the southern reservoir system and LHD-3, LHD-6 and LHD-7 in the boundary margin of the prospect area (Robert, 1987; Siahaan et al., 2005).

The development of wells LHD-8 to LHD-16 at Lahendong geothermal field were drilled from 1991 to 1998 and the first 20 MW power plant Unit I was commenced in 2001. The development stage continued from 2005 to 2007 in which 7 production wells were drilled which generated electricity 2x20 MW for power plant Unit II and III and was commenced in 2007 and 2009. In line with the increasing electricity need in North Sulawesi, the Lahendong geothermal field has been expanded with an additional 20 MW for unit IV starting 2008. Parallel with this development 2x20 MW of units V and VI also developed in the Tompaso prospect in the southern part of the Lahendong. 12 wells have been planned for this development 10 of which are already drilled and 2 wells remaining to be drilled.

The stratigraphy of Lahendong geothermal field has been studied on the surface (Figure 3) and in the wells and can be divided into 3 main lithological units (Figure 4), i.e. Pre-Tondano, Tondano and Post Tondano units (Robert, 1987). The basement rocks of the Pre-Tondano unit are comprised of thick hyaloclastite rocks, basaltic andesite, andesite, pyroclastics with inter-bedded of sedimentary rock formed during the Miocene time. The sedimentary formation which is included in the Pre-Tondano unit includes limestone and silty marl with foraminifera identified in wells LHD-1, LHD-2 and LHD-3 (Robert, 1987; Siahaan et al., 2005).

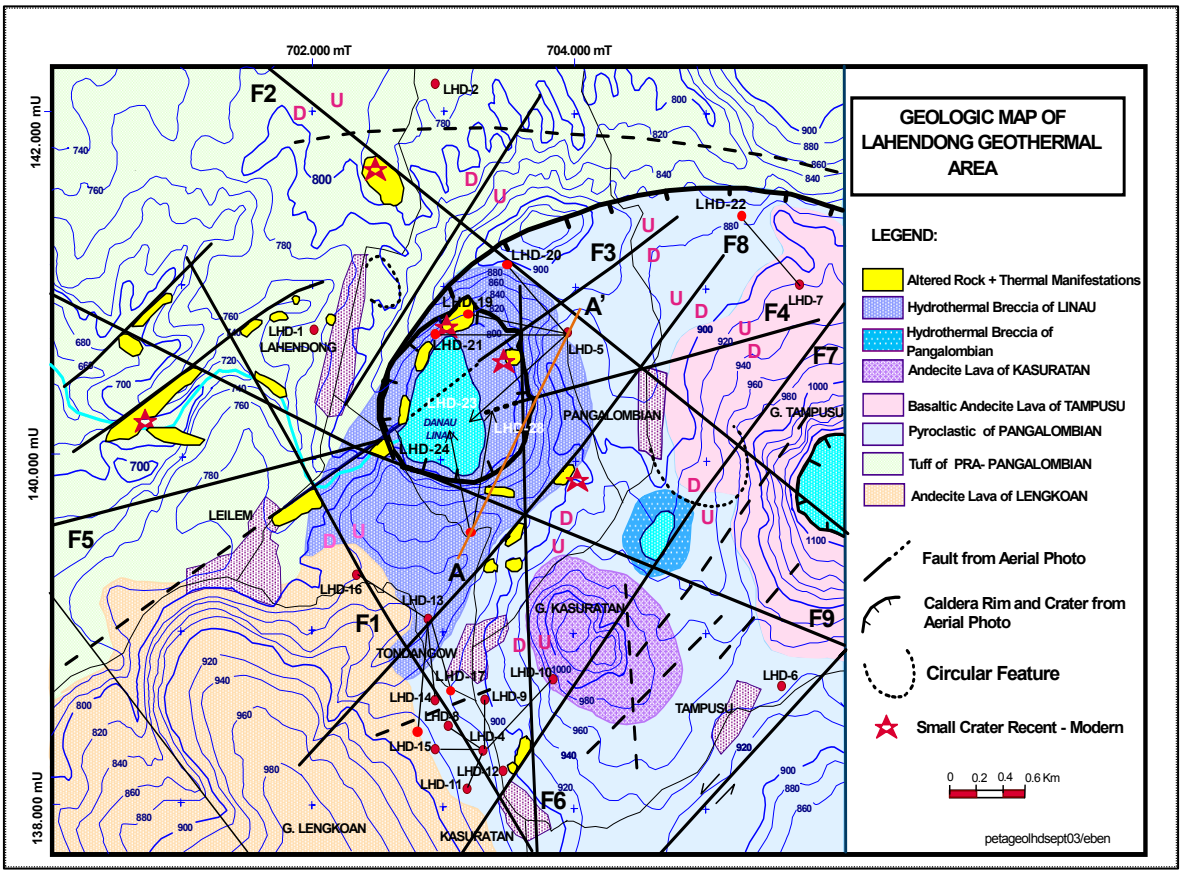

FIGURE 3: Geological and structural map of Lahendong geothermal field (Siahaan, 2000)

The Tondano depression is the important structure in the area and is formed due to the huge eruption which occured on the Late Miocene or Early Pliocene time. Tondano unit is made up of rhyo-dacitic pumices rich ignimbrites in the upper part, but the influence of micro dioritic intrusion in the lower part makes it difficult to determine the lithological character (Siahaan et al., 2005).

The Post Tondano Unit is commonly found covering the upper part of the stratigraphy and comprises pumice, tuff and volcanic breccia in the upper part and basaltic andesite in the lower part. The Post-Tondano unit consists of 2 sub-units, the Pre-Pangolombian and Post-Pangolombian sub-units. The Pre-Pangolombian sub-unit mainly consists of basaltic andesite lava deposited in the northern and southern part of Pangolombian depression. The second sub-unit, the Post-Pangolombian, was composed by eruptions located in the central and peripheral areas of the depression. The chronological sequence from early to late deposition is described as basaltic andesite lava of Kasuratan, Linau breccia consisting of volcanic breccia and pyroclastic rock, Tampusu basaltic andesite lava and pyroclastic rock, product of Mt. Lengkoan andesitic lava, obsidian and tuff breccia, and altered ground located in the northern side of Kasuratan village extending to Pangolombian rim, in Leilem creek and in the eastern side of Lahendong village (Figure 3). Linau Lake and its crater rim were

Lithologic column	Rock unit & type	Thickness (m)	Age (Ma)*	Geothermal significance
	Pangolombian unit : andesite lava, breccia, tuff, welded ignimbrite	350 - 850	Not yet determined	Cap rock Shallow reservoir
	Tondano unit: rhyolitic tuff, breccia, pumiceous rhyolite lava	< 100 - 600	0.871±0.097 Early Pleistocene	Deep reservoir
	Pre-Tondano unit: andesite breccia, lava, water-laid tuff	≥ 600	2.19±0.03 Late Pliocene	Deep reservoir
	Diorite intrusion	?	Not yet determined	Heat source (?)

FIGURE 4: Simplified of subsurface stratigraphy of the Lahendong geothermal field (Slightly modified from Utami et al., 2005). Age data is taken from Gondwana, 1988

formed due to the hydrothermal eruption activities and are believed to be the centre of surface thermal manifestations in the field (Siahaan, 2000; Siahaan et al., 2005).

2.2 Tectonic structure

The study on the distribution of the geological structure of the Lahendong Geothermal Field has been carried out by Pertamina since 1982. Ganda and Sunaryo (1982) mapped the geology of the area. Later in 1987, Geoservice studied the geology and the structure of the field based on aerial photographs. Robert (1987) compiled the data of Geoservice together with the well data. A head on Resistivity Survey was carried out by Pertamina in 1988. An aerial photograph, Landsat interpretation and a surface manifestation evaluation were done by Siahaan (2000). Tectonically, five main structures were encountered in Lahendong geothermal field. The structures are Pangolombian rim, and faults striking NE-SW, E-W, NW-SE and N-S (Figure 3).

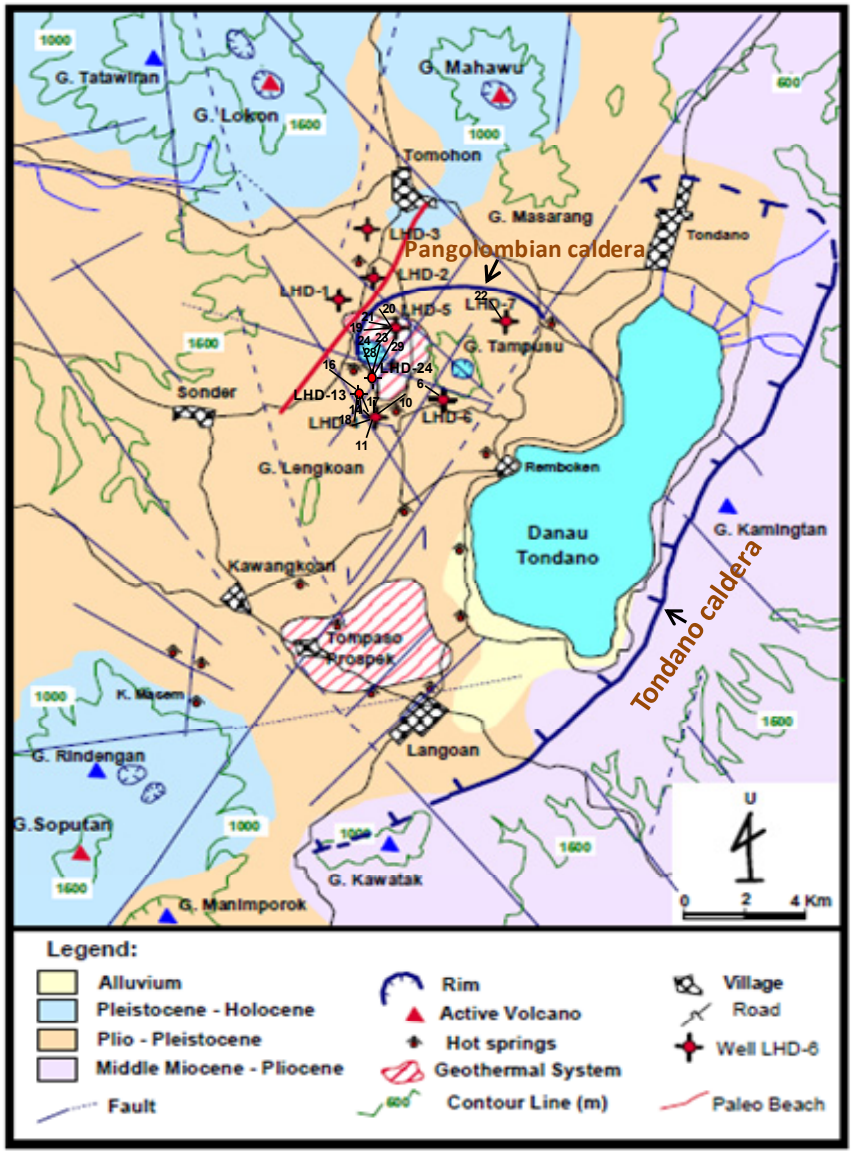

FIGURE 5: Fault pattern of Minahasa compartment (Siahaan et al., 2005)

The active strike slip left lateral fault trending NE-SW and is located in the crest of volcanic inner arc of Minahasa. It aligns from Mt. Soputan on the south-west side to the north-east side direction. This fault controls the development of Tondano and Pangolombian calderas and may also separate the geothermal system of the Lahendong field and the Tompaso prospect (Figure 5). The eastern rim of Tondano caldera can be delineated whereas the western and southern rims were covered by lava from recent activities of Mt. Lengkoan, Mt. Sempu and Mt. Soputan (Siahaan et al., 2005).

The Pangolombian caldera has an ellipsoidal shape, about 5 km long and 3.5 km wide and was formed after the Tondano caldera (Robert, 1987; Siahaan et al., 2005). The northern rim of Pangolombian can be outlined clearly based on topography as it forms hills and ridges. The southern rim was covered by the lava product from Mt.Lengkoan. The western side of Pangolombian caldera or around Linau Lake is predicted as the most intensive faulted area in the Lahendong as shown in the fracture density map (Figure 6).

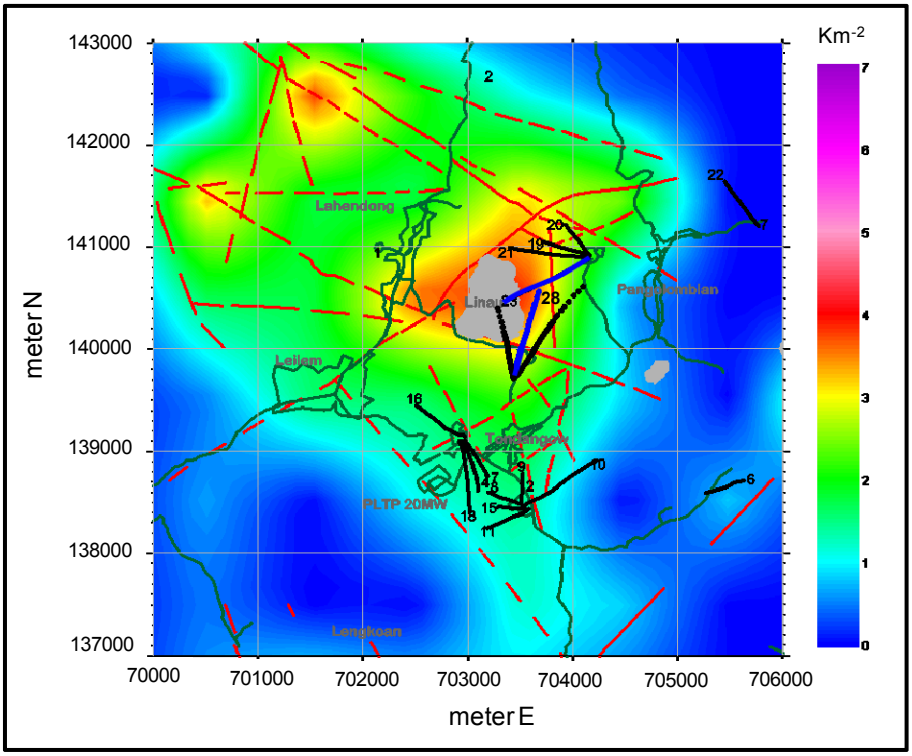

FIGURE 6: Fracture density map of Lahendong field (Pertamina geothermal database)

The Pangolombian structure is a caldera rim that is interpreted to provide the good permeability to geothermal in the field. The NE-SW fault structure is normal and lateral fault, acting as the major volcanic axis. The E-W fault structure is lateral and a transcurrent fault. The NW-SE fault and N-S faults are normal faults which are interpreted to provide a good permeability to the geothermal system (Robert, 1987). The important faults structure controlling the geothermal systems in the fields are F-1 to which wells in the well pads LHD-4 and LHD-13 reach and F-2 and Pangolombian rim to which wells on well pad LHD-5 reach and may F-6 and F-9 for well pad LHD-24. These four well pads are the production site, whereas wells in well pad LHD-7 in the western part are the reinjection wells. The geological structure of the Lahendong geothermal field is shown in the Figure 3 and 5.

2.3 Geophysics

The geophysical methods used to assess the geothermal system are resistivity, MT and gravity and have been conducted in this field since its discovery in 1982.

The Schlumberger resistivity and MT survey was carried out in the Lahendong field in 1983. A total of 291 profiles and 144 soundings were measured. The results of Schlumberger resistivity (AB/2=1000 m) and magnetotelluric (MT-5 EX) showed that the width of the geothermal prospect area, identified by low resistivity anomaly (<10 ohmm), is around 15 to 25 km^2. This prospect area has centred in around of Linau Lake (Figure 7). At the same time, 201 MT soundings were measured and results indicate the existence of a huge conductive zone limited in southern part by a resistive block.

In 1985, a microearthquake survey was carried out around Lahendong field and showed that the northern and eastern part of Mt. Tampusu has a relatively high frequency of earthquakes and mostly occured at depth between 2 to 10 km. Silitonga et al. (2005) used the Poisson's ratio from Wadati Diagram to determine fractures by analysing the hypocenter distribution of earthquakes. The value of Poisson's ratio with depth in the Lahendong geothermal field can be divided into two zones which correspond to shallower and deeper zone. The shallower zone with interval of Poisson's ratio varies from 0.35 to 0.43 has depth from surface to 2000 meters and the deeper zone, with interval of Poisson's ratio varying from 0.27 to 0.35, has a depth of greater than 2000 m. The correlation between cores and Poisson's ratio data provide the two reservoir zone. The shallower zone is distinguished by the intensively fractured rock, partial to high circulation losses and sudden change in the rate of penetration. On the other hand, in the deeper zone, the rock is highly silicified and circulation losses are absent (Silitonga et al., 2005).

Detailed MT survey was done in 2005 and reported in 2008 by modelling of 3D MT inversion and showed an up-dome resistivity structure at around Linau Lake. The updome resistivity structure is characterized by the resistivity value of 20-60 ohmm which is interpreted as the propilitic zone (Figures 7 and 8). At depth about 1.5 km, the size of the dome is around 3x4 km^2. This zone is covered by the conductor resistivity structure with value <10 ohmm as the clay cap and part of the argillic zone (Raharjo, et.al, 2008).

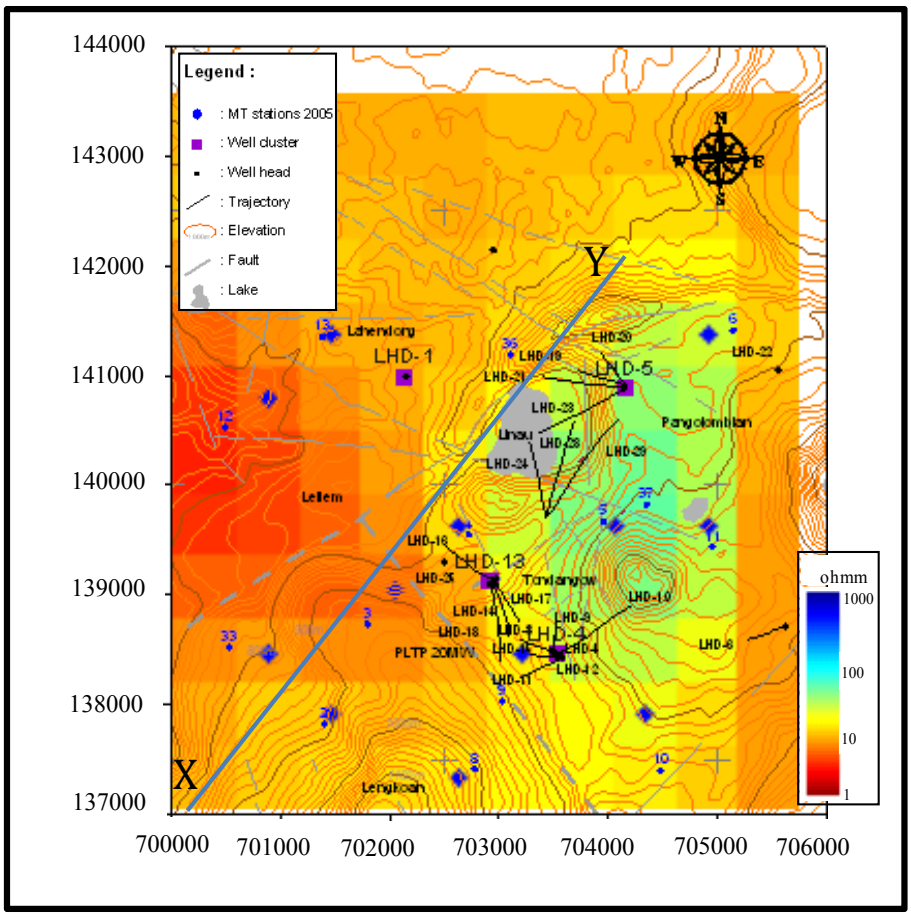

FIGURE 7: Map shows well direction and MT resistivity slice at depth of 1.5 to 1.6 km (Raharjo et al., 2009)

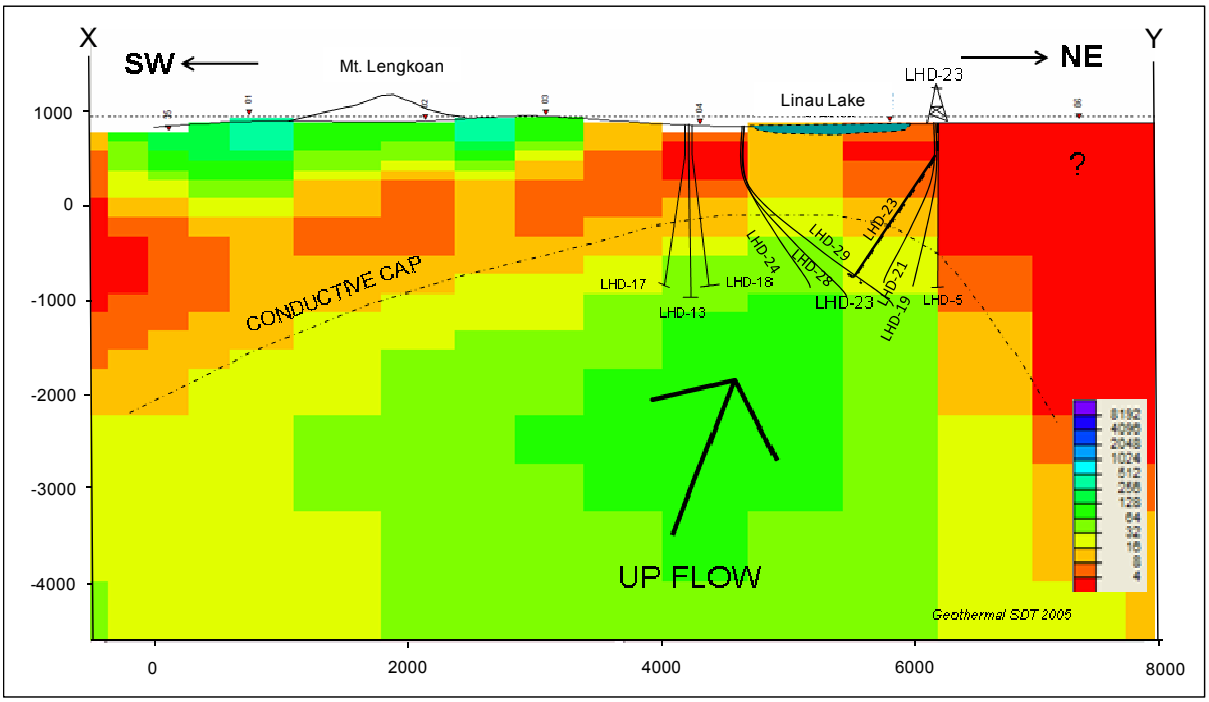

FIGURE 8: MT cross section of SW-NE direction of Lahendong geothermal field showing the directional of the wells (Raharjo et al., 2009)

2.4 Fluid chemistry

The surface manifestations of the geothermal system in this field include hot springs, mud pools, fumaroles, and altered rock. The field is a two phase reservoir systems where the boiling of fluids is occurring in the reservoir and results in excess steam in wells on surface.

The Lahendong geothermal field can be divided into two groups of hot water based on their chemical characteristics of the Cl-B ratio, i.e. Lokon-Mahawu group and Lahendong-Tompaso group. Lokon-Mahawu group is located in the Northern part and is characterized by low silica content and low temperature while the concentration of Ca, Mg and SO_4^{2-} is relatively high. The ratio of Cl/B in this group is higher (188) than the second group (13). The second group is Lahendong-Tompaso group. This group is located in the Middle and Southern part of the field. The temperature estimation based on the gas geothermometry is around 322°C (Prijanto et al.,, 1984).

Based on the Cl-SO_4-HCO_3 triangular plot (Figure 9), the Lahendong surface manifestations plot either as steam heated or volcanic waters and are still immature as indicated by the Na-K-Mg triangular plot proposed by Giggenbach (Figure 10). The fluids discharged by neutral wells in the Lahendong geothermal field plot within the mature Cl-type waters while acid well LHD-23 discharge is categorized as Cl-SO_4 type of water. Figure 10 also suggests that both the neutral and acidic well discharges have either attained only partial equilibrium with the rocks or are mixtures of lower temperature fluids (160-200°C based on the K-Mg geothermometer) and a hotter component with Na-K geothermometry of 300-340°C for neutral wells and 220-240°C for acid well LHD-23. Lower T-qtz of acid well LHD-23 at 191°C can also be indication of secondary processes like dilution or cooling that affect its discharge water chemistry.

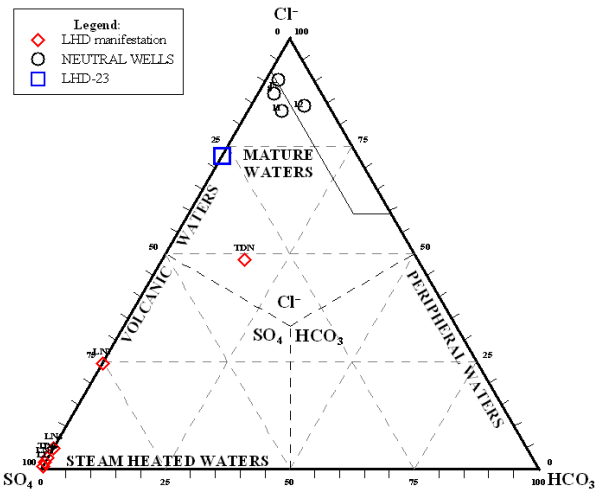

FIGURE 9: Cl-SO_4-HCO_3 triangular diagram of thermal fluids in Lahendong (Batan, 2005; Batan 2009)

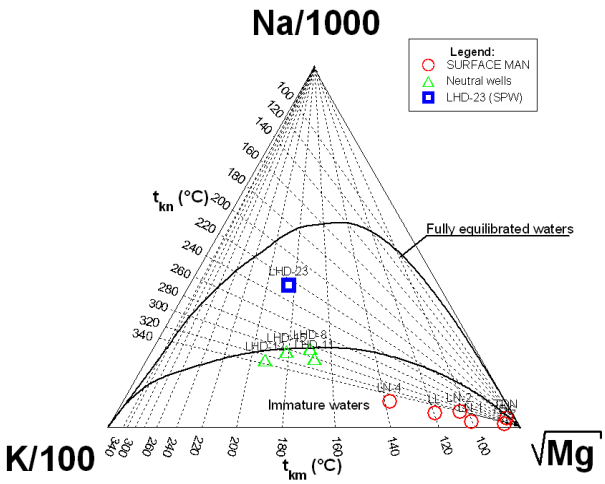

FIGURE 10: The Na-K-Mg triangular diagram of thermal fluids in Lahendong (Batan, 2005; Batan 2009)

The chemistry of gases as positioned in the CO_2-CH_4-N_2 triangular plot (Figure 11) indicates the contribution of either low-CH_4 magmatic gases or fluids from an oxidizing environment to the hydrothermal discharges in Lahendong. The neutral well fluids are predominantly from meteoric waters while the acid well LHD-23 and surface manifestation LN-3 samples have relatively more magmatic components based on the CO_2-N_2-Ar triangular plot (Figure 12). For acid well LHD-23, a higher T-H_2/Ar geothermometer of about 268°C relative to water geothermometers may suggest an initial vapour fraction in the original aquifer fluid.

Isotope study of ^{18}O and δ^2H were carried out started at 1991 and reviewed at 2005. The study shows that the reservoir fluid of the Lahendong field is originated from meteoric water. The reservoir fluid of the Lahendong field is derived from the local meteoric water recharge from the elevation between 600 to 900 m above sea level (Batan, 1991; Batan 2005).

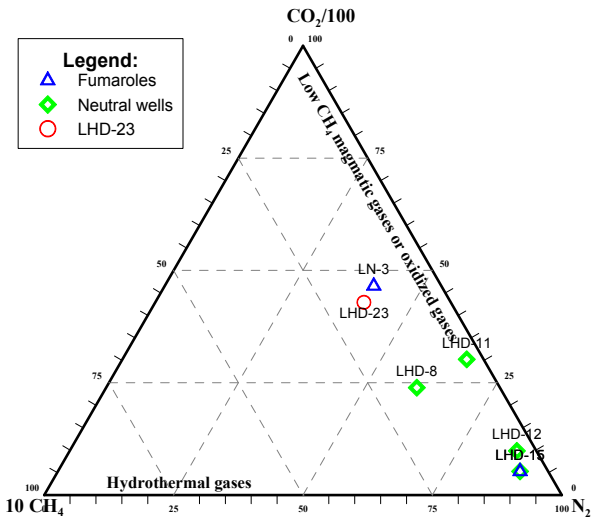

FIGURE 11: The CO2-CH4-N2 ternary plot of the gases in Lahendong (Batan, 2005; Batan 2009)

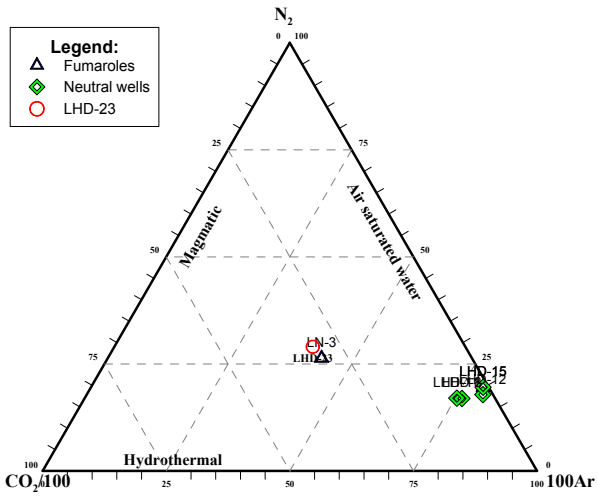

FIGURE 12: The N2-CO2-Ar ternary plot of the gases in Lahendong (Batan, 2005; Batan 2009)

TABLE 1: Representative water chemistry of wells and surface manifestation in Lahendong (Batan, 2005; Batan 2009)

No	Sampel	pH	Cond	Na^+	K^+	Ca^{2+}	Mg^{2+}	Li^+	Fe total	NH_4^+	B	SO_4^{2-}	Cl^-	SiO_2	HCO_3^-
				ppm	ppm	ppm	ppm	ppm	ppm	ppm	ppm	ppm	ppm	ppm	ppm
1	LHD-8	5.17	1263	180.47	33.05	0.74	<0.1	0.61		1.39	22.19	35.06	316.84	659.88	11.52
2	LHD-11	5.5	1038	149.00	31.34	0.98	<0.1	0.84		1.66	23.85	36.24	301.81	603.72	24.88
3	LHD-12	5.15	1638	203.90	57.67	0.47	<0.1	1.91		0.99	24.37	20.64	354.75	736.25	45.57
4	LHD-15	5.3	1174.5	202.88	44.36	0.50	<0.1	1.21		0.89	21.43	24.97	314.86	652.68	8.76
5	LHD-23	2.45		1335.00	123.10	0.04	0.67	3.18	9.61			584.50	1561.80	232.70	0.00
6	LN-1	3.2	725.5	30.38	20.50	11.37	2.60	0.00		1.60	24.40	265.61	4.36	211.02	
7	LN-2	2.5	2790	239.39	65.95	34.72	19.43	0.55		1.47	21.45	642.52	209.84	342.96	
8	LN-4	4.3	280	55.22	21.22	0.18	0.24				2.46	73.88	3.83	85.07	
9	LL	7	1877	35.38	16.01	0.09	0.44	0.00		1.43	2.96	694.03	4.87	103.95	
10	TDN	6	1220	168.50	13.27	3.09	38.26	0.09		0.11	10.75	120.00	167.33	145.27	56.85
11	TDG	3.2	1448	5.70	1.66	0.14	0.24			0.10	2.13	125.82	3.53	73.85	

Note: No. 1 to 5 are wells, no.6 to 11 are surface manifestations

TABLE 2: Representative gas chemistry of wells and surface manifestation in Lahendong (Batan, 2005; Batan 2009)

No.	Sample code	Y	CO_2	H_2S	CH_4	H_2	N_2	Ar	He	NH_3	weight %
		Total discharge (mmol/100 mol steam)									
1	LHD-8	0.46	80.26	16.03	0.05	3.08	2.02	0.09	0.08	0.05	0.50
2	LHD-11	0.47	64.65	16.87	0.01	1.67	1.43	0.06	0.23	0.10	0.41
3	LHD-12	0.38	39.27	10.42	0.02	1.16	3.45	0.16	0.08	0.03	0.31
4	LHD-15	0.39	27.11	9.88	0.03	2.62	4.61	0.19	0.08	0.05	0.24
5	LN-3		9319.85	147.29	2.61	162.03	80.85	1.33	4.18	2.54	18.83
6	LL		6893.44	313.48	0.59	32.34	17.30	1.29	1.85	4.83	14.58
7	LHD-23		988.69	69.76	0.39	2.71	9.29	0.13	0.00	0.00	2.51

3. SAMPLING AND ANALYTICAL TECHNIQUES

3.1 Sampling

In various stages of drilling, sampling and analysis of cuttings is important and crucial for the success of the better understanding of the subsurface conditions in a geothermal system in the area. The sampling is employed to many kind of purposes such as to determine lithology and stratigraphy sequence, to analyze the alteration assemblage, to assist the rig personnel and management in deciding the position of casing depth, to give information to prevent the problem during drilling include the appearance of swelling clay, collapse lithology, the possibility of appearance of magmatic zone, and so on (Reyes, 2000). For this purpose the sampling is an important procedure during drilling as all the information that will be collected depends on the quality of the sample. It also should be noted that drilling a well is very expensive so care should be taken during sampling. Compared to the core sample, the cutting samples are cheaper and easy and are taken at 2 or 3 meter interval during drilling.

In this study, cutting samples from two wells, LHD-23 and LHD-28, in Lahendong geothermal field were collected and analyzed. The samples were taken every 3 m depth interval is customary in Pertamina geothermal areas.

3.2 Analytical techniques

3.2.1 Binocular microscope analysis

Preparation of samples is the first and basic procedure before any analysis. Samples are initially put into small plastic bags, washed to remove the dust and the impurities and then placed in the small container and put in the mounting stage of the Binocular microscope and lastly analyzed. The samples were prepared and analyzed using Olympus SZ12 binocular microscope with a magnification range of 6X to 80X. The analysis of cutting takes note of the the colour of the cuttings, rock type, grain size, structure, texture, original/primary mineralogy, alteration mineralogy, alteration intensity, whether a stratigraphic unit or a possible intrusion and even data that points to a possible aquifer. The quality of the samples may deteriorate, with depths becoming finer in size and when mixing occurs on route from deep levels in the well. To solve the latter the dominant part of the cutting was used to determine the lithology.

3.2.2 Petrographic microscope analysis

The petrographic thin section analyses determines in more detail the rock type, the porosity, vein fillings, alteration of primary minerals, precipitation sequence of secondary minerals, and mineral paragenesis. The analysis was done using an *Olympus SZX*, *Leitz Wetzlar* with a binocular magnification of 4X to 25X. Representative number of samples from the different lithologic units within the wells were selected and analyzed. The quality of the thin section is very important to get maximum information on the petrography. The quality of the thin sections that were made in Indonesia was quite variable.

3.2.3 X-ray diffraction analysis

The XRD analysis is method to examine crystallized materials based upon the scattering of X-rays according to the crystal type of the material.

The X-ray diffractometer analyses were carried out usually to distinguish various clay minerals. In this study, the samples were prepared from wells LHD-23 and LHD-28 which represent the different rock and the degree of alteration intensity. Such analyses are useful in determining the alteration zones along with other index minerals found in binocular and petrographic analysis. The procedure of preparation of clay mineral samples are described in the Appendix A.

3.2.4 Fluid inclusion analysis

Fluid inclusions are small portions of fluid, which are trapped in a growing or a fractured crystal. Inclusions formed during the growth of a crystal are called primary inclusions, while a fluid inclusion is called secondary if it forms within a crack after the formation of the crystal (Goldstein and Reynolds, 1994).

Fluid inclusions from selected samples of quartz and anhydrite were analyzed from the two wells. The analyses were done using Linkam TMS 94. The crystal with inclusion is heated up carefully until the fluid homogenizes. The homogenization temperature is marked by the disappearance of inclusion bubble.

3.2.5 Electrone microprobe analysis

Electron microprobe analysis is principally used for the major element analysis of minerals and generally not trace elements. The principle is that the sample is excited by a beam of electrons. Energy-dispersive electron microprobe analysis utilizes energy versus intensity spectrum and allows the simultaneous determination of the elements of interest (Rollinson, 1995).

Selected samples of epidote, sulfides, feldspar, and clay minerals were polished and analyzed using electron microprobe analysis at 15 kV with 15 nA of sample current and a beam diameter of 2 to 3 micrometers. The analysis of minerals was carried out using an electron microprobe instrument at the University of Iceland.

3.2.6 ICP-OES

Inductively coupled plasma Optical Electron Spectroscopy (ICP-OES) is a rapid analytical method for silicate analysis. The method is based upon the observation that atoms of an element can absorb electromagnetic radiation. This occurs when the element is atomized and the wavelength of light absorbed is specific to each element (Rollinson, 1995). The rock compositions of 10 samples from the two wells were analyzed. The samples were prepared at the University laboratory. During preparation samples were weighed in with lithium metaborate and fluxed in graphite crucible for 30 min at 1000°C. After melting the resulting glass beads were dissolved with continuous agitation in 100 times its weight of acid mixture (75 g for reference samples, 30 g for the unknowns). The acid mixtures are made of deionized water with volume of 5% nitric acid, 1.33 volume % of hydrochloric acid and 1.33 volume % of semi-saturated oxalic acid. The ICP analyses were made with a cross-flow nebulizer at sample consumption about 2 ml/min. The argon plasma was run at 1200 V. Measurements were made in four 25 second reading sessions after 40 second flushing of the nebulizer with the sample itself. The overall and detailed preparation of the samples is included in the Appendix B.

4. SUBSURFACE GEOLOGY

4.1 Drilling history

Two wells namely LHD-23 and LHD-28 from Lahendong geothermal field in North Sulawesi, Indonesia was selected for this study. Both wells are directional as part of the development of Lahendong unit-3, 4 and 5. Brief history about the drilling of these two wells can be explained as follows:

Well LHD-23 is located in the LHD-5 pad, Pangolombian village at surface coordinates X= 703979 mE, 532; Y= 140733 mN, 32; Z= 877.91 masl and bottom coordinates X= 703728.36 mE; Y= 140608.83 mN; Z= -808 masl. The well is directional with direction S 64°C, inclination 47° and KOP at 250 m. The well was drilled for development unit-3 in this area. The drilling target of this well is the Fault F-6 trending N-S and Pangolombian rim. The well was drilled from 30 December 2005 and finished on 19 March 2006 and spent time about 80 days calendar with last depth of the well is 2000 mMD/ 1693 mTVD (Figure 14). The drilling was carried out in five stages. The well was dug manually with diameter 36'' and cementing casing 30'' through depth 13 m. The first stage was 26'' drilling from 13 m to 208 m and cased cemented using a 20'' casing with casing shoe at 205 m. The second stage was drilling to 834.5 m and cased cemented by 13 3/8'' with casing shoe at 831.5 m. The third stage was drilling by 12 1/4'' to 1708 m and cased by slotted liner 9 5/8'' and hanged at 808.14 m. The last stage was drilling by 8 1/2'' to 2000 m and cased by slotted liner 7'' and hanged at 1703.48 (Table 3; Figure 13). Mud was used during drilling in all stages and only changing to water after encountering total circulation loss which started at 1703 m and remained to 2000 m.

TABLE 3: The casing design of wells LHD-23 and LHD-28
(Silaban et al., 2006: Pertamina drilling department, 2010)

Hole diameter (inch)	Depth (m)	Casing diameter (inch)	Casing depth (m)	Remark
WELL LHD-23				
36	15	30	0-13	
26	208	20	0-205	
17.1/2	834,55	13.3/8	0-831,5	
12.1/4	1704	9.5/8	808,14 – 1704	Slotted liner
8.1/2	2000	7	1701,68 - 2000	Slotted liner
WELL LHD-28				
36	36	30	0-36	
26	455	20	0-451,75	
17.1/2	1011	13.3/8	0-1008	
12.1/4	1600	10.3/4	959-1007,59	Blind liner
			1007,59 – 1600	Perforated liner
9.7/8	2181	8.5/8	1552,10 - 2181	Perforated liner

Well LHD-28 is located in the well pad LHD-24 area in the Tondangow village. The well has coordinates location are X = 703428 mE, Y = 139717 mN, Z= 820 masl, and the bottom coordinates are X = 704002 mE, Y = 140537 mN, Z = -1093 masl. The well is directional with direction N 19 E, inclination 33° and KOP at 500 m. The well is deliniation well to prove the relationship between two different reservoir systems of northern and southern part of the area. The well is also part of the program for the development of the Lahendong unit-4 and unit-5. The drilling target of the well is the structure of F-9 trending SE-NW and Pangolombian rim. The well was drilled started at 10 July 2009 and accomplised at 14 August 2009 or only 36 days (Figure 15). The total depth of the well is 2181 mMD/1924 mTVD. The hole 36'' was drilled to 30 m and 30" casing cemented to 30 m. The first stage was the drilling of 26'' hole starting from 30 m to 455 m and cased and cemented at 451.75 m. The second stage was drilling of hole 17 1/2'' to 1011 m and cased cemented 13 3/8'' at depth 1008 m. The third stage was drillling of hole 12 1/4'' to the depth of 1600 m and 10 3/4'' liner set from 959 to 1600 m. The last stage was drilling of 9 7/8'' hole to the bottom of the well and a 8 5/8" perforated liner set at 2181 m with top of liner hanger at 1552 m (Table 3; Figure 13). Drilling mud was used

during alll stages of drilling except from 1729 m was drilling encountered total circulation loss and the drilling fluid changed from mud to aerated fluids.

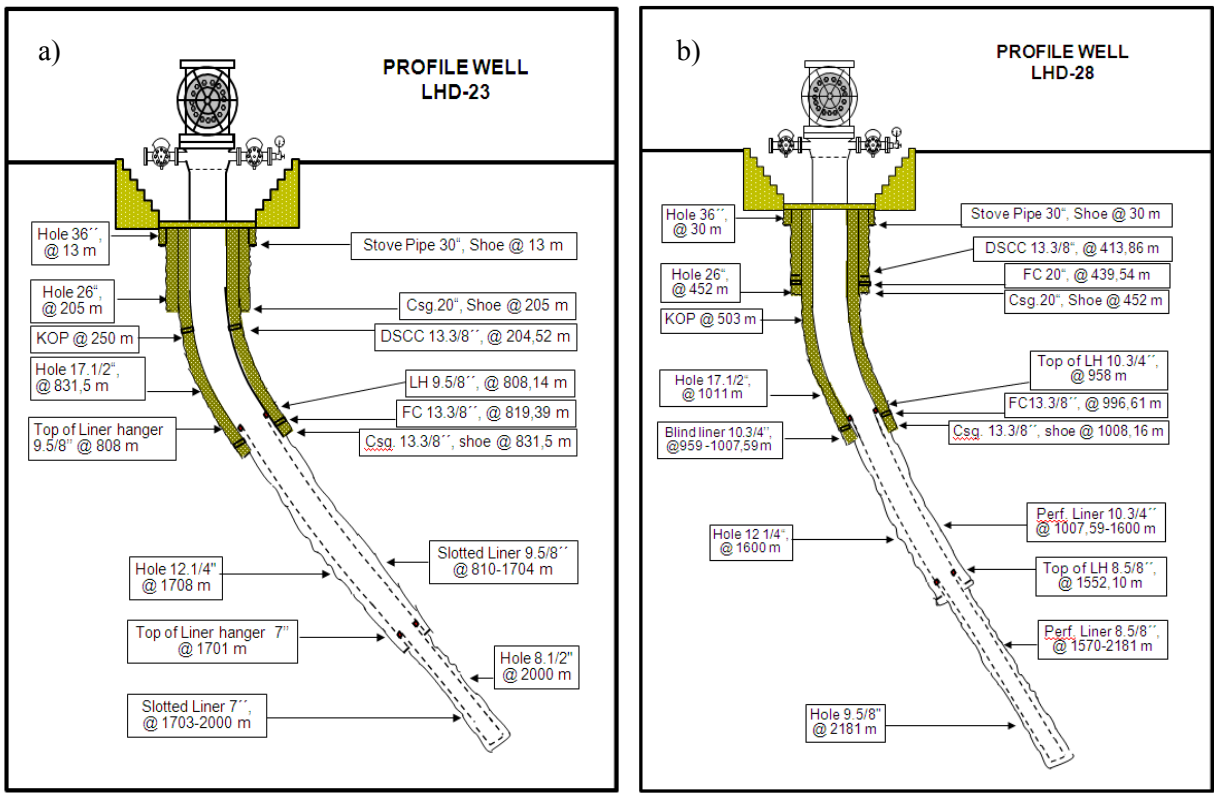

FIGURE 13: Well design of wells a) LHD-23 and b) LHD-28
(Silaban et al., 2006: Pertamina Drilling Department, 2010)

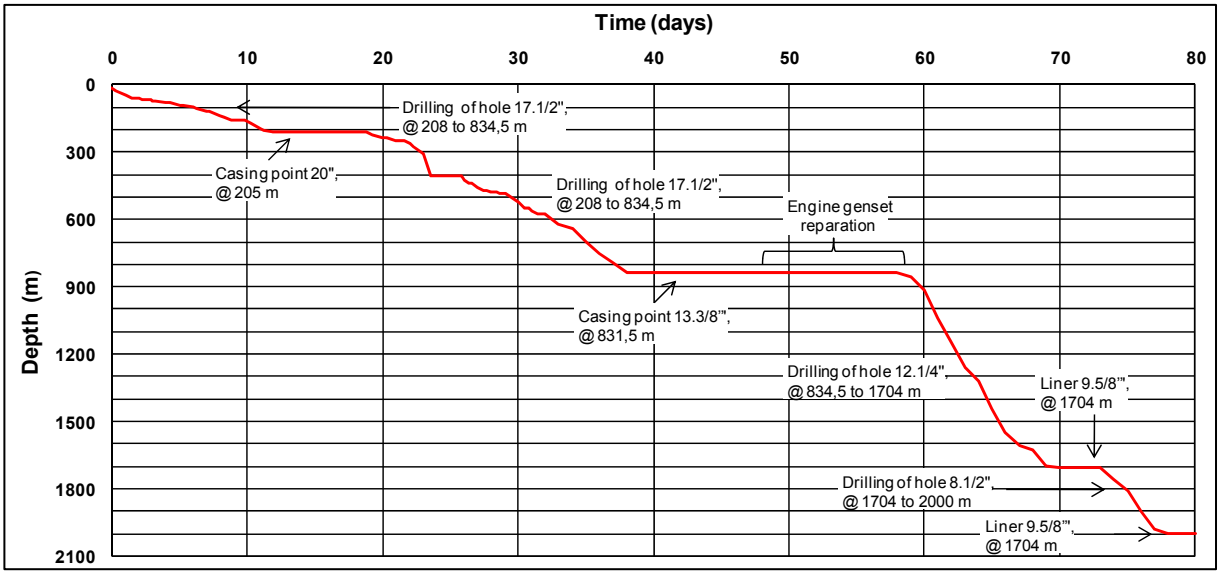

FIGURE 14: Drilling progress of well LHD-23 (Silaban et al., 2006)

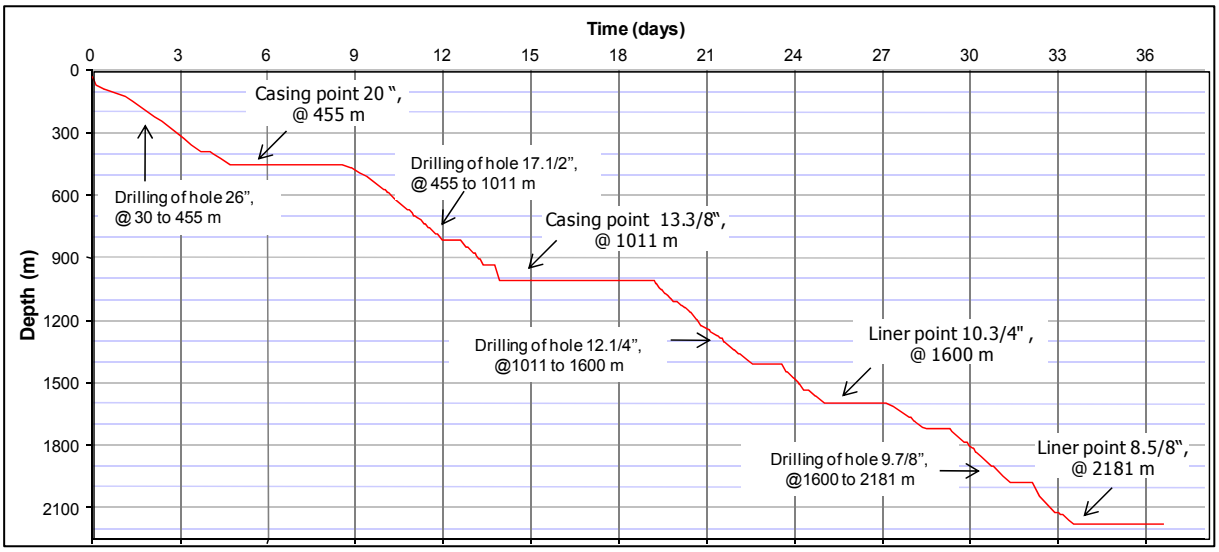

FIGURE 15: Drilling progress of well LHD-28 (Pertamina Drilling Department, 2010)

4.2 Subsurface geology of the well LHD-23 and LHD-28

4.2.1 Lithology

Previous study on the subsurface geology in the Lahendong was carried out by Robert (1987), Azimudin and Hartanto (1997), and Utami et al. (2005). Basically the wells drilled in Lahendong geothermal field encounter thick sequences of basaltic andesitic to rhyolitic rock compositions belonging to the Post Tondano, Tondano, and Pre-Tondano units. Micro diorite dyke was found in the well LHD-5 and has been postulated to form a part of the heat source of the geothermal system. Robert (1987) stated that The Post Tondano unit consists of the Tampusu sub-group of basaltic andesites and pyroclastic products, Kasuratan subgroup is made up of very viscous extrusive magma and Linau sub-group which made of volcanic breccias and pyroclastics. Volcano sedimentary rocks are found as lenses within the Pre-Tondano unit in the northern part of the area but not developed in the Pangolombian, perhaps due to active volcanism inside the caldera.

The rocks found in Lahendong consist of basaltic andesite, breccia, rhyolite, tuff and tuff breccia. Basaltic andesite is characterized by pyroxene-plagioclase porphyritic texture in a microcrystalline groundmass. Breccia is characterized by mixture rock of crystallized basaltic andesite lava and glass tuff. Rhyolite is variably feldspar porphyritic and commonly shows sperulitic texture in the groundmass. Tuff breccia is mixture of glass tuff and basaltic andesite with dominantly tuff.

The units in wells LHD-23 and LHD-28 have been divided in accordance with previous work, i.e. the Post-Tondano, Tondano and Pre-Tondano units. These units are subdivided into formations based on their mode of occurrence and compositions. The layers are based on cutting analysis which limits to some extent the resolution on exact boundaries.

Well LHD-23
Post Tondano Succession
Unit A (0-175 m)(0-175 mTVD)(878-710 masl)
Unit A has thickness at about 175 m and consists of tuff, tuff breccias and basaltic andesite. These layers are products of several volcanic eruptions. The tuffs and tuff breccias is a thin layer at about 10 to 15 m, moderately altered, commonly weak and shows vesicles which filled by secondary minerals such as calcite and pyrite, where the glass tuff is commonly altered to clay. Basaltic andesite lavas are found with thicknesses varying from about 15 to 50 m, greyish to darkish grey in colour, plagioclase and pyroxene porphyritic set in a microcrystalline groundmass. These show oxidation in the some parts of the rock.

Unit B (175-320 m)(175-320 mTVD)(710-565 masl)
This unit is about 145 m thick and consists of basaltic andesite in the lower part and tuff breccia in the upper one. The tuff breccia is greyish green to whitish, highly altered with abundant pyrite. Vesicles are often open but also filled by secondary minerals. In this rock, calcite, pyrite and oxidation are commonly found. Basaltic andesite is blackish grey coloured, porphyritic texture of plagioclase and pyroxene in microcrystalline plagioclase and pyroxene groundmass, some oxidation in the upper part but decreases downward. Rare calcite and pyrite and a few veins are found filled by calcite and pyrite.

Unit C (320-423 m)(320-423 mTVD)(565-462 masl)
This unit is made of tuff and about 103 m thick. The rock is whitish, greenish and grayish in colour, very soft and intermediate to highly altered to clay which may be kaolinite. Two colour textures of tuff are found which has fine grain light colour and course grained darker colour. Minor amount of crystallized fresh looking plagioclase-pyroxene porphyritic andesite fragments are found in the some part.

Unit D (423 – 659 m)(423-637 mTVD)(462-247 masl)
The unit consists of a basaltic andesite lava unit with a total thickness of 236 m. It is dark grey, plagioclase-pyroxene porphyritic in a microcrystalline groundmass of pyroxene and plagioclase minerals, and only slightly altered. Alteration increases between 530 and 545 m where the phenocrysts become moderately altered. In this depth range tuff fraction enters the samples indicating a contact between two lavas.

Tondano Formation (659-830 m) (637-771 mTVD) (247-114 masl)
This formation consists of tuff breccias in the upper part and breccias in the lower part. The thickness of the unit is about 171 m. Tuff breccia is dominantly whitish grey, greenish grey, consists of mixture of white glass tuff and basaltic andesite fragment in various ratios. The rock is moderately altered, vitric crystal tuff, plagioclase and glass fragment in glassy matrix. Local choritisation and silicification occur in some samples, calcite and pyrite are moderately common in the rock. Breccia is found in the lower part of the unit, consisting of a mixture of basaltic andesite and glass tuff, whitish green, darkish grey in colour, the basaltic andesite fragments have plagioclase and pyroxene porphyritic texture in the groundmass of aphanitic material, moderately altered. From 776 m, the rock shows dominantly yellow-green colour. Oxidation is common in the rock at 662-773 m.

Pre-Tondano Succession
Unit-1 (830-956 m)(771-872 mTVD)(114-13 masl)
The uppermost unit is basaltic andesite lava, quite similar as found above the Tondano succession. The thickness of the unit is 126 m. The rock is darkish grey, is plagioclase-pyroxene porphyritic in a microcrystalline groundmass. Slightly-moderately altered. Moderately altered tuff is found at 863 - 869 m and 902 - 911 m which may indicate lava boundaries. A relatively fresh basaltic andesite at 911 – 923 m depth may indicate a possible intrusion.

Unit-2 (956-1088 m)(872-981 mTVD)(13 to -97 masl)
The unit is consists of tuff breccias in the upper part and breccias in the middle and lower part. The unit has thickness of 132 m. The unit is probably intruded by about 3 m dyke of porphyritic basaltic andesite. Tuff breccia is whitish to greenish white; consisting of lithic fragment of andesite in the glass matrix. The crystallized part becomes more common with depth. Oxidation is low and intermittent.

Unit-3 (1088-1352 m)(981-1212 mTVD)(-97 to -328 masl)
The unit is 264 m thick and consists of two basaltic andesite lavas (Figure 16), separated by a layer of tuff-breccia. A breccia layer is also found as the bottom of this unit. The lavas are darkish grey to darkish green, plagioclase-pyroxene porphyritic in the microcrystalline groundmass. The upper unit is less altered than the lower one. The breccia is a mixture of crystallized fragments and tuff. Breccia is found observed as mixture of plagioclase-pyroxene porphyritic of andesite and glass tuff. The rock is highly altered and chloritized. Tuff breccia is whitish due to higher alteration. Probable intrusion is found at depth 1187-1190 m, characterized by fresh-slight altered of dark grey porphyritic basaltic andesite (Figure 17).

FIGURE 16: Basaltic andesite at depth 1140 m well LHD-23

FIGURE 17: Possible intrusion of basaltic andesite at depth 1187 well LHD-23 in tuff breccia formation

Unit-4 (1352-1703 m)(1212-1490 mTVD)(-328 to -606 masl)

This unit which is about 350 m thick is of rhyolitic composition (Figures 18 and 19). It is very light coloured, feldspar porphyritic in the groundmass of feldspar and quartz. Spherulitic texture is found intermittently in a groundmass below 1355 m. From 1703 to 2000 m, total circulation loss occurred. ICP analysis of selected samples from depth 1421 m, 1523 m, 1586 m and 1688 m show SiO_2 content of about 78.78 wt%, 75.01 wt%, 74.52 wt%, and 74.56 wt%, respectively. A plot of SiO_2 against major elements and a comparison between fresh rocks from the surface sampling shows that the trend of SiO_2 follows the expected evolutionary trend, which implies that the high silica content may not be due to silicification from outside.

FIGURE 18: Rhyolite lava observed at depth of 1360 m well LHD-23. Sparsely feldspar porphyritic and sulfides disseminated in the groundmass

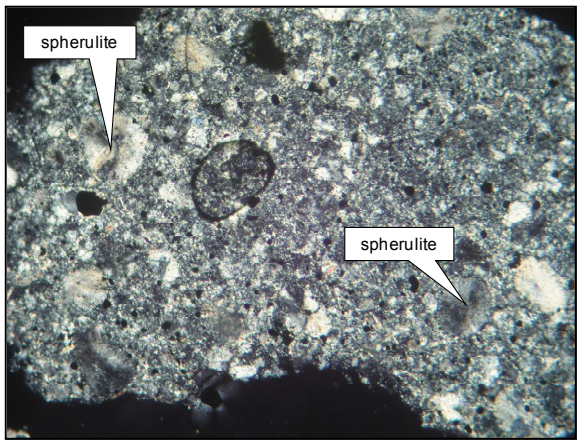

FIGURE 19: Spherulitic texture in rhyolite lava well LHD-23 at depth of 1355 m

Well LHD-28

Post Tondano Succession

Unit 1 (0-180 m)(0-180 mTVD)(820-651 masl)

This unit consists of andesite pyroclastics in the upper part and breccias in the middle and lower parts. Andesite pyroclastic is found on the surface of the area. The breccia is a mixture of crystallized fragments and glass tuff.

Unit 2 (180-309 m)(180-309 mTVD)(651-522 masl)

This unit is about 130 m thick and consists of a variable mixture of tuff and crystallized basaltic andesite. It is greyish white, fragmental textures with a few crystallized rocks. The basaltic andesite

is dark grey to grey in colour, plagioclase-pyroxene porphyritic in the aphanitic groundmass, slightly altered, showing some oxidation. Breccia is greenish grey to grey and is moderately to strongly altered.

Unit 3 (309 – 402 m)(309-402 mTVD)(522-429 masl)
This unit consists of a 90 m thick layer of tuff. The unit is predominantly glassy tuff with minor crystallized fragments. The rock is greyish to white but becomes greenish in the middle part. Plagioclase and pyroxene phenocrysts are rare. Oxidation is observed especially at about 384 m depth. Veins are noteable in the middle part mostly filled by chalcedony quartz, calcite and pyrite.

Unit 4 (402-549 m)(402-549 mTVD)(429-282 masl)
The unit is about 150 m thick basaltic andesite lava, light to dark grey, dark greenish in colour, predominantly plagioclase and pyroxene porphyritic in the microcrystalline groundmass and becoming more crystalline in the lower part. It is slightly - moderately altered.

FIGURE 20: Abundant pyrite in the matrix of vitric crystal tuff at 558 m depth, well LHD-28

FIGURE 21: Vein in tuff filled by pyrite and quartz at 558 m depth, well LHD-28

Tondano Formation (549-741 m) (549-732 mTVD) (282 – 99 masl)
This unit is a tuff breccia in the upper part (Figures 20 and 21) and breccia in the lower. The unit is 192 m thick. Tuff breccias are greyish white in colour, fragmental, and consist of a mixture of tuff and crystallized fragments. The breccia is a mixture of greenish crystallized basaltic andesite and tuff in various proportions. Some of the basaltic andesite has porphyritic and vesicular texture.

Pre-Tondano Formation
Unit-1 (741-879 m)(732-855 mTVD)(99 to -24 masl)
This basaltic andesite lava is 138 m thick. It is greyish green, altered, plagioclase-pyroxene porphyritic and vesicular

Unit-2 (879-950 m)(855-915 mTVD)(-24 to -84 masl)
This 70 m thick breccia is greyish green in colour and strongly altered, a mixture of tuff and crystallized fragments of basaltic andesite. The rock is locally intensely chloritized.

Unit-3 (950-1578 m)(915-1425 mTVD)(-84 to -594 masl)
This unit is considered to be about 630 m thick. It consists of a very thick succession of basaltic andesite lavas and breccias. A thin layer of rhyolite is found in the middle of the unit. The top layer is 202 m thick basaltic andesite lava. It is greyish green in colour, pyroxene-plagioclase porphyritic and vesicular texture in the microcrystalline groundmass. It is highly altered and variable oxidation is observed. Below the thick lava unit is a sequence of five basaltic andesite lavas separated by breccia and tuff layers. The lava layers range in thickness from 24 m to 40 m, and the breccias layers range in thickness from 21 to 34 m. A thin layer of rhyolitic composition occurs at 1293 m to 1305 m depth. It is recognizable by the very light colour near to white and is sparsely feldspar porphyritic.

Unit-4 (1578-2181 m)(1425-1924 mTVD)(-594 to -1093 masl)
This sequence of silicic rock has a thickness of about >603 m. The unit is characterized by being very whitish in colour and feldspar porphyritic. In thin section the groundmass is patchy siliceous groundmass along with microlaths of feldspars. Spherulitic texture is sometimes found but not always. The rock is commonly feldspar porphyritic. Chemical analysis at 1590, 1635, and 1830 m depths are 76.97 wt%, 72.37 wt% and 73.72 wt%, respectively. Total circulation losses were found in this unit starting at 1981 m depth to the bottom of the well.

4.2.2 Stratigraphic correlation

The detailed character of the lithological sequence is described above, based on the cutting analysis represented in appendix C. In this section, an attempt is made to correlate between the two wells of this study and then expand that to other neighbouring wells that were drilled in the same pads as those two wells. The distance between the wellpads is about 1.1 km and one would expect some variation in lithology, as individual lava units may be variably extensive. The uppermost ca. 1000 m succession within each pad should correlate well but diminish as the wells deviate out in different directions. Stratigraphy has been dealt with in previous work (e.g. Ganda and Sunaryo, 1982 and Robert, 1987; Azimudin and Hartanto, 1997). Tondano is the mega volcanic caldera structure, and the eruptive material from the subsidence episode is found on the caldera rim. Lahendong which is both within that caldera is also within the smaller Pangolombian caldera (Figure 5). The tuffs and breccias formed during the Tondano subsidence is found at 500-700 m depth in most of the wells in Lahendong. For that reason the formations are divided according to whether they pre- or postdate the Tondano caldera formation.

Figures 22 and 23 show how the units connect stratigraphically. The correlation from the two wells of LHD-23 and 28 show that the Post-Tondano unit forms between 0-659 m (878-247 masl) and 0-549 m (820-247 masl), respectively. The Tondano Unit is forms from 659-830 m (247 to 114 masl) and 549-729 m (282-110 masl), respectively, and the Pre-Tondano unit below 830 m (114 masl) and 729 m (110 masl) to the bottom of the wells, respectively.

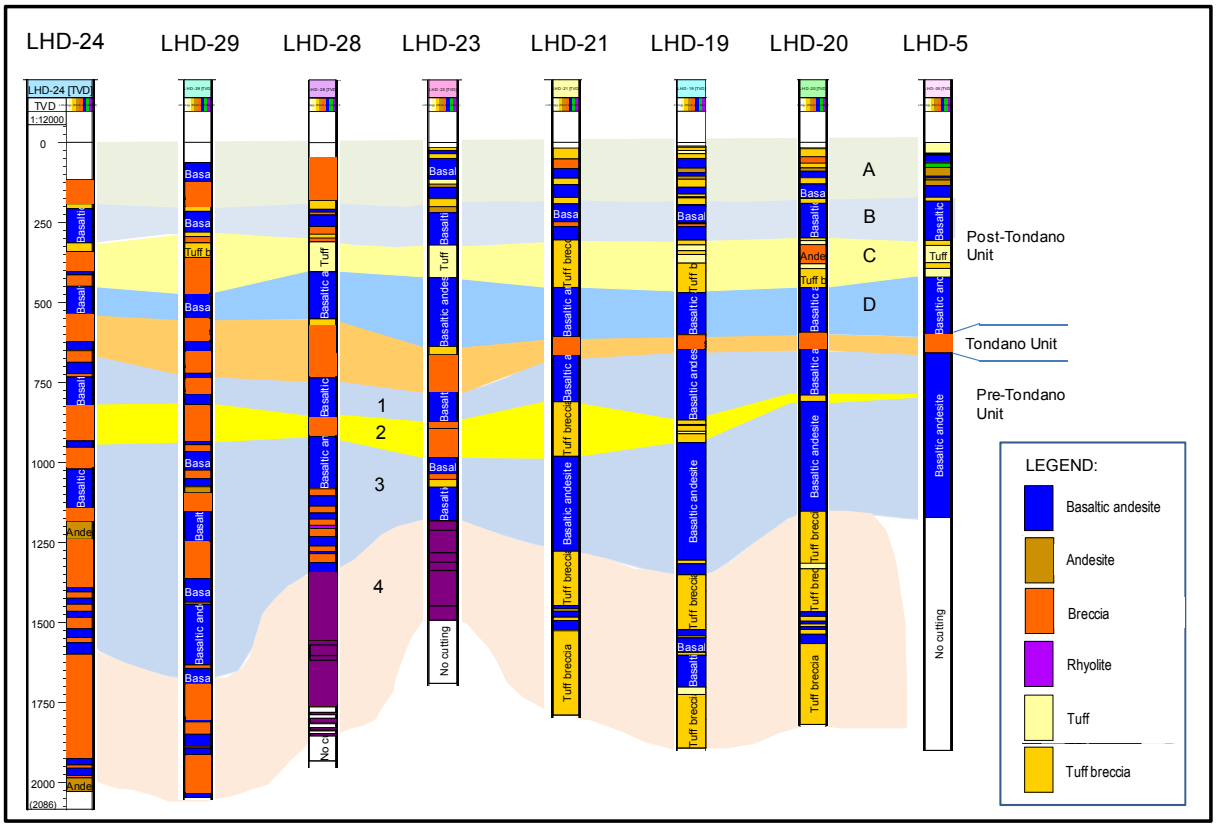

FIGURE 22: Lithologic correlation from well LHD-23 (well pad LHD-5) and well LHD-28 (well pad LHD- 24)

The Post Tondano unit (LHD-23: 0-659 m (878-247 masl) and LHD-28: 0-549 m (820-247 masl))

The Post Tondano unit consists of pumice, tuff and volcanic breccias from Kasuan, Tampusu or Lengkoan and Linau, respectively. The bottom of this sequence is marked by the sequence of basaltic-andesite with a thickness about 140 to 580 m probably a product of Mt. Tampusu (Robert, 1987).

In both wells LHD-23 and LHD-28, this unit consists of intercalation between basaltic andesite, breccias and tuff to tuff breccia. The total thickness of this sequence is about 659 and 549 m in well LHD-23 and 28, respectively. The bottom part of this sequence is marked by the appearance of different thicknesses of the basaltic andesite sequence in the wells, with thickness 236 m and 90 m in well LHD-23 and 28, respectively. The difference in thickness is probably due to the fact that well LHD-28 is further away from Mt. Tampusu than well LHD-23 or could also be influenced by the paleotopography when the unit was deposited (Figure 3).

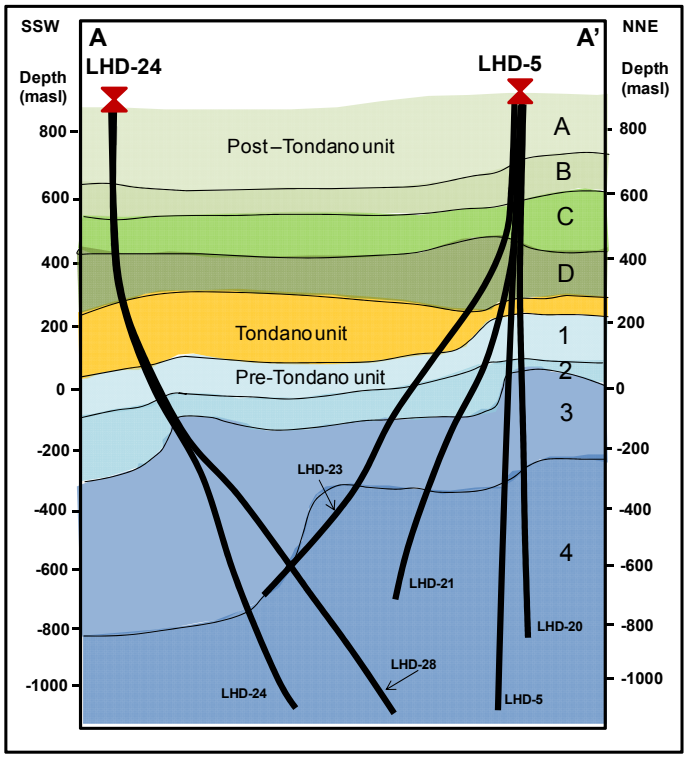

FIGURE 23: SSW-NNE cross section shows formation unit in well LHD-23 (well pad LHD-5) and well LHD-28 (well pad LHD- 24)

The Tondano unit (LHD-23: 659-830 m (247 to 114 masl) and LHD-28: 549-729 m (282-110 masl))

The Tondano formation is derived from the Pliocene period as an eruptive product of the huge Tondano volcano-tectonic depression. The rock unit has good porosity and permeability and consists of rhyo-dacitic ignimbrites in the upper part (Robert, 1987). Utami et al., (2005), reported that Tondano unit consists of rhyolitic tuff, breccias, and pumiceous rhyolite lava.

In wells LHD-23 and LhD-28, the Tondano unit is encountered at depth 659 m to 830 m (247 to 114 masl) and 549-729 m (282-110 masl), respectively. The rock units encountered in this depth are made up of tuff breccias in the upper part and breccias in the lower part. This unit is interpreted as the shallow reservoir of the Lahendong geothermal system and is found in almost all the wells.

The Pre-Tondano unit (LHD-23: below 830 (114 masl) and LHD-28: below 729 (110 masl).

This unit is made of volcanic and sedimentary formations prior to the formation of the Tondano volcano tectonic depression during the Miocene period. The sediments are well developed especially in the northern part of Lahendong but not around Pangolombian probably because it was already forming a volcanic highland (Robert, 1987). Pre-Tondano successions build up of basaltic andesitic to rhyolitic formations, a mixture of lavas and intercalated tuff and breccia layers at depths below 600 m to 1000 m (Siahaan, 2000).

The succession in wells LHD-23 and LHD-28 is composed of basaltic andesite, andesite and rhyolite lavas with intercalated breccias and tuffs. The lavas sometimes show good vesicular structures, especially those found in well LHD-28. Similar vesicular structures are found in wells LHD-6 and 7 and are reportedly associated with circulation losses during drilling (Siahaan, 2000). The Pre-Tondano unit is believed to be the main reservoir rock of the Lahendong system. This is especially true in the

central and southern parts of the field, while wells LHD-3, LHD-6 and LHD-7 show low temperature alteration and provide the location for reinjection at the boundary of the field.

The unit in Pre-Tondano were assessed to be dominantly andesite to dacite in binocular and petrographic microscope analysis. Petrochemistry (Section 4.3) shows, however, more silicic compositions. This makes correlation of the Pre-Tondano unit more difficult to other neighboring wells as seen in Figure 22. Further chemical analyses are underway on the main stratigraphic units in wells LHD-23 and LHD-28 to confirm better this relation.

4.3 Petrochemistry

The volcanic succession of Lahendong field is divided into three groups: Pre-caldera Tondano caldera, and Post-caldera formations (Robert, 1987; Azimudin and Dradjat, 1997; Siahaan et al., 2005; Utami et al.,, 2005). These formations are considered to be dominated by basaltic andesite compositions (Gondwana, 1988). Volcanic product from the Pre-caldera group has an age range of 2.63 (Late Pliosen) – 0.832 m.y. (Early Pleistosen). Volcanic product from Post-caldera is formed by volcanic activity which has an age range of 0.586 m.y. (Middle Pleistosen) to Holocene. The formation of the Tondano caldera is believed to have occurred between Late Pliosen to Early Pleistosen or 600 to 800 10^3 years ago (Gondwana, 1988). The Linau Lake and Tampusu eruptions around Lahendong have an age of about 500 10^3 years.

Geochemical analysis shows that rock compositions range from basalt to rhyolitic compositions, with predominance of basaltic andesites. These analyses (Figure 24) show that they fall within three volcanic evolutionary trends: Calc-alkali-potassic, calc alkali and tholeiitic trends (see also table in appendix B). The series appear to cover these evolutionary series within the basaltic andesite range but follow the calc-alkali trend in the andesitic to rhyolitic compositions these trends probably bear witness to the complex magmatic environment during the build up of the crust including crustal assimilation, magma mixing and fractional crystallization (Gondwana, 1988; Siahaan et al., 2005). These different magmas trends are characteristic in the tectonic orogenic environment related to the subduction system in the eastern or northern parts of Sulawesi.

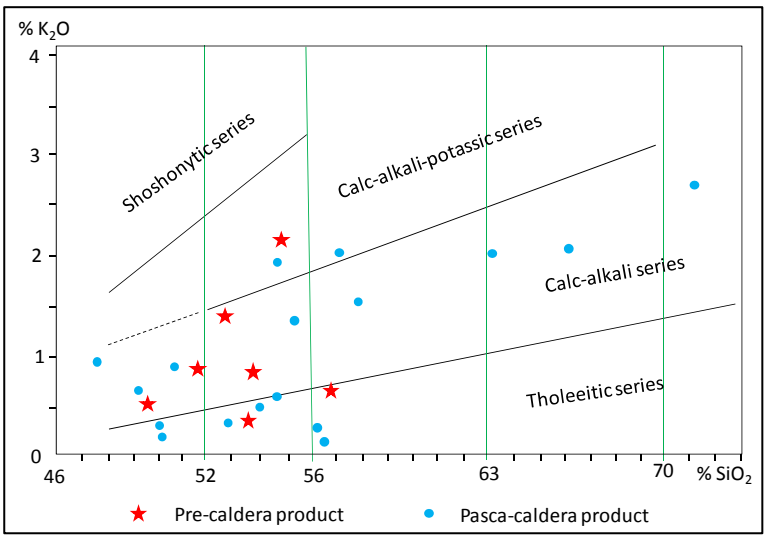

FIGURE 24: Diagram K_2O/SiO_2 of Lahendong rock samples from Peccerillo and Taylor, 1976 (Gondwana, 1988)

Ten samples were taken from wells LHD-23 and LHD-28 at various depths and analyzed using ICP at the University of Iceland. The samples were taken from variably altered rocks as has been discussed in Section 4.2. The samples were analyzed for major and trace elements (Table 4). The chemical composition of fresh rocks from surface mapping is used for comparison with the altered rocks of the two wells. Fresh rocks from surface mapping were only analysed for major element analysis, hence the comparison between the analysis of samples from this work (wells LHD-23 and LHD-28) and fresh rocks from surface mapping (Gondwana, 1988) is based on major element data.

Figure 25 shows the relationship between various oxides plotted against SiO_2 in comparison with fresh rocks. Overall, the samples fall within the evolutionary field of the fresh samples, indicating alteration insignificant chemical transport during alteration. The only oxides that appear changed during are K_2O depletion and P_2O_5 and CaO enrichment in three samples. TiO_2 and FeO are very stable during

TABLE 4: Major and traces elements analysis of wells LHD-23 and LHD-28 (in wt%)

Wells	LHD-23	LHD-23	LHD-23	LHD-23	LHD-23	LHD-23	LHD-28	LHD-28	LHD-28	LHD-28
Depth (m)	1247	1331	1421	1523	1586	1688	444	1590	1635	1830
SiO_2	66.74	69.96	78.78	75.01	74.52	74.56	61.36	76.97	72.37	73.72
Al_2O3	15.39	15.01	12.42	13.65	14.08	13.89	17.46	13.00	14.71	14.54
FeO	4.93	3.15	1.17	1.68	1.79	1.79	6.16	1.82	2.51	1.65
MnO	0.11	0.09	0.03	0.07	0.07	0.06	0.12	0.05	0.07	0.08
MgO	1.83	1.21	0.39	0.70	0.84	0.75	3.15	0.65	0.90	0.86
CaO	5.91	5.32	0.96	2.07	2.26	2.37	8.02	1.72	2.80	2.35
Na_2O	3.38	3.24	3.02	3.89	3.64	3.73	1.73	2.85	4.09	4.46
K_2O	0.80	1.37	2.90	2.46	2.30	2.34	0.91	2.55	2.07	1.93
TiO_2	0.61	0.41	0.19	0.26	0.28	0.27	0.69	0.21	0.27	0.23
P_2O_5	0.20	0.14	0.04	0.10	0.11	0.10	0.30	0.07	0.11	0.10
Ba	0.017	0.023	0.039	0.036	0.032	0.035	0.013	0.035	0.033	0.031
Co	0.001	0.001	0.000	0.000	0.000	0.000	0.002	0.000	0.000	0.000
Cr	0.001	0.001	0.000	0.001	0.000	0.000	0.002	0.001	0.000	0.004
Cu	0.004	0.004	0.001	0.003	0.002	0.002	0.006	0.001	0.003	0.002
La	0.001	0.002	0.002	0.001	0.001	0.001	0.003	0.002	0.002	0.001
Ni	0.001	0.001	0.001	0.001	0.001	0.001	0.002	0.001	0.001	0.001
Rb	0.008	0.015	0.022	0.021	0.017	0.021		0.018	0.015	0.008
Sc	0.002	0.001	0.001	0.001	0.001	0.001	0.002	0.001	0.001	0.001
Sr	0.025	0.022	0.009	0.016	0.015	0.014	0.022	0.009	0.016	0.016
V	0.012	0.007	0.001	0.003	0.003	0.003	0.020	0.003	0.004	0.003
Y	0.004	0.003	0.005	0.003	0.004	0.003	0.003	0.005	0.003	0.003
Zn	0.005	0.004	0.002	0.003	0.005	0.028	0.006	0.003	0.004	0.003
Zr	0.014	0.014	0.021	0.016	0.017	0.015	0.021	0.024	0.016	0.015
Total	100.00	100.00	100.00	100.00	100.00	100.00	100.00	100.00	100.00	100.00

alteration (Franzson et al., 2008). Plotting SiO_2 against CaO and K_2O shows a slight enrichment in CaO from a sample taken at 444 m depth in well LHD-28 and 1247 m and 1331 m depths from well LHD-23 but depleted in K_2O. Plotting SiO_2 against P_2O_5 shows that there are two samples is off trend from depth 1247 and 444 m in well LHD-23 and LHD-28, respectively.

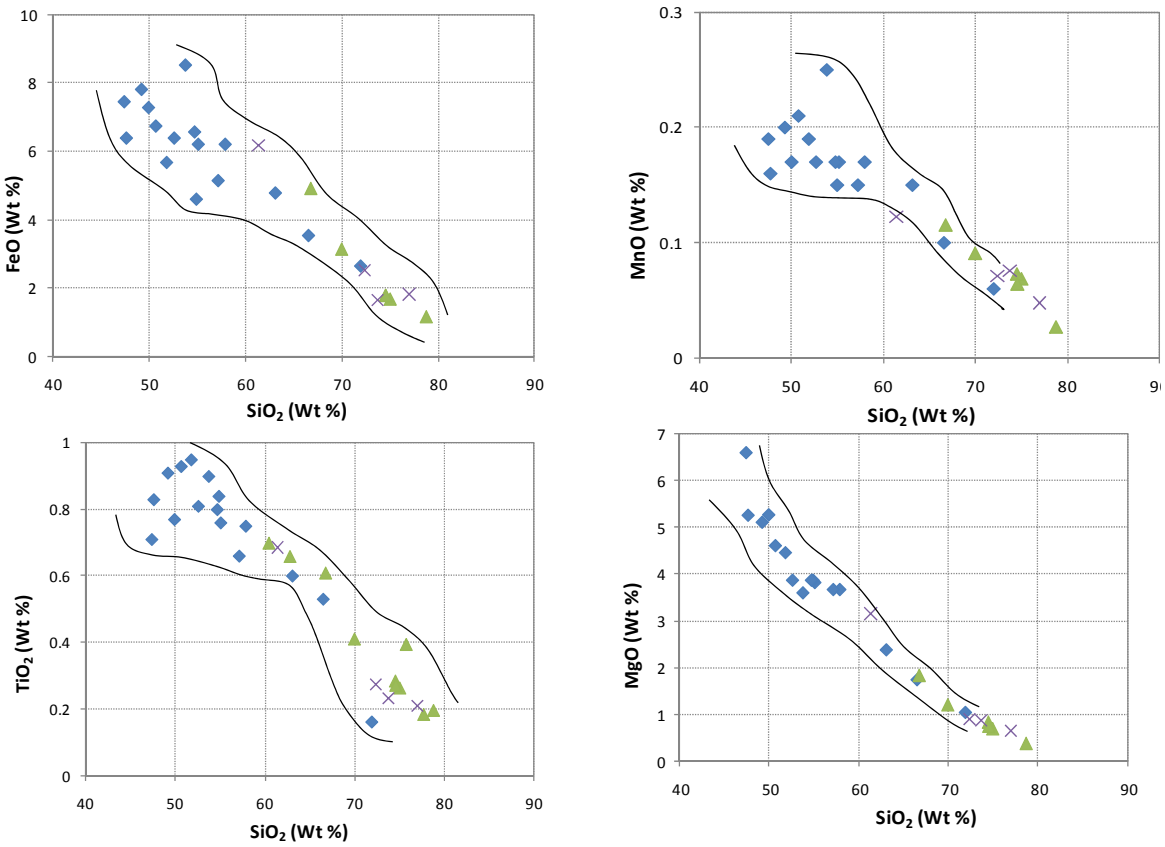

FIGURE 25: Oxide components plotted against silica from selected surface rock samples (Gondwana, 1988) and altered rock samples from wells LHD-23 and LHD-28

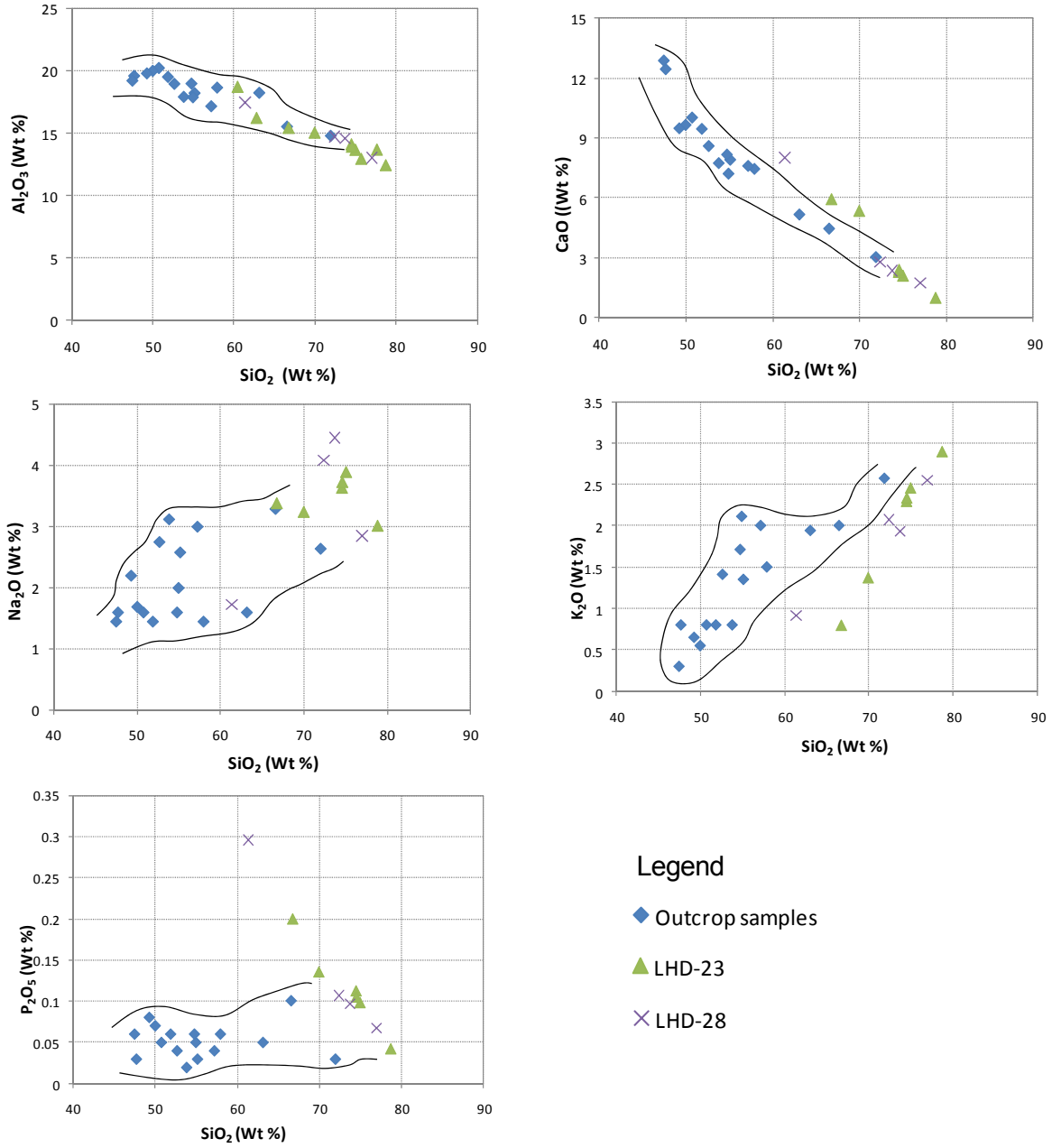

FIGURE 25: (Continued)

4.4 Aquifers and connection to geological structure

The main aim of geothermal drilling is to intersect good permeability within the reservoir. An aquifer may be a fracture, joint, lithological contact, intrusive boundary, porosity, like in breccia, etc. Aquifers or feed points can be monitored as circulation losses or gains during drilling, the larger the losses, the bigger the aquifer. Fractures along dyke and faults provide high permeable zones in the Icelandic geothermal system (Franzson, 1983; Franzson, 2000; Franzson et al.,, 2002). Other evidences of aquifers may be a sudden increase in the penetration rate.

Fault intersections are the major sources of permeability in the Philippines systems. Quartz, adularia, anhydrite, wairakite, illite, hyalophane, abundant pyrite, abundant calcite are the minerals indicative of good permeability in Philippines geothermal wells (Reyes, 2000). There the identification of the aquifer or permeability from the wells is loss circulation, and an intense degree of alteration. Silicic pumice breccia and pyroclastic rocks are the main aquifers in the Wairakei and Broadlands system in New Zealand (Browne, 1995).

The methods to locate aquifers in this study mostly utilized temperature logs. The interpretation data from temperature logs were combined with the data of circulation loss, rate of penetration (ROP), distribution of veins filling, rock formation and degree of alteration intensity. These data were plotted in the figure to see the correlation between the aquifer and the geological evidence. In wells LHD-23 and LHD-28, temperature measurement was done using the kuster temperature element (KTE). The measurement was done at every 50 m to 100 m depth intervals without using water injection during the measurement. Therefore, the accuracy and sensitivity on reading the aquifer in the well formation was less precise compared to the digital temperature measurements done during water injection into the well such as is done in Icelandic wells. The P and T measurements in Icelandic wells are done continuously along the well hole so that the interpretation of aquifer location becomes more accurately detail (Stefansson and Steingrimsson, 1980).

TABLE 5: Location of aquifers in wells LHD-23 and LHD-28

Well	No.	Depth (m)	Circ. loss (l/m)	Temp. Profile	Alt. Intensity	Geological evidence	Relative size
LHD-23	1.	350		S	HA	Frac	S
	2.	450		S	SA	Frac	S
	3.	600		S	MA	Ukn	S
	4.	700		S	MA	Ukn	S
	3	1006		M	HA	Abundance Pyrite/Frac?	S
	4	1352		M	HA	Strat	S
	5	1370	40	M	HA	Frac/2nd Porosity	M
	6	1451	50	M	HA	2nd Porosity	M
	7	1472	61	M	HA	Strat, Frac	M
	8	1577	130	M	HA	Veins/vesicles/Frac	M
	9	1703-2000	TCL	H	HA	Frac (?)	H
LHD-28	1	400		M	MA	Strat	S
	2	549		S	MA	Strat	S
	3	828		L	HA	Unk	S
	4	1000		M	HA	Strat, ves	S
	5	1100		S	MA/HA	Strat	S
	6	1416		S	HA	Unk	S
	7	1600		S	HA	Strat	S
	8	1659	30 - 200	M	HA	Unk	S
	9	1728	100 – 600	S	HA	Frac	M
	10	1751	100 – 630	S	HA	Unk	M
	11	1771	32 – 3100	S	HA	Strat	H
	12	1845	80 – 3800	M	HA	Strat	H
	13	1902	235 – 1750	S	HA	Unk	M
	14	1961	700 – 1100	M	HA	Unk	M
	15	1981-2181	TCL	H	HA	F-6 (?)	H

Circ.=Circulation, Temp.=Temperature, Alt.=Alteration, TCL=Total circulation loss, S=Small, M=Moderate, H=High, NA=No alteration, SA=Slight alteration, MA=Moderate alteration, HA=Highly alteration, Strat=Stratigraphic boundary, Frac=Fracture, Unk=Unknown relationship.

Four zones were found at shallow depth (above the production casing) in wells LHD-23 and well LHD-28. The entire aquifer zone at these depths is categorized as small size since no circulation losses were encountered at that depth. Wells LHD-23 was drilled with mud throughout the drilling stage but changed to water after encounter total loss circulation and well LHD-28 was drilled with mud but changed to aerated fluids after encountering total circulation loss. Drilling using mud sometimes minimizes the possibility circulation loss. The correlation of the aquifer with the geological structure is dominantly controlled by stratigraphy, fractures and some unknown relationship. Fracture can be observed in the cuttings on grounds of abundant micro mineral veins that in these wells were predominantly filled by pyrite and quartz and with or without calcite.

In wells LHD-23 and LHD-28, no circulation losses were found in the shallow depths of the production part of the wells. The first depths where both of wells encountered partial circulation loses were at 1370 m and 1659 m, in wells LHD-23 and 28, respectively. At depth of 1703 m in well LHD-23 and a depth of 1901 m in well LHD-28, total circulation losses started.

In well LHD-23, seven possible aquifers were found within the production casing. No circulation losses were encountered at the first two aquifers at 1006 m and 1352 m depths but pyrite was abundant. The evidence for aquifers there are deviations in the temperature logs and the occurrence also acid alteration. This aquifer is possibly related to some fractures and a stratigraphic boundary at 1006 and 1352 m depths, respectively.

Below these two possible aquifers partial loss of circulation occurred at depth of 1370, 1451, 1472, and 1577 m. The aquifers at these depths are predominantly related to fractures (vein fillings abundant in cuttings at about 1300 and 1350 m depths), the stratigraphic boundary and possibly due to the appearance of secondary porosity. Below those aquifers, at 1703 m depth, total circulation loss occurred (Figure 26). The cause of the permeability is not known from subsurface data. It must be noted, however, that the well was directed towards Linau Lake, where the maximum density of fractures in the Lahendong area occurs, so the probability of entering into a permeable fracture zone is considered high. It is interesting to note the gradual increase in secondary porosity from about 1350 m depth down to the total circulation loss, seen in the preferential dissolution of feldspar phenocrysts in the rock. This coincides with acid alteration indicating that the dissolution is caused by the acid fluid.

The aquifers in well LHD-28 are shown in Figure 27. Above the end of the production casing, three aquifers were identified by the temperature logs and zones of intense vein fillings in the cuttings. Some 11 aquifers were identified, in the production part. No circulation losses were observed in the first three, i.e. at 1100, 1416 and 1600 m depths, but were seen in temperature logs as internal flow between aquifers. It is interesting to note that the 1416 m aquifer coincides with minor intrusions at that depth, and vein fillings are relatively abundant in cuttings below 1500 m down towards 1600 m where the aquifer was encountered, indicating a fracture relationship.

Partial circulation loss started at a depth below 1659 m to 1961 m. The geological evidence related with this aquifer is stratigraphy, fracture and an unknown relationship. A completion test done in well LHD-28 showed that the aquifers are located at the depth interval of 1550 to 2000 m, with a major aquifer probably located at a depth of about 1800 m to 2000 m (Handoko, 2009). These major aquifers are marked by high partial to total circulation losses. This main aquifer may be related to the N-S geological structure of F-6 and was one of the targets of the well. At the location of the total circulation loss at 1950 m a temperature minimum occurs in the T-log indicating a flow of colder circulation fluids into the aquifer during drilling. Below, a steep gradient takes over indicating that the well is tight.

The aquifers in both wells also relate to acid aquifers. Acid aquifers are found at depths in wells LHD-23 and LHD-28. An acid aquifer may be observed by the appearance of sulphur and the distribution of gypsum fungi in cutting samples at those depths. Acid alterations were found intermittently and sometimes were observed as narrow zone. Possible acid alteration was found intermittently below 320 m, 752 m, 1022 m and 1346 m in well LHD-23. In well LHD-28, acid alterations were found at depths below 1512 m and 1692 m. The relationship between the location of the aquifer and acid alteration is shown in the Figures 26 and 27.

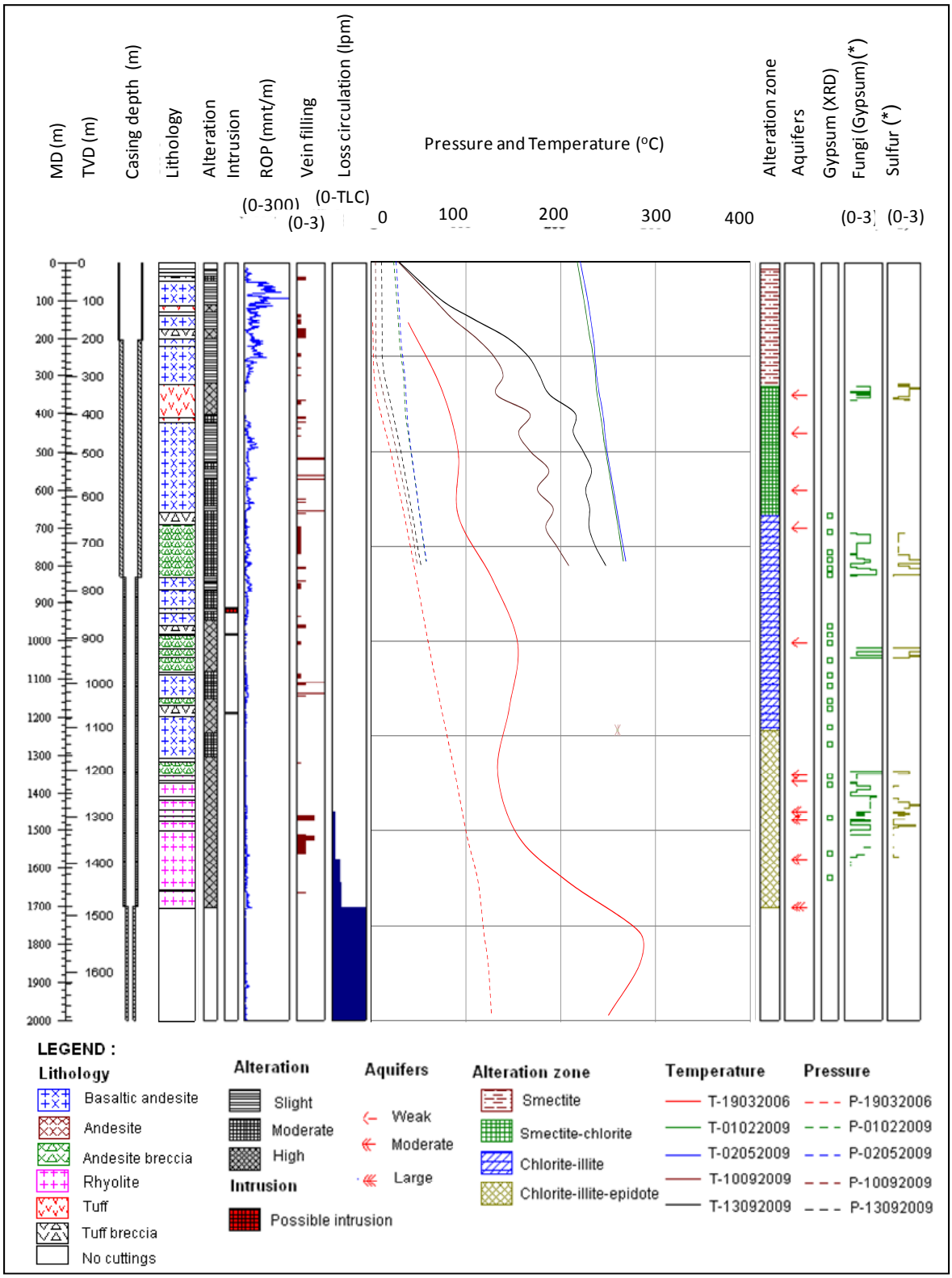

FIGURE 26: The location of the aquifers related to the geological evidence and the appearance of probable acid evidence in well LHD-23; (*) = probably appears after sampling

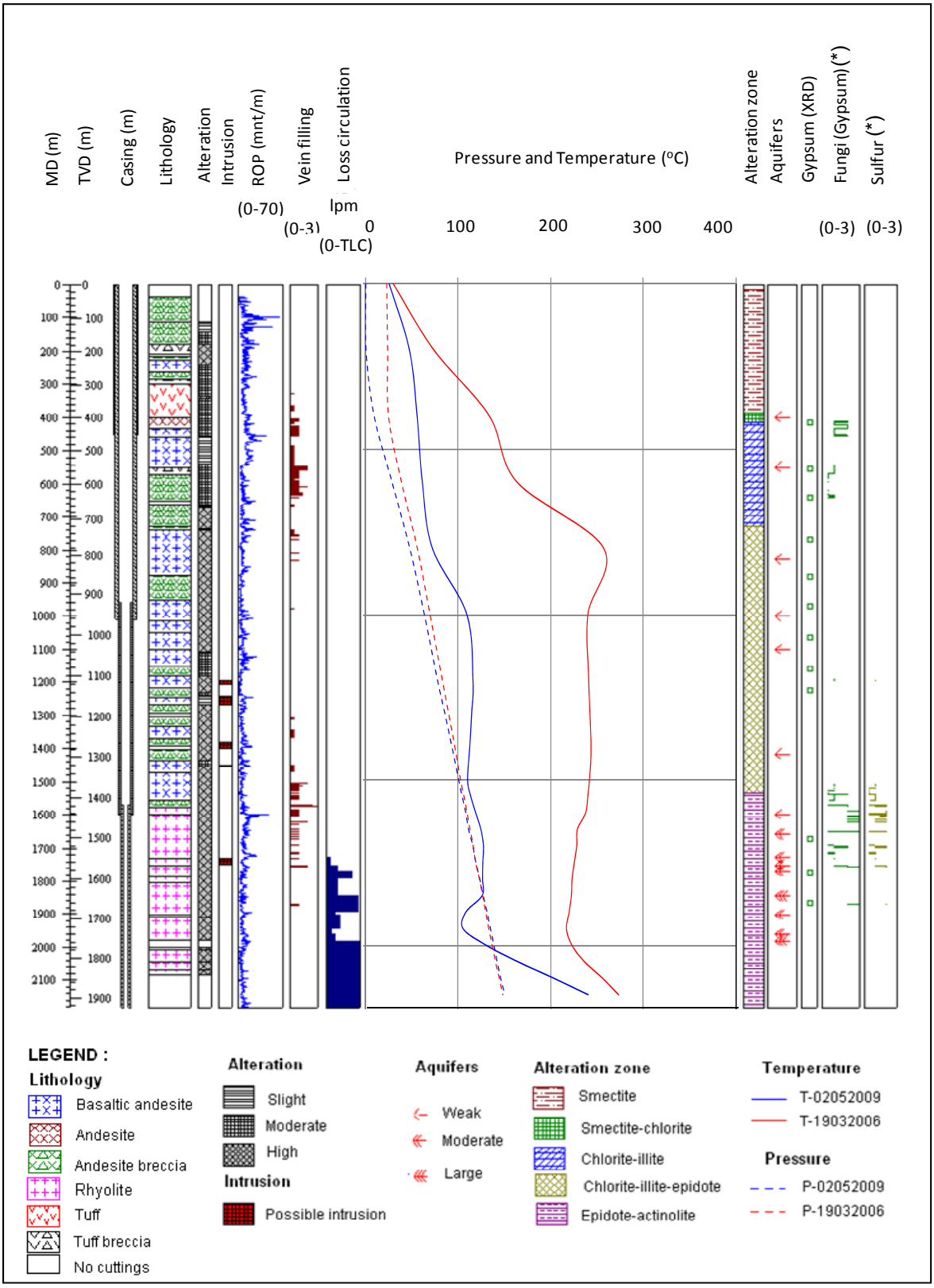

FIGURE 27: The location of the aquifers related to the geological evidence and the appearance of probable acid evidence in well LHD-28; (*) = probably appears after sampling

5. HYDROTHERMAL ALTERATION

5.1 Hydrothermal alteration of well LHD-23 and LHD-28

Hydrothermal alteration is the result of the interaction of individual primary rock minerals and various ions present in the geothermal fluids (Steiner, 1977). In geothermal systems, hydrothermal alteration is a product of water-rock interaction and the parent rock influences hydrothermal alteration mainly through the control of permeability by texture and porosity.

The formation of hydrothermal minerals is affected by temperature, pressure, parent rock types, reservoir permeability, fluid composition and duration of activity (Browne, 1978) and the number of hydrothermal regimes (Reyes, 1990). Time is also an important factor since it controls whether the alterations are incipient, partial or complete (Steiner, 1977).

The hydrothermal alteration minerals in geothermal systems can be used as geothermometers, in determining depth of production casing, in estimating fluid pH and other chemical parameters, predicting scaling and corrosion tendencies of fluids, measuring permeability and possible cold-water influx into wells, as a guide to field hydrology and to roughly estimate the thickness of the eroded overburden, see Figure 28 (Reyes, 1990).

Hydrothermal alteration is divided into two suite types based on the composition of hydrothermal fluids. Two types of the hydrothermal assemblages are neutral pH and acid alteration. Neutral pH alteration is formed by hot, near-neutral pH, and alkali chloride fluids, while acid alteration is formed by the passage of low pH, high-sulphur bearing (possibly gassy) fluids. In this type of suite, acid alteration is accompanied by hydrogen metasomatism, base-cation leaching, and sulfate metasomatism (Hemley and Jones, 1964). In Philippines geothermal systems, the most common acid alteration minerals are aluminium and silica rich minerals such as kandite, pyrophyllite, diaspore and iron or titanium rich such as pyrite, leucoxene and rutile (Reyes, 1990).

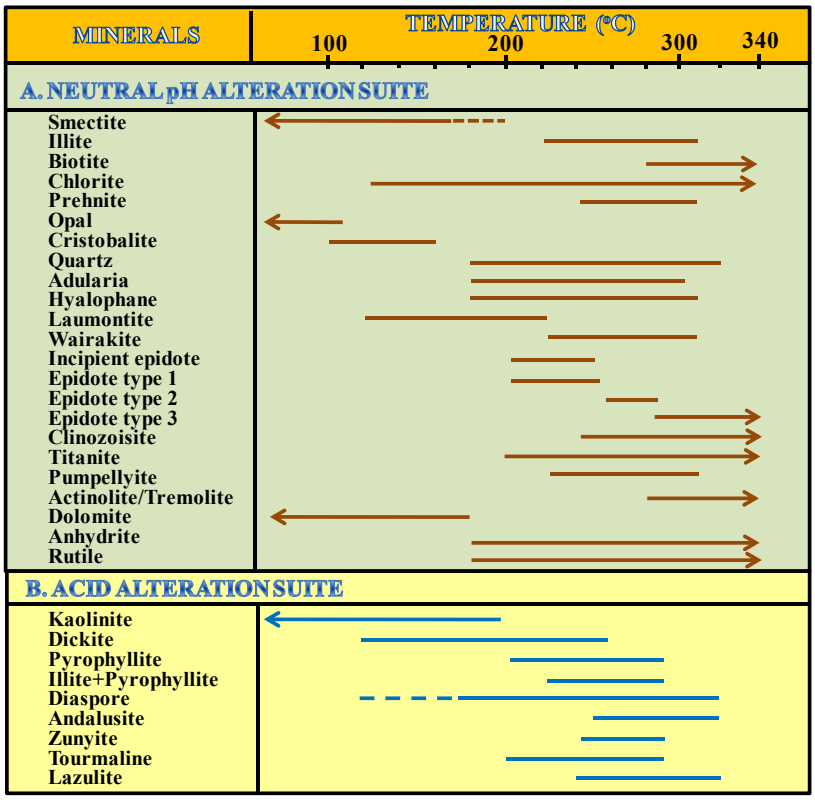

FIGURE 28: Common hydrothermal minerals used as geothermometers in Philippines geothermal systems (redrawn from Reyes, 1990)

In two wells of LHD-23 and 28, the neutral pH alteration mineral assemblage is dominant compared to acid alteration mineral assemblages that found discontinous, locally, sometimes narrow and usually related to the fracture systems or aquifers. Common neutral alteration assemblages were found in wells LHD-23 and LHD-28 include calcite, quartz, chalcedony, wairakite, albite, epidote, adularia, while actinolite and wollastonite are found only in well LHD-28. Acid alteration assemblages found in wells LHD-23 and LHD-28 included kaolinite, pyrophylite and diaspore (only found in well LHD-23).

Commonly, in subsurface conditions, the degree of alteration intensity increases with depth. The alteration intensity in the Lahendong geothermal field was variable and the degree of alteration intensity varied with depth. The alteration intensity was high in the porous and permeable rocks and low in tight formations. The alteration intensity is especially high in tuff, tuff breccias and breccias, but lower in the compact basaltic andesite lavas in wells LHD-23 and LHD-28.

5.1.1 Distribution of hydrothermal alteration minerals

Hydrothermal alteration depicts the effect of the geothermal fluid on the rocks it flows through. The hydrothermal minerals form as precipitates from the geothermal fluid or as an alteration of the rock. Two types of hydrothermal alteration assemblages were found in the both wells LHD-23 and LHD-28. The dominant one is neutral alteration assemblage and the second one is acid alteration assemblage. The distribution of hydrothermal minerals in wells LHD-23 and LHD-28 is shown in a later section in Figures 54 to Figure 57 and described further below.

Neutral alteration assemblage

Calcite is one of the common alteration minerals in geothermal systems. In wells LHD-23 and LHD-28 it starts to form at the top of the geothermal system and becomes very common in the chlorite zone, but appears to decrease and disappear at about 1600 m depth in well LHD-23 and at about 1450 m in well LHD-28. Calcite is found as direct deposition and also as replacing glass, plagioclase and pyroxene. The abundance of calcite may relate to some extent to the lithology as it seems to be in general more abundant in tuffaceous rocks. In Iceland, calcite disappearance is sometimes associated with temperatures surpassing about 290°C. Calcite is considered to be more common at the outer perimeter of geothermal systems in the Philippines (Reyes, 1990) and the same may apply to the Icelandic geothermal systems.

Pyrite is a common mineral and is found at almost all depths of the wells (Figure 29). Pyrite mostly forms in the vein and vesicle fillings associated with quartz, calcite, chlorite and epidote. Pyrite is also commonly disseminated in the matrix of tuffs and embedded in the groundmass of rhyolitic lava. Studies from Mahanagdong, Mt. Apo and Pinatubo in the Philippines show that pyrite often exists as vein fillings in acid wells but seldom in neutral wells. Chalcopyrite veins in drill cuttings can be used to predict acidic fluid discharge of the wells (Dulce et al., 1995). In LHD-23 and LHD-28, pyrite is the most common mineral found in the wells from the surface to the bottom part as shown in probe analysis (see Section 5.3).

FIGURE 29: Pyrite associated with epidote and quartz at a depth of 1560 m, well LHD-23

FIGURE 30: Quartz crystal forms at 582 m depth in well LHD-28

Quartz is colourless to white coloured, hexagonal shaped and commonly found as subhedral to euhedral crystals (Figure 30). Under thin section, quartz commonly shows a mosaic texture. Quartz mostly forms in open spaces and as a vein filling minerals, and commonly also forms as a replacement of plagioclase phenocrysts. A common prismatic of euhedral quartz is found in the veins and vesicles. In both wells, quartz occurs from the shallow depth to the bottom of the wells. Below 1300 m and

1400 in wells LHD-23 and 28, respectively, quartz is commonly formed in the secondary porosity associated with epidote, chlorite and sulphides. Fluids are apparently saturated with respect to quartz and/or anhydrite at temperature ≥180°C (Reyes, 2000).

Sphene/Titanite: This mineral is recognized as a white coloured mineral usually found as a replacement of opaque minerals. From thin section sphene is identified by very high relief brownish to dark brown colour and shows dusty-cloudy discoloration that formed by altering opaque minerals. The mineral is formed sporadically below 425 m and 233 m in well LHD-23 and 28, respectively. The mineral formed in the wide range of temperature but seems to start altering the opaques near to 200°C (Franzson, pers. comm.). In the Philippine geothermal systems, the occurrence of sphene may indicate weak permeability and porosity (Reyes, 2000).

Chalcedony is characterized by a colourless-light blue colour under binocular microscope. Under thin section petrography, the mineral is seen as a light white colour thin layered lining in vesicles and is often replaced by quartz. In well LHD-28 in the vesicular texture of the andesite rock, vesicles are commonly filled by chalcedony and chlorite. Chalcedony is found intermittently at depths below 863 m and 363 m in wells LHD-23 and LHD-28, respectively. Chalcedony starts to forms at temperatures above 120°C (Kristmannsdóttir, 1979)**.**

Anhydrite was mostly analyzed petrographically and more rarely by binocular microscope (Figures 31 and 32). It is a colourless, commonly blocky crystal and tabular and has usually high birefringence. The occurrence of anhydrite is found below 750 m depth in well LHD-23 and below 400 m in LHD-28. It is mostly found replacing feldspar in wells LHD-23 and LHD28, but is also commonly found as direct precipitation into veins and vesicles. Anhydrite is found as an alteration in both neutral and acid geothermal systems, as widely evidenced in the Philippines geothermal systems (Reyes, 1990; Reyes, 2000). The minimum temperature of formation is about 200°C in neutral systems but about 185°C in acid alteration.

FIGURE 31: Ortorhombic anhydrite crystal at a depth of 1496 m well LHD-23

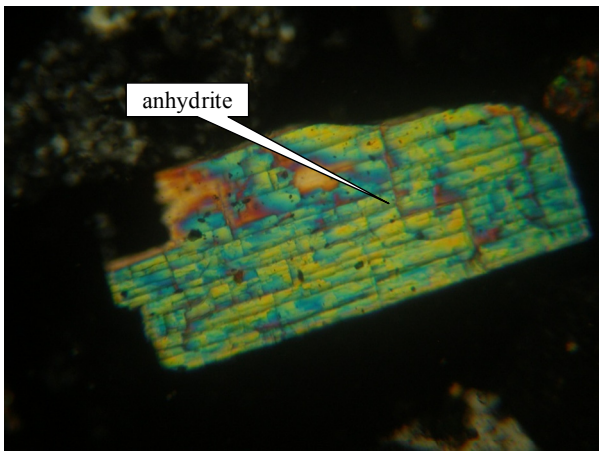

FIGURE 32: Crystal anhydrite at a depth of 1884 m well LHD-28

Wairakite is characterized by a colourless to low grey colour and has an isometric crystal structure (Figures 33 and 34). Under petrographic thin section, wairakite shows low birefringence and two sets of twin lamella. Wairakite commonly replaces primary plagioclase phenocryst and forms in the veins and vesicles. The mineral is found in the tuff, breccias and basaltic andesitic rock. In well LHD-23, wairakite occurs rarely and intermittently below 824 m depth, whereas in well LHD-28 it forms earlier and more commonly at depths below 603 m. Wairakite forms at 200-300°C (Saemundsson and Gunnlaugsson, 2002) or above 230°C where wairakite associates with epidote (Steiner, 1977; Reyes, 2000) or at temperatures >240 up to 300°C (Henley and Ellis, 1983). The precipitation of wairakite over epidote is favoured by cooling or decreasing pH (Browne and Ellis, 1970). In the Wairakei geothermal area, wairakite commonly replaces primary Na-Ca plagioclase phenocryst and locally replaces pumice fragments and lapilli, lines or fills rock pores, vugs, veinlets and fractures associated with quartz and rarely with calcite (Steiner, 1977).

FIGURE 33: Cubic colourless crystal of wairakite formed in the vesicles at 674 m depth in well LHD-28

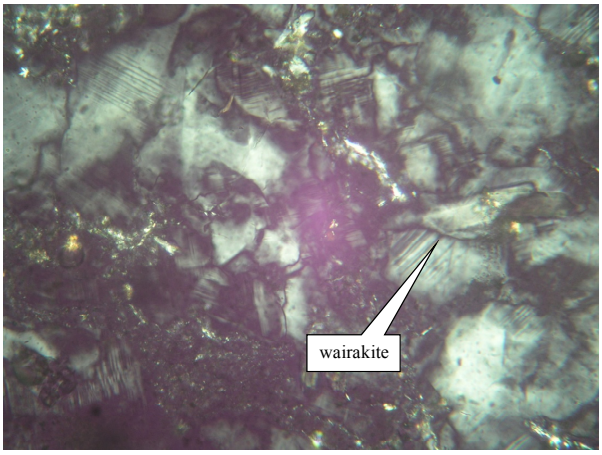

FIGURE 34: Cross polarized petrographic photo showing the cross hatched twinning in Wairakite in a vesicle at a depth of 632 m in well LHD-28

Epidote is recognized by its yellow-green to green colour in rock, as euhedral to subhedral prismatic crystals and radiating needle-liked crystals (Figures 35 and 36). Under thin section the mineral shows green pleochroism and high birefringence. Epidote forms as fracture filling, veins or vesicles and replaces feldspar and pyroxene. Commonly epidote is associated with others minerals such as quartz, anhydrite, chlorite, pyrite, and calcite. In both wells, epidote occurs intermittently to commonly as seen in Figures 54 to 57. Anhedral epidote appears at depth 953 m and becomes common subhedral to euhedral at below 1232 m depth in well LHD-23. In well LHD-28, anhedral epidote starts to appear at 588 m and becomes abundant as euhedral crystals below 732 m depth. In the deeper part, especially below 1313 m in well LHD-23, epidote forms in the vesicles and secondary porosity is caused by feldspar phenocryst dissolution. Epidote starts to form at temperatures above 250°C (Browne, 1984; Henley and Ellis, 1983) and above 240°C in Iceland geothermal system (Franzson, 1998).

FIGURE 35: The formation of epidote, filling in the secondary porosity, associated with quartz and chlorite at 1532 m depth in well LHD-23

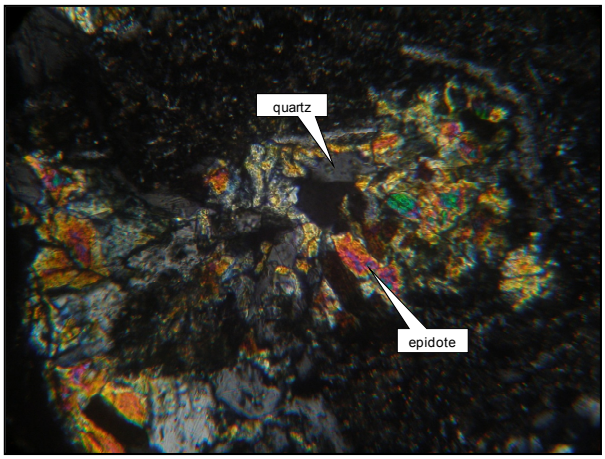

FIGURE 36: Cross polarized of epidote and quartz replacing plagioclase at a depth of 963 m in well LHD-28

Albite was mostly analysed in the petrographic microscope and was found as the replacement of primary andesine groundmass and phenocrysts but may also be found as direct precipitation from the geothermal fluid. Albite is related to temperature as shown in the figures, it is first seen at similar or slightly deeper than epidote, and may indicate permeability (Browne, 1984). Albite is less abundant in the low permeability andesite lavas than breccias and tuffs. The upper boundary of albite is at 834 m in LHD-28 but is considerably deeper in LHD-23 at a depth of 1157 m.

Wollastonite is white and fibrous shaped under binocular microscope (Figures 37 and 38). Under thin section, the mineral wollastonite is colourless, has a hairy-fibrous structure, and is found associated with epidote. Wollastonite is recognized by binocular and petrographic microscope in well LHD-28 at depths below 1533 m. The paragenesis sequence of the minerals in the vesicles shows that wollastonite precipitates before epidote. Wollastonite has a minimum formation temperature of about 270°C.

FIGURE 37: Wollastonite and epidote crystal forms as vein fillings at 1536 m depth, well LHD-28

FIGURE 38: White colour of fibrous crystal of wollastonite formed at depth 1557 m in well LHD-28

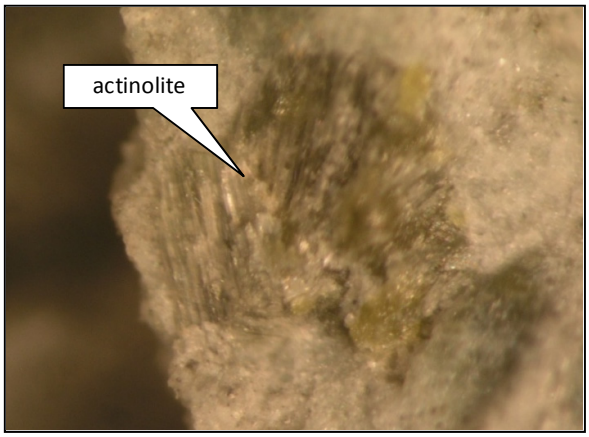

FIGURE 39: Acicular crystal of actinolite replacing pyroxene at depth 1536 m, well LHD-28

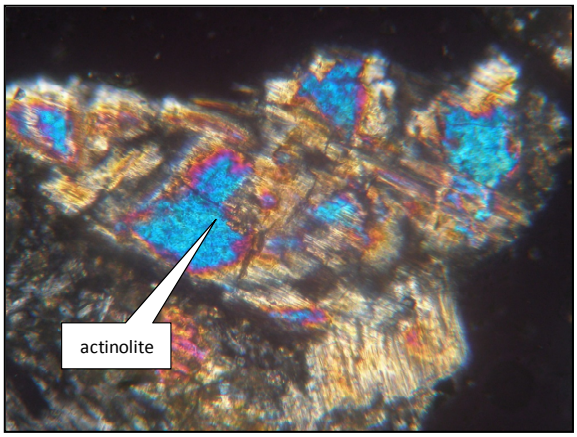

FIGURE 40: Cross pollarized actinolite replaces pyroxene at depth 1542 m, well LHD-28

Actinolite: The mineral actinolite is pale green, has moderate pleochroism, a fibrous-acicular crystal shape and has high birefringence (Figures 39 and 40). In the wells, actinolite was found under binocular and petrographic microscope. Actinolite was rare below 1533 m under petrographic thin section in well LHD-28. Under binocular microscope, actinolite was recognized intermittently from 1536 to 1734 m in well LHD-28. Actinolite was found as veins and vesicle filling and as a replacement of primary minerals of pyroxene. Actinolite starts to form at a temperature of about 280 to 350°C (Reyes, 2000) or remains stable at temperatures of about 300°C or more (Henley and Ellis, 1983).

Adularia is recognized by diamond shaped crystals. In wells LHD-23 and LHD-28, the mineral was difficult to recognize under binocular microscope and was only found during petrographic investigation. The mineral was observed under thin section at a depth below 1732 in well LHD-28. This mineral forms commonly as a replacement of feldspar and precipitates in the veins. In well LHD-28, adularia usually associated with quartz and epidote at depths near the aquifer, identified by the appearance of circulation losses. Adularia is one of the minerals that indicate permeability (Reyes, 2000).

Smectite is found in the upper part of the well from the surface down to 347 m and 385 m in wells LHD-23 and LHD-28, respectively. Smectite is also found in the unit of slightly altered rock of basaltic andesite at depths between 423 m to 602 m in well LHD-23 and 459 m to 555 m in well LHD-28. The mineral is found in the tuff, breccias and andesite to basaltic andesite porphyritic at slight to highly altered intensity. Smectite commonly replaces glass, feldspar and pyroxene phenocryst. Based on XRD analysis, in both wells, smectite has peaks at around 12 to 15 Å for untreated, 12 to 15 Å for glycolated and 9 to 10 Å for heated conditions (Figure 41). Smectite is stable at temperature below 140°C (Browne, 1984) or at temperatures below 200°C (Kristmanndóttir, 1979).

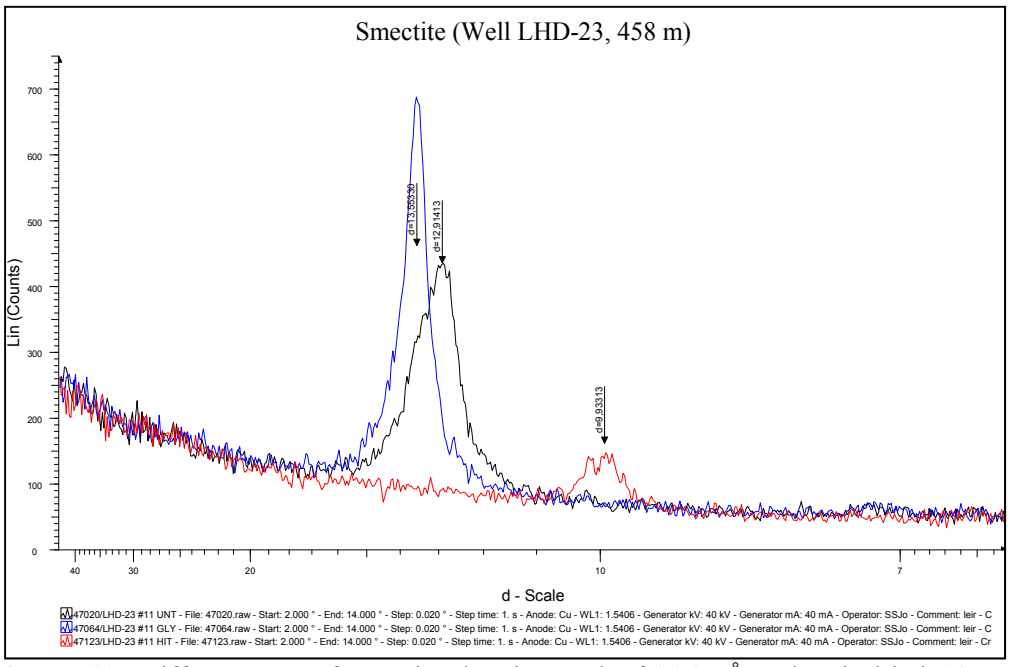

FIGURE 41: Diffractogram of smectite showing peak of 12.91 Å under air dried, 13.55 Å under glycolated and 9.93 Å under heated conditions in well LHD-23 at a depth of 458 m

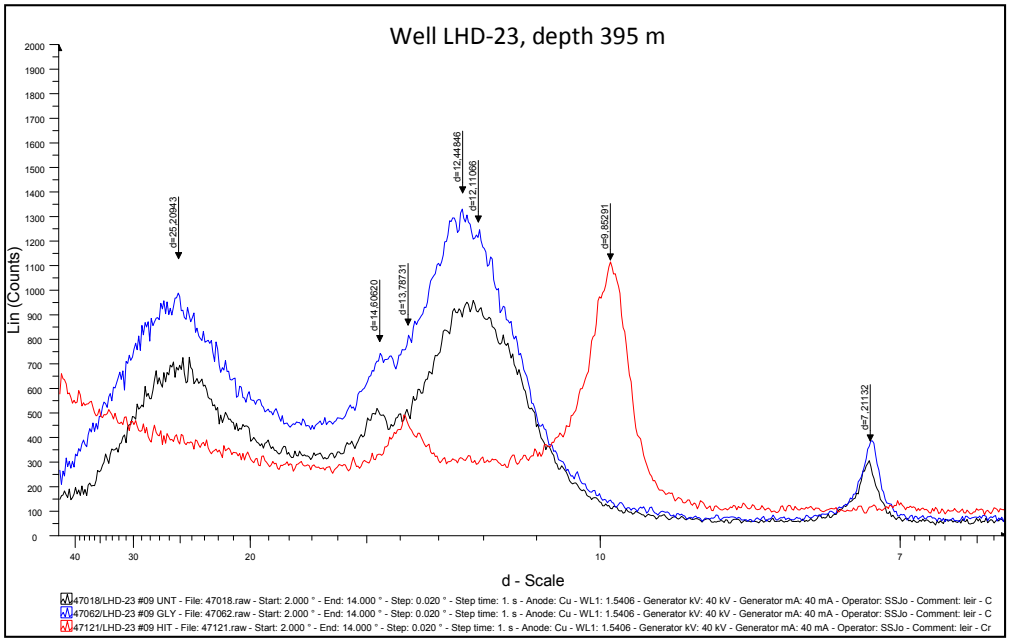

FIGURE 42: A mixture of smectite and MLC in well LHD-23 at depth 395 m, shows a significant portion of clay that swells and collapses to 9.85 Å, representing the smectite. Remaining part is related to MLC as a peak at 7.21 Å and some layer is visible at 25.21 Å

Smectite is also found as a mixture of smectite and mixed layer clay (MLC). In well LHD-23 at depths of about 395 (Figure 42), 419, 824 and 1316 m, smectite shows peaks of 25,21 to 25,75 Å,

whereas, in well LHD-28, the typical peak of this kind of mineral is not present. This mixture of peaks point to the occurrence of mixed layer clay in the drilled hole at Mahio, in the Philippines geothermal system and implies disequilibrium condition (Reyes, 1979).

Chlorite forms in various colours from green to bluish green. In thin section, chlorite shows light to dark green colours, low birefringence with light to medium grey colours and shows a fibrous type or radial shape. This mineral was identified under XRD-analysis by peaks at about 14 Å without change during air dried, glycolated and heated conditions, and some chlorite has peak 7 Å for untreated, glycolated conditions and then commonly collapsed after heating to 550°C. In well LHD-23 and LHD-28 chlorite commonly formed as replacement mineral of pyroxene and plagioclase and precipitated in veins and vesicles. Common chlorite depositing in vein and vesicles is associated with chalcedony, quartz, epidote, illite and pyrite. In the porphyritic vesicular texture of andesite, chlorite commonly precipitates in the vesicles associated with chalcedony as a common part of the paragenesis sequence of chalcedony>chlorite in the early stage. This typical chlorite was commonly found especially at depths from 732 m to 1173 m in well LHD-28. Chlorite generally indicates temperatures exceeding 230°C (Kristmannsdóttir, 1979).

Illite is mostly white to light green in colour, replaces feldspar and precipitates also in veins and vesicles (Figures 43 and 44). Under petrographic microscope, illite is fine to coarse grained clay, colourless in plane polarized light, and is seen as matted flakes or fibrous aggregates, it has variable refractive indices and birefringence. Illite is commonly found in tuff and breccias but less in andesite to basaltic andesite lavas. In porphyritic lava, illite is commonly found replacing feldspar and pyroxene phenocrysts and microporphyritic groundmass of the rock. Illite starts to form at 425 m and 533 m in wells LHD-23 and LHD-28, respectively. Illite forms from Ca-smectite due to increasing temperature (Steiner, 1977). Under XRD analysis, illite shows no change of peak at about 10 Å during air dried, glycolated and heated conditions. XRD analyses show that illite starts to form at depth 668 m and 414 m in wells LHD-23 and LHD-28, respectively. Illite is stable at temperatures above 220°C (Browne, 1984).

FIGURE 43: Illite associated with chlorite as replacement mineral of plagioclase at a depth of 1460 well LHD-23

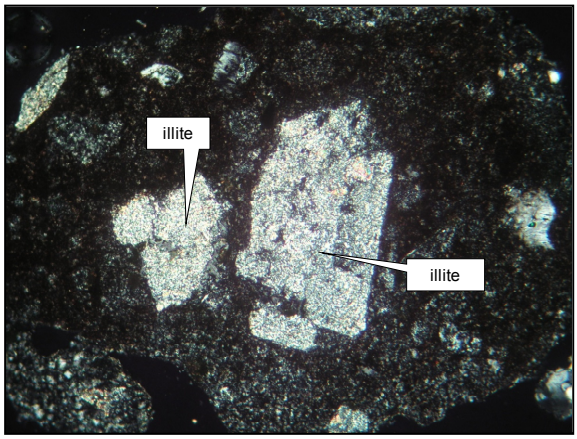

FIGURE 44: XPL aggressive illite replacing phenocryst of plagioclase and pyroxene at a depth of 1220 well LHD-23

Acid alteration assemblage

Kaolinite is white in colour and commonly found in the altered rock of tuff to tuff breccias. Kaolinite was found in the narrow depth interval of 323 m to 347 m with peaks of 7.17 to 7.19 Å in well LHD-23 and below 249 m in well LHD-28, respectively. Kaolinite is commonly found associated with smectite and quartz. Kaolinite is found only in the shallow levels of both wells. Kaolinite is common as supergene minerals in New Zealand and Philippines geothermal systems. Supergene kaolinite is normally found replacing plagioclase phenocrysts and has a peak of about 7.19 Å (Steiner, 1977). Kaolinite occurs at temperatures below 120°C (Browne, 1984), common associated with Mg-Fe chlorite (Reyes, 1979). At deeper levels in Mahio wells, Philippines, kaolinite is commonly found associated with anhydrite, quartz, pyrophyllite and diaspore (Reyes, 1979).

Sulphur is yellow to pale yellow. Sulphur is recognized under binocular microscope and XRD analysis (Figures 45 and 46). Under binocular microscope, sulphur was identified by the appearance of the yellow colour after the samples were put under humid conditions. Sulphur is commonly associated with the formation of gypsum. In well LHD-23 sulphur was found intermittently at depths below 320-365 m, 752-830 m, 1022-1049 m, and intermittently below 1346-1571 m. In well LHD-28, sulphur was found at depth 1512-1608 m and intermittently below 1692 m. Two samples with a trace of of sulphur were found at depth 1430 and 1436 m under XRD analysis. Sulphur is commonly found as an acid alteration mineral in Philippines geothermal systems and is associated with alunite and pyrite or marcasite as virulent acid alteration. Sulphur forms at temperatures from 50 ^{o}C to about 280°C (Reyes, 2000).

FIGURE 45: Crystal sulphur forms at a depth of 788 m well LHD-23

FIGURE 46: Gypsum and may be yellow sulphur form at 1430 m depth, well LHD-23

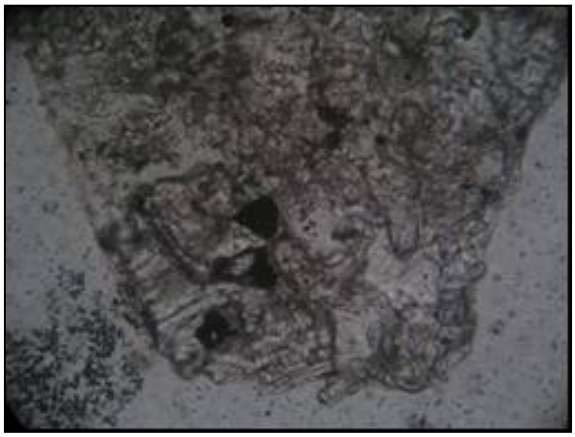

FIGURE 47: Plain polarized thin section showing diaspore at depth about 1562 m, in well LHD-23

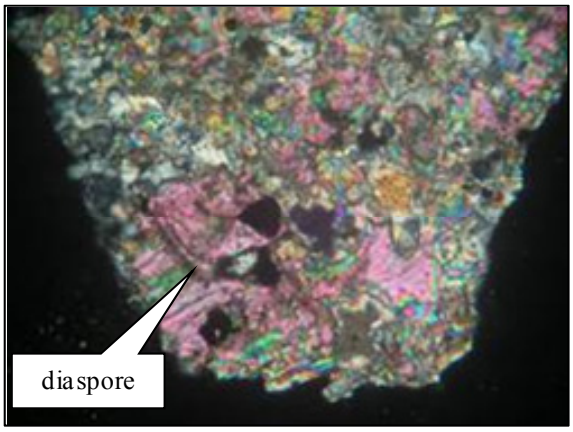

FIGURE 48: Cross polarized thin section showing diaspore at depth about 1562 m, in well LHD-23

Diaspore is colourless, has a high refractive index and is pleochroic. Diaspore is identified in one depth from XRD analysis at 1490 m depth and thin section at depth of 1562 m in well LHD-23 (Figures 47 and 48). Diaspore is found as acid alteration in Philippines geothermal systems and starts to form at temperatures ranging above 120°C to 320°C (Reyes, 2000).

Pyrophyllite is only identified under XRD analysis. The pyrophyllite mineral was found at depth of 1559 m in well LHD-23 with peak of 9.33 Å (Figure 49) and in well LHD-28 is found at depths of 1587 m with peaks of 9.35 Å. The peak of pyrophyllite under XRD analysis did not change during air dried glycolated and untreated conditions. Pyrophyllite forms at temperatures above 250°C as a replacement mineral of dickite (Browne, 1984). These peaks did not change upon glycolation and heating. Pyrophyllite results from the reaction of low pH fluids with rocks and may represent earlier

alteration (high sulphidation or surficial acid) of leach zones above boiling geothermal systems (Thompson and Thompson, 1996).

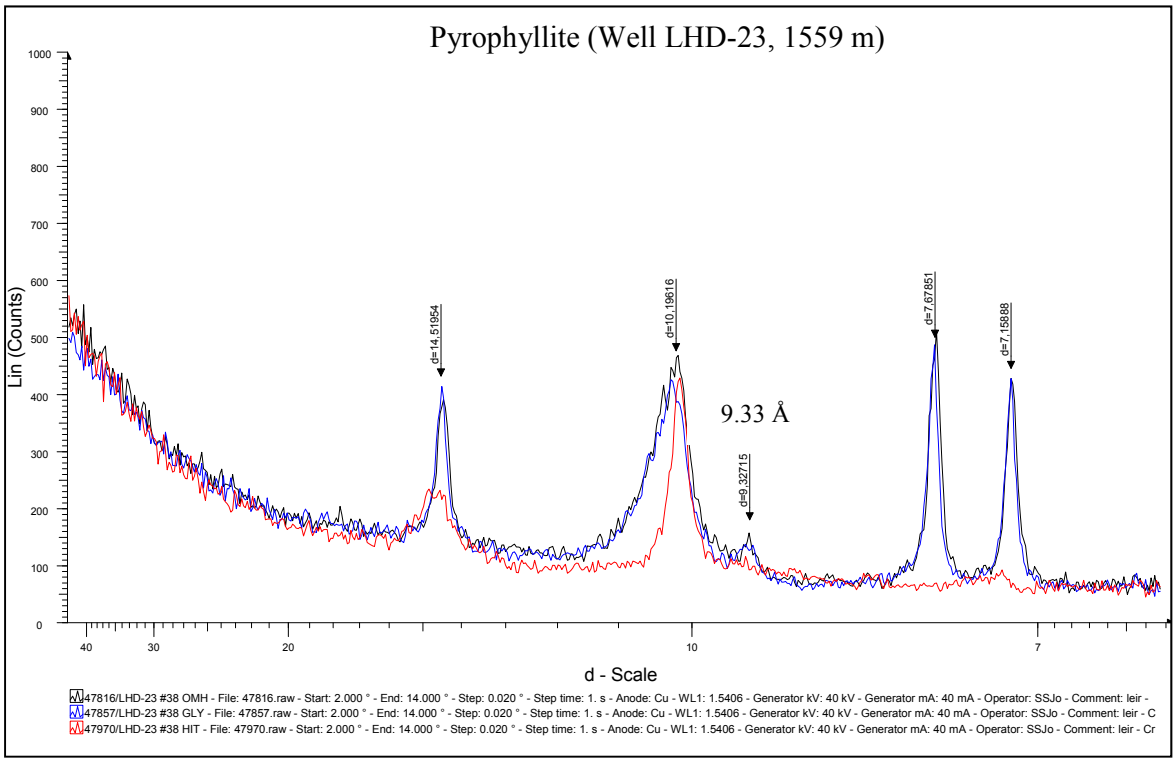

FIGURE 49: XRD analysis of pyrophyllite showing peaks at 9.33 Å for all runs

Gypsum was recognized under XRD analysis and has a distinct peak of about 7.7 Å (Figure 50). In well LHD-23, gypsum was found intermittently below 668 m (Figures 48, 51 and 52). In well LHD-28, gypsum was found intermittently below 414 m. Gypsum may form as a secondary mineral and

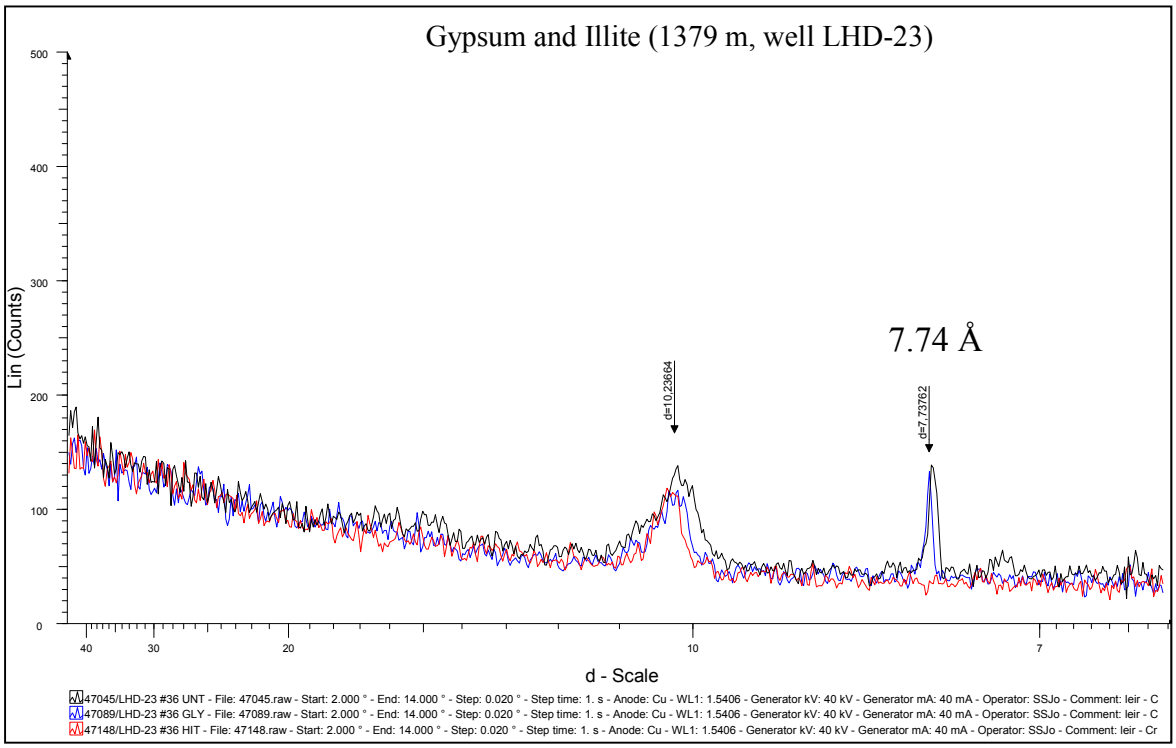

FIGURE 50: Gypsum has a peak of 7.74 Å in untreated, glycolated and collapsed after heating at depth of 1379 m in well LHD-23

may also form by precipitating in the cuttings if the cutting is placed in humid conditions. Crystal gypsum was analysed at depth 1022 and 1430 m as precipitation on the surface of the rock (Figure 53). In Philippines geothermal systems, gypsum commonly occurs in veins associated with quartz and is also found as patches in the rock matrix. It is commonly found where intense silicification is observed (Reyes, 1979).

FIGURE 51: Gypsum forms in the surface of the rock at 1028 m depth in well LHD-23

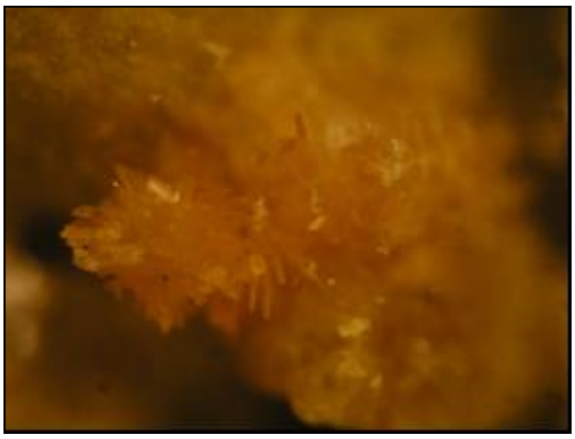

FIGURE 52: Yellow crystal of Gypsum forms in the surface of the rock at 1028 m depth in well LHD-23

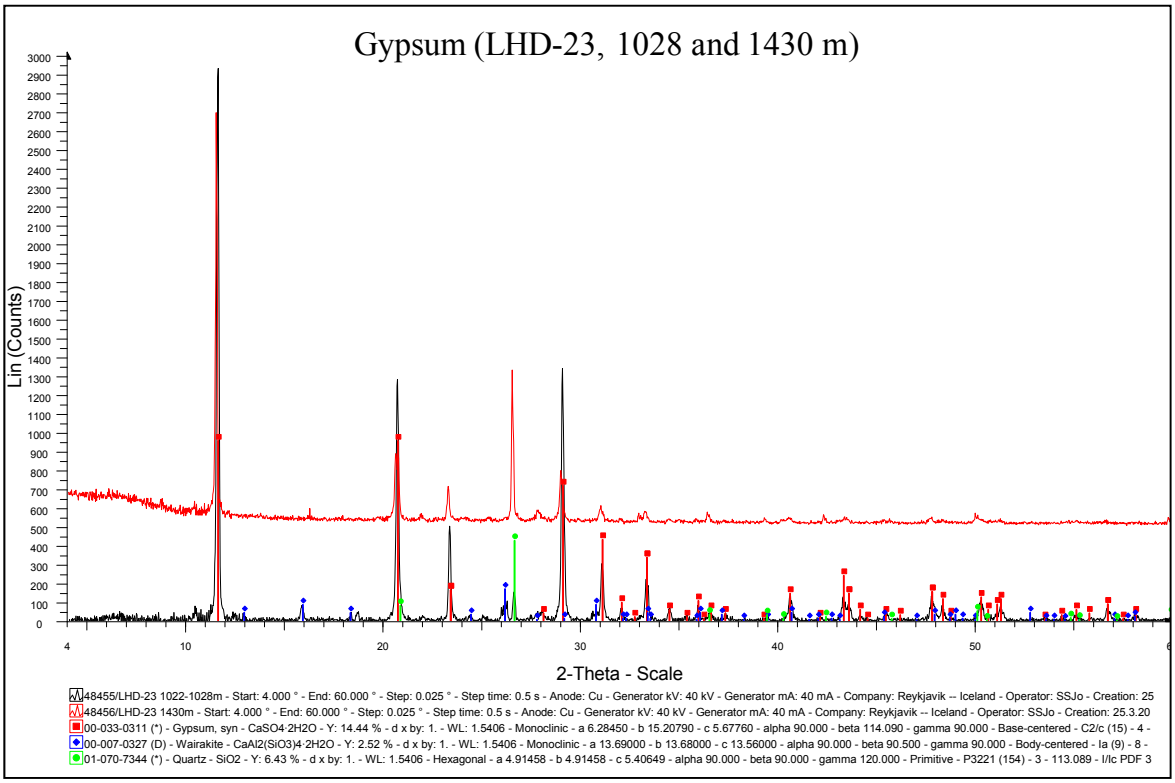

FIGURE 53: XRD analysis of gypsum at 1028 m and 1430 m depth in well LHD-23

5.1.2 Alteration of primary minerals

The stratification in Lahendong is largely built up of volcanic rocks ranging from basaltic- andesites to andesites, dacites and rhyolitic compositions, and range from tuffaceous to holocrystalline rocks as discussed in detail in Section 4.2. The main constituents of these rocks are glass, plagioclase, quartz, pyroxene, opaques and amphibole in variable proportions and compositions. The extent of the alteration of these depends on their resistance, temperature, and the accessibility of the geothermal

fluids (permeability). The intensity of the alteration of the rock was visually assessed during the cutting analysis and shown in Figures 54 to 57.

Hydrothermal minerals in Lahendong occur as replacements of primary minerals, replacement and deposition in vein and cavities. The replacement hydrothermal minerals record the interactions between the wall rocks and the hydrothermal fluids, while space-filled minerals reflect the processes that affected the circulating fluid. Other factors which can affect the formation of hydrothermal

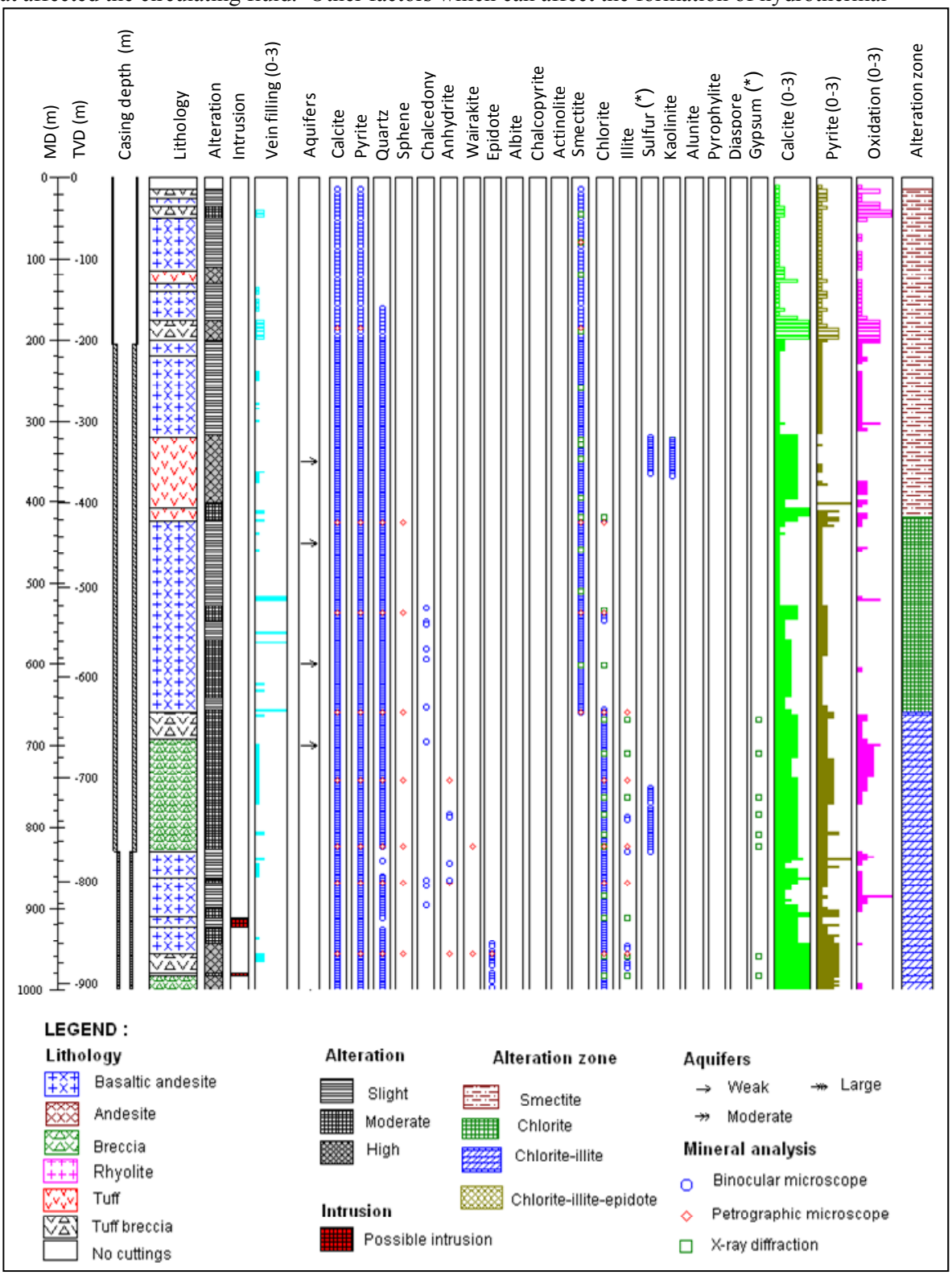

FIGURE 54: Lithology, distribution of hydrothermal alteration minerals and zonation in well LHD-23 at depth 0 to 1000 m; (*) = probably appears after sampling

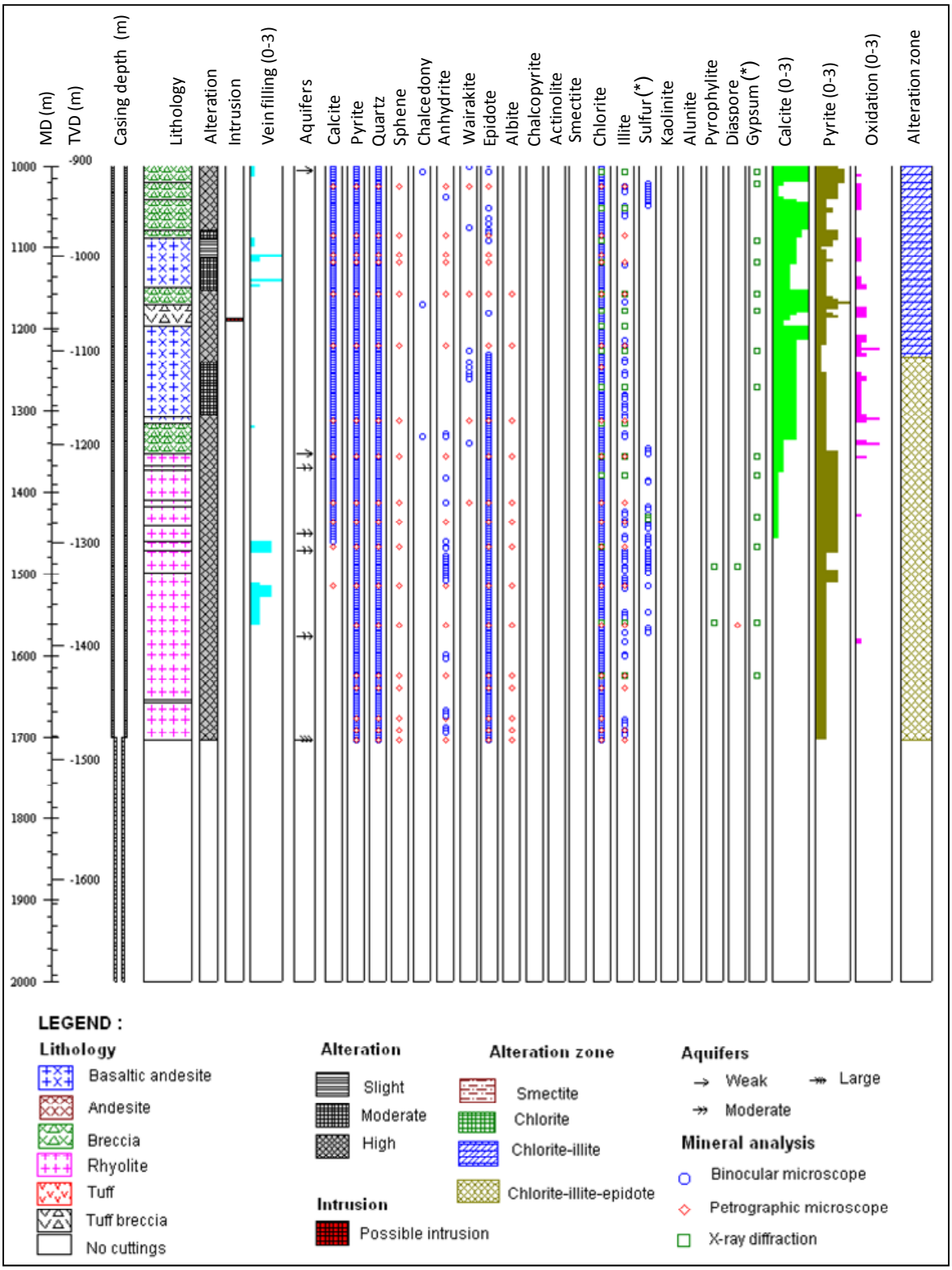

FIGURE 55: Lithology, distribution of hydrothermal alteration minerals and zonation in well LHD-23 at depth 1000 to 2000 m; (*) = probably appears after sampling

minerals are temperature, pressure, parent rock type, reservoir permeability, fluid composition and duration of activity (Browne, 1978).

The subsurface lithology of the Lahendong geothermal field is dominated by andesitic rocks except in the Tondano Unit which is mostly comprised of rhyolitic type rocks (Utami et al., 2005). The alteration minerals at shallow depth are dominated by calcite, quartz, hematite and iron oxide. Anhydrite is formed by the partial replacement of plagioclase and pyroxene. Clay minerals commonly

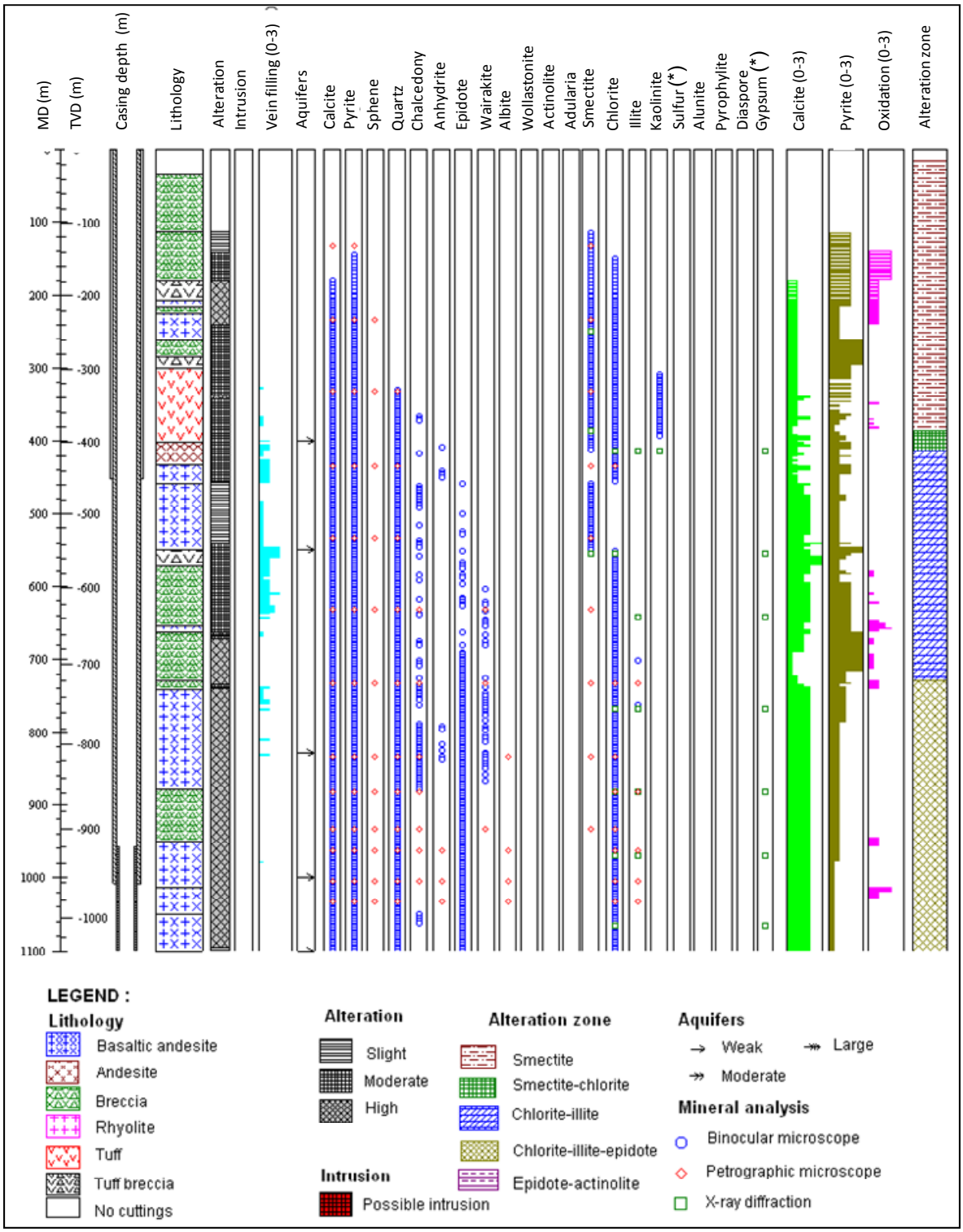

FIGURE 56: Lithology, distribution of hydrothermal alteration minerals and zonation in well LHD-28 at depth of 0 to 1100 m; (*) = probably appears after sampling

found are smectite and interlayered smectite-chlorite at shallow levels. Chlorite is relatively more commonly found than illite (Utami et al., 2005).

The primary minerals of andesitic type are predominantly plagioclase, pyroxene and opaque minerals and minor amphibole. The main phenocrysts are dominantly plagioclase with less pyroxene. Amphibole phenocrysts are rarer and are usually more pleochroic varieties than actinolite which that may be associated with hydrothermal alteration. The plagioclase and pyroxene are found as main groundmass constituents. Glass is found in the pyroclastic tuff and is mostly altered to smectite and

chlorite clay and the more acidic tuffs also to quartz and feldspar. The replacement of the primary constituents is summarized in Table 6 and in the text below.

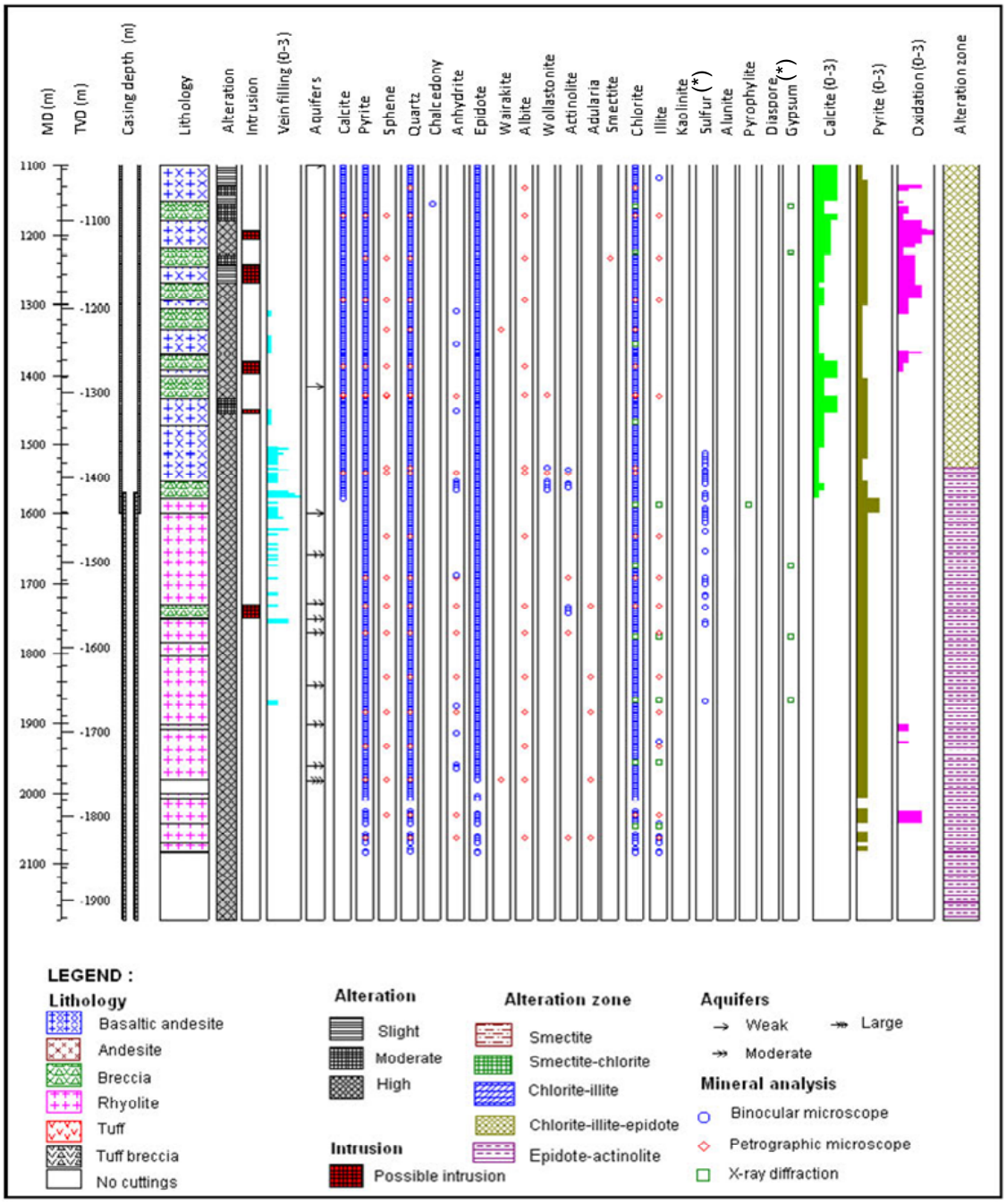

FIGURE 57: Lithology, distribution of hydrothermal alteration minerals and zonation in well LHD-28 at depth 1100 to 2181 m; (*) = probably appears after sampling

TABLE 6: Primary rock constituents and their alteration products as found in well LHD-23 and LHD- 28

Glass	Smectite, chlorite, illite, quartz, calcite
Plagioclase	Quartz, calcite, smectite, chlorite, illite, anhydrite, epidote, wairakite, adularia
Pyroxene	Quartz, calcite, chlorite, smectite, epidote, illite
Opaques	Sphene (titanite)

Glass is the most sensitive to alteration. Glass is commonly altered to clay. It alters to smectite at lower temperatures and chlorite at higher temperatures. It also recrystallizes to quartz, especially the more acidic varieties. The glass starts to alter to smectite at below about 80 m and 133 m depths in wells LHD-23 and 28 respectively, and then to chlorite at below about 395 m and 414 m in wells LHD-23 and 28, respectively, and to illite at depths of 743 m and 632 m in wells LHD-23 and LHD-28, respectively.

Plagioclase is very common as phenocryst and groundmass in the rocks. All the rhyolitic-andesitic rocks are sparsely to densely plagioclase porphyritic. Plagioclase is altered to variable secondary minerals such as quartz, calcite, smectite, chlorite, illite, anhydrite, epidote and wairakite (Figures 58-61). The first indication of plagioclase being altered to calcite and smectite is found at depths of 185 m and 133 m in wells LHD-23 and LHD-28, respectively. Chlorite alteration starts below 425 m and 434 in wells LHD-23 and LHD-28, respectively. Illite alteration started at 425 m and 533 m depths in well LHD-23 and LHD-28 respectively. The replacement of plagioclase by wairakite started at depth 1025 m and 732 in wells LHD-23 and LHD-28, respectively, and replacement to epidote is first noted below 1085 m and 732 m depth in well LHD-23 and 28, respectively. Plagioclase replaced to adularia starting at 2084 m depth in well LHD-28. An interesting dissolution of feldspar phenocryst became noteable below 1355 m depth in well LHD-23 all the way to the zone of total circulation loss at 1703 m depth.

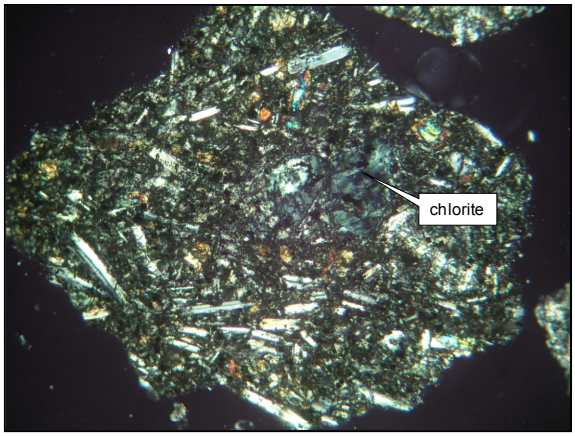

FIGURE 58: Chlorite alteration of pyroxene phenocryst in andesite at 1436 m depth in LHD-23

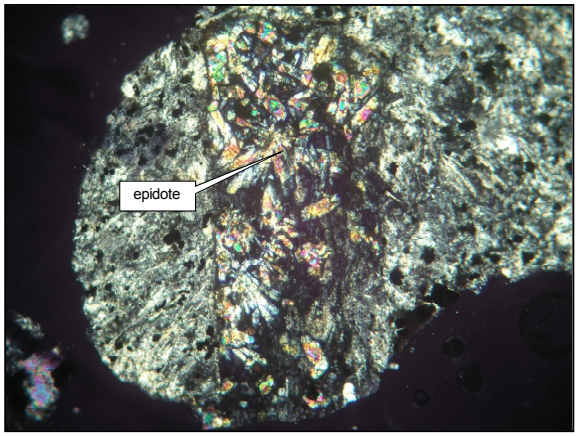

FIGURE 59: Plagioclase replaced by epidote at 1436 m depth in well LHD-23

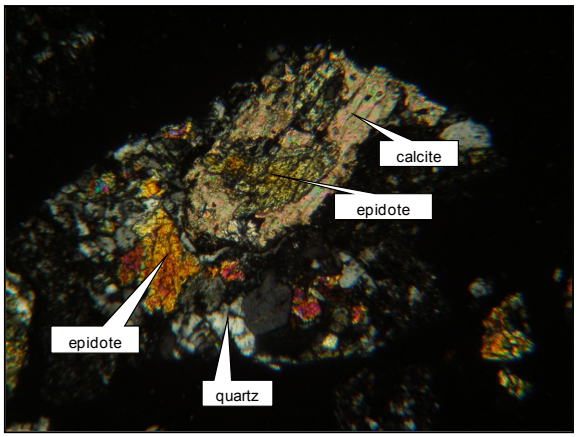

FIGURE 60: Calcite and epidote alteration of plagioclase phenocryst at 963 m depth in well LHD-28

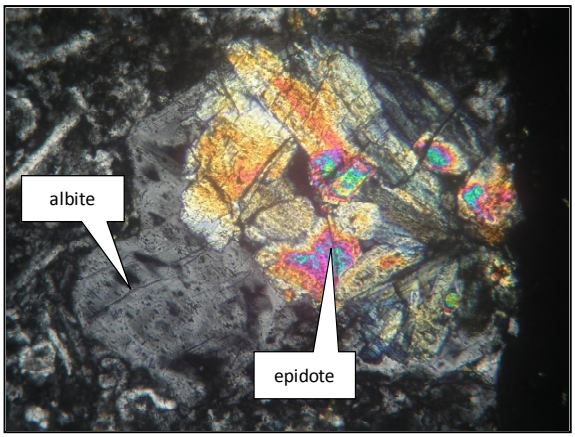

FIGURE 61: Epidote and albite replace plagioclase phenocryst at 1632 m depth in well LHD-28

Pyroxene is the second most abundant primary mineral in the porphyritic andesite - basaltic andesite rock. Pyroxene both appears as phenocryst and in groundmass. This mineral starts to alter to smectite and calcite at 185 m and 233 m depths in wells LHD-23 and 28, respectively. Pyroxene is dominantly

altered to chlorite below 425 m and 434 m depth in wells LHD-23 and 28, respectively, but less commonly to quartz, epidote and illite.

The abundance of opaque minerals is quite variable being most common in basaltic andesites but least in the rhyolitic units. The opaques are predominantly altered to sphene (titanite). Secondary opaque minerals may also be found near intrusive margins such as at depth interval 1194 to 1206 m in well LHD-28.

5.1.3 Sequence of mineral deposition

Most hydrothermal minerals found in geothermal fields can deposit directly from solution into void spaces such as joints, faults, hydraulic fractures, unconformities, veins, vugs, and pores (Browne, 1984). Studies have shown that these minerals often form time related sequences and thus depict changes that have taken place in the geothermal systems (e.g. Franzson, 2000; Franzson et al., 2002). Utami et al. (2005) studied mineral sequences in core samples from Lahendong wells LHD-1, LHD-3, LHD-4, LHD-5, LHD-6, LHD-7, LHD-10, and LHD-13. She reported 5 stages of mineral deposition in the wells studied. Chlorite forms in the first stage, followed by calcite which forms in stage-2. Quartz and calcite precipitate in stage-3. Stages-4 and 5 are more complex probably due to the more complex fluid flow patterns. Epidote, albite, wairakite and prehnite form in stage-4 at temperatures about 200-300°C and indicate near neutral pH. Stage-5 contains commonly minerals such as of hematite, calcite or quartz probably representative of the present condition in the geothermal system.

The mineral sequences deposited from the geothermal system into vesicles and veins were studied petrographically in cutting samples from wells LHD-23 and LHD-28 and are shown in Tables 7 and 8.

TABLE 7: Mineral sequence of well LHD-23

Depth	Degree of alteration	Depositional sequence							Filling type
		Early	→					Late	
956	high			anhy	epi		wai		vein
					epi	qtz			vein
1085	moderate					qtz		anhy	vein
1157	high			anhy		qtz			vein
1220	high		cc		epi	qtz	wai		vesicle
1412	high				epi	qtz			vesicle
				anhy	epi				vein
1436	high				epi			anhy	vein
1625	high				epi	qtz			vesicle
1691	high	chl			epi				vesicle

Abbreviations: anhy = anhydrite, cc = calcite, chal = chalcedony, chl = chlorite, epi = epidote, qtz = quartz, wai = wairakite, woll = wollastonite.

In well LHD-23, the mineral paragenesis is more commonly found in veins than in vesicles. Chlorite and calcite are found in the early stages of the sequence. At later stages anhydrite precipitates in veins followed by the deposition of epidote ± quartz. Anhydrite and wairakite are formed in the last stage of the sequence. Secondary porosity, mainly seen as the dissolution of feldspar phenocrysts, is found in the deeper part of the well LHD-23. Mineral depositions in those voids are mostly epidote ± quartz. The paragenesis sequence in well LHD-28 is predominantly found in the vesicles and shows a more complex interrelationship compared to the depositional sequences in veins (Figures 62-65). Vesicle fillings are common at several locations below 700 m especially in the vesicular andesite. These vesicles are predominantly filled by thin linings of chalcedony followed by chlorite. Chlorite commonly fills the central part of vesicles, but may, in some instances be followed by deposition of quartz as was found at a depth of 882 m. A more complex paragenesis of chalcedony > chlorite±calcite > quartz is found at depth 882 m and then later epidote ± quartz may deposit at still

TABLE 8: Mineral sequence of well LHD-28

Depth (m)	Degree of alteration	Depositional sequence									Filling type
		Early	→							Late	
434	medium		cc		qtz						Vesicle
732	high	chal				wai					Vesicle
		chal	chl								Vesicle
834	high	chal	chl								Vesicle
		chal			qtz			epi			Vesicle
882	high	chal	cc+chl								Vesicle
				ill				epi+qtz			Vesicle
		chal	chl		qtz			epi			Vein
932	high				qtz			epi		cc	Vesicle
963	high	chal	chl±cc	ill							Vesicle
								epi±qtz	cc±qtz		Vesicle
			chl					anhy		cc	Vesicle
1005	high	chal	chl								Vesicle
1173	moderate	chal	cc+chl								Vein
			chl					epi+qtz			Vesicle
1293	high							epi	qtz		Vesicle
1431	high							epi	qtz		Vesicle
1533	high							epi		cc	Vesicle
							woll	epi			Vesicle
1632	high							epi	qtz		Vein
1770	high				qtz					anh	Vein
1884	high					wai		epi+qtz			Vesicle
1980	high							epi	qtz		Vein

later stage. Below 963 m, calcite and quartz are commonly found as the last minerals to deposit in the system. At a deeper level at 1533 m, wollastonite precipitates and then followed by epidote ± quartz. Wairakite deposits in the vesicles associated with quartz and sometimes also with epidote as found at depth of 1884 m.

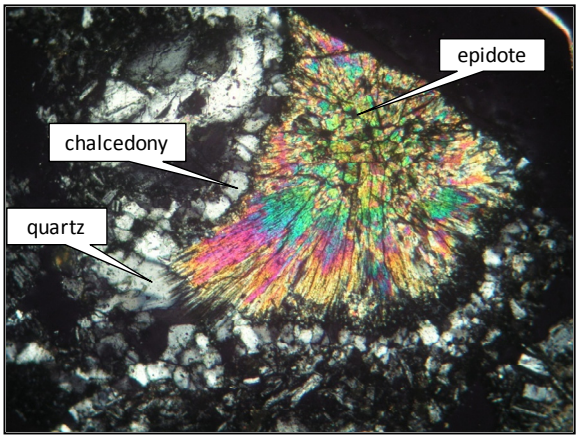

FIGURE 62: Sequence of chalcedony > quartz > epidote, well LHD-28 at 834 m depth

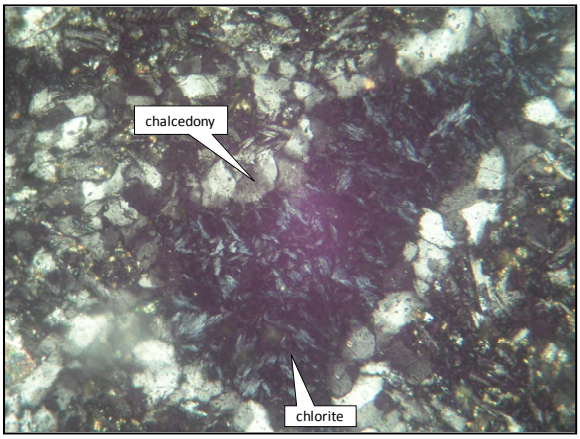

FIGURE 63: Paragenesis sequence of the chalcedony>chlorite, well LHD-28 at 834 m depth

Additional data is needed before the mineral sequence is conclusive. There is, however, a strong conformity with the sequence reported by Utami et al. (2005). It is proposed here that the search for mineral sequences should be continued in future wells to be drilled in Lahendong field.

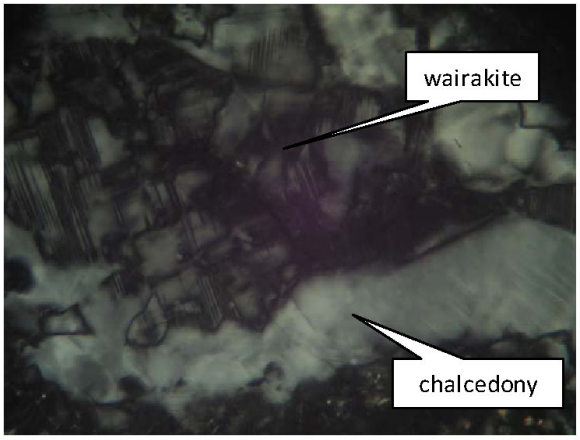

FIGURE 64: Paragenesis sequence of chalcedony > wairakite in well LHD-28 at 732 m depth

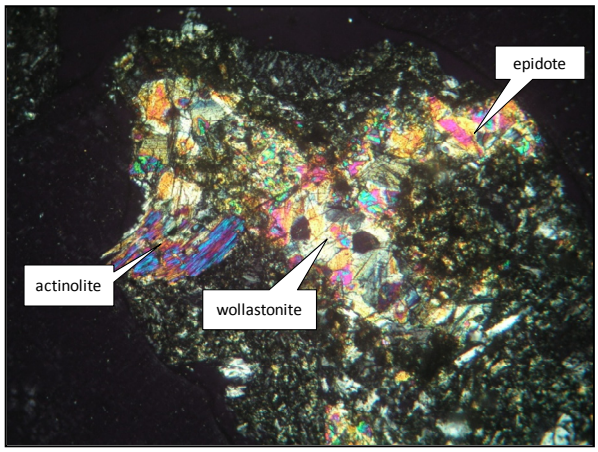

FIGURE 65: Mineral sequence of wollastonite > epidote, well LHD-28 at 1533 m depth

5.1.4 Hydrothermal alteration zonation

Clay minerals of smectite, chlorite and illite are commonly found in the Lahendong geothermal field. The identification of the different types of clays is done mostly by XRD-analysis. Two types of alteration mineral zonations were found in both wells. This zonation is based on the composition of the hydrothermal fluid. In both wells two suites of alteration mineral assemblages were found, derived from neutral pH fluids and acid fluids. These two different assemblages later were divided into several zones which are based on the combination of the clay minerals and other temperature dependent alteration minerals. These were based on the first appearance of particular minerals, such as epidote and actinolite.

Some hydrothermal alteration minerals have a specific temperature range for crystallizing so they can be used as geothermometers. Clay minerals such as smectite crystallizes below 200°C (Krismanndottir, 1977) and randomly become interlayered with chlorite at temperature between 200°C to 230°C, whereas illite has a minimum formation temperature of about >220°C (Browne, 1984). The andesitic rock type of Philippines and Indonesia, albite, quartz, chlorite, epidote, calcite ± pyrite ± adularia ± illite has typical equilibrium assemblage at 260°C (Browne, 1984) or about 220 ^{o}C to 340°C in the presence of chlorite and epidote (Reyes, 2000). In Philippine geothermal systems, the appearance of wairakite starts to forms at temperature above 230°C and at temperature above 280°C for actinolite-tremolite (Reyes, 2000). Kaolinite commonly forms in the shallow depths at temperatures <200°C (Reyes, 1990) or occur below about 120°C and for pyrophyllite which forms at temperatures above 250°C (Browne, 1984).

For the neutral pH alteration assemblages, five hydrothermal alteration zones were found in wells LHD-23 and LHD-28 in the Lahendong geothermal system: the smectite zone (< 200°C), the smectite-chlorite zone (200 - 220°C), the chlorite-illite zone (220 - 230°C), the chlorite-illite-epidote zone (>260°C) and epidote-actinolite zone (>280°C) Figure 66).

The smectite zone (< 200°C). The smectite zone occurs above 419 m in well LHD-23 and above 385 m in well LHD-28, extending to the surfaces. This zone is marked by the appearance of the smectite especially based on the XRD analysis data. The bottom boundary of this zone is marked by the first appearance of chlorite. A mixture of swelling smectite and mixed layer clay is found at a depth of 395 m in well LHD-23. Kaolinite is found in this zone identified by peaks under XRD of 7.17 to 7.19 Å. In both wells, this zone is found in the Post Tondano unit.

The smectite-chlorite zone (200 - 220°C). The zone occurs at 419 m to 668 m and 385 m to 414 m in well LHD-23 and 28, respectively. This zone is marked by the first appearance of chlorite at the upper boundary and the first appearance of illite at the lower boundary. The determination of the clay minerals is based on XRD analysis. The smectite-chlorite zone in both wells is found in a tuff layer in

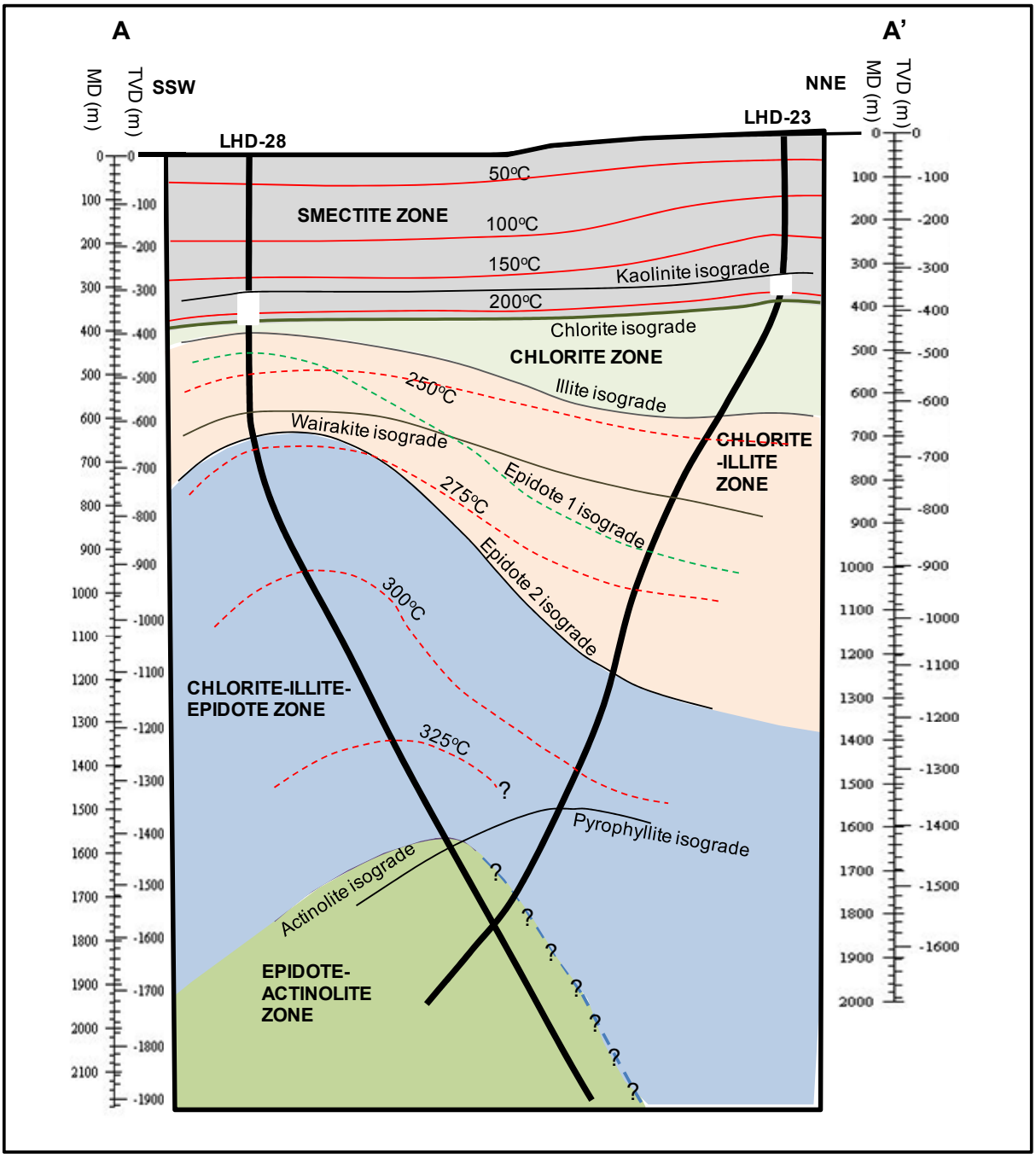

FIGURE 66: The correlation between wells LHD-23 and LHD-28 showing the neutral pH and acid assemblage alteration mineral zonation, possible formation temperature and the first appearance of alteration minerals (note:epidote 1=anhedral, found intermittently at depth, epidote 2=euhedral crystal and found commonly and continously)

the upper parts, and in basaltic andesite lava in the lower part of well LHD-23 and a tuff unit in well LHD-28. In well LHD-23, smectite-chlorite is commonly recognized in the depth range but in some locations only smectite is found such as in the denser basaltic andesite lava and only chlorite in some of the breccias layers. Other alteration minerals are found in this zone such as calcite, pyrite, quartz, sphene and chalcedony. This zone is found in the Post Tondano and Tondano units in well LHD-23 and in the Post-Tondano unit in well LHD-23.

The chlorite-illite zone (220 - 230°C). The zone appears at 668 to 1235 m and 414 to 729 m depths in well LHD-23 and LHD-28, respectively. This zone is marked by the first appearance of illite at the upper boundary and the first appearance of euhedral crystal of epidote (epidote type-2) at the bottom. In well LHD-23, the chlorite-illite zone is made of alternating units of tuff breccias, breccias and

basaltic andesite lavas. In well LHD-28 on the other hand, this unit is made of andesite, basaltic andesite, tuff breccia and breccia. In well LHD-23, this zone consists of chlorite- illite (668 to 764 m, 911 to 1052 m, 1157 to 1226 m) and chlorite (668 to 911 m, 1052 to 1157 m). In well LHD-28, this zone is made of chlorite (555 m) and chlorite-illite (642 m). It is found in the Tondano to Pre-Tondano units and Post-Tondano to Tondano units in wells LHD-23 and LHD-28, respectively. Other alteration minerals found in this zone are calcite, pyrite, sphene, quartz, chalcedony, anhydrite, epidote, wairakite, and albite.

The chlorite-illite-epidote zone (>260°C). The chlorite-illite-epidote zone appears from 1235 m to the bottom of the well and from 729 m to 1533 m depths in well LHD-23 and 28, respectively. This unit was identified by the first appearance of euhedral crystals of epidote in both wells. The bottom boundary of this zone was marked by the first appearance of actinolite in well LHD-28 and the bottom of well LHD-23 since no actinolite mineral was found in this well. This zone is located in the Pre-Tondano unit in well LHD-23 and Tondano to Pre-Tondano unit in well LHD-28. The alteration minerals that were found in this zone are calcite, pyrite, sphene, quartz, chalcedony, anhydrite, epidote, wairakite, and albite.

The epidote-actinolite zone (>280°C). This zone was only found in well LHD-28. This zone is identified by the first appearance of actinolite at a depth of 1533 m. Actinolite was recognized under binocular, thin section and XRD analysis. Actinolite is found intermittently below 1533 m depth in LHD-28. No indication of actinolite was found in well LHD-23. Actinolite was found as replacement of pyroxene phenocryst and precipitate in vesicles, associated with epidote, quartz and wollastonite. This zone is located in the sequence of basaltic andesite, breccias and rhyolitic lava. The appearance of actinolite shows a range of temperatures of 280-350°C (Reyes, 2000). This zone is sited in the Pre-Tondano unit in well LHD-28. Common alteration minerals found in this zone are calcite, pyrite, sphene, quartz, chalcedony, anhydrite, epidote, wairakite, albite, adularia, wollastonite, and actinolite. The high temperature acid alteration mineral prophyllite was found at depth 1559 m and 1587 m in wells LHD-23 and LHD-28, respectively.

In the acid alteration suite, two main zones of acid alteration assemblages were found in well LHD-23 and LHD-28. These zones were identified using the appearance of the acid alteration assemblages found in both wells. The identification of the acid alteration clay is predominantly is recognized by XRD analysis.

Two main acid alteration zonations are:

*Kaolinite zone (<120°C).*_Kaolinite zone is found at depths of 323 to 368 m and 309 to 393 m in wells LHD-23 and LHD-28, respectively. The zone is made of tuff formation, moderately to highly altered. Kaolinite is identified using XRD with peak at about 7.17 to 7.19 Å in untreated and glycolated conditions, but collapses after heating.

Pyrophyllite and illite zone (>250°C). The pyrophyllite and illite zone is marked by the appearance of pyrophyllite and illite. This may be a very narrow zone since it is only found in one location by XRD analysis. Pyrophyllite was identified using XRD and has peaks of 9.33 Å at 1559 m and 9.35 Å at 1587 m depths in wells LHD-23 and 28, respectively. The peak was stable in untreated, glycolated and heated conditions. The pyrophyllite is found associated with chlorite, illite and gypsum under XRD analysis. In well LHD-23, the zone is also associated with diaspore that was found under thin section at 1562 m depth. The zone is very limited and this is common in acid alteration zone that usually has narrow aquifer zone (Reyes, 1990).

5.2 Fluid inclusion geothermometry

Methods used to assess the formation temperature in the geothermal reservoirs include the study of temperature dependent alteration minerals, especially important as the first temperature assessment during drilling, secondly temperature logging and thirdly homogenization temperatures in fluid

inclusions. The first reflects the longterm condition in the geothermal system and the second the possible present formation temperature if done after the heating of the well. Fluid inclusions reflect the temperatures at the formation of the respective alteration mineral or later. Careful consideration must be given on the reliability of each of these logs to represent the present condition in the geothermal system. A comparison of these logs is given for wells LHD-23 and LHD-28 below in Figures 67 and 68, while Figures 69 and 70 show the measured temperature and pressure, hydrothermal alteration and fluid inclusion T_h of the wells LHD-23 and LHD-28.

The temperature logs were taken at various times. The first was taken only about 1 day after the completion of the well, and clearly indicates that the well has not equilibrated to the formation

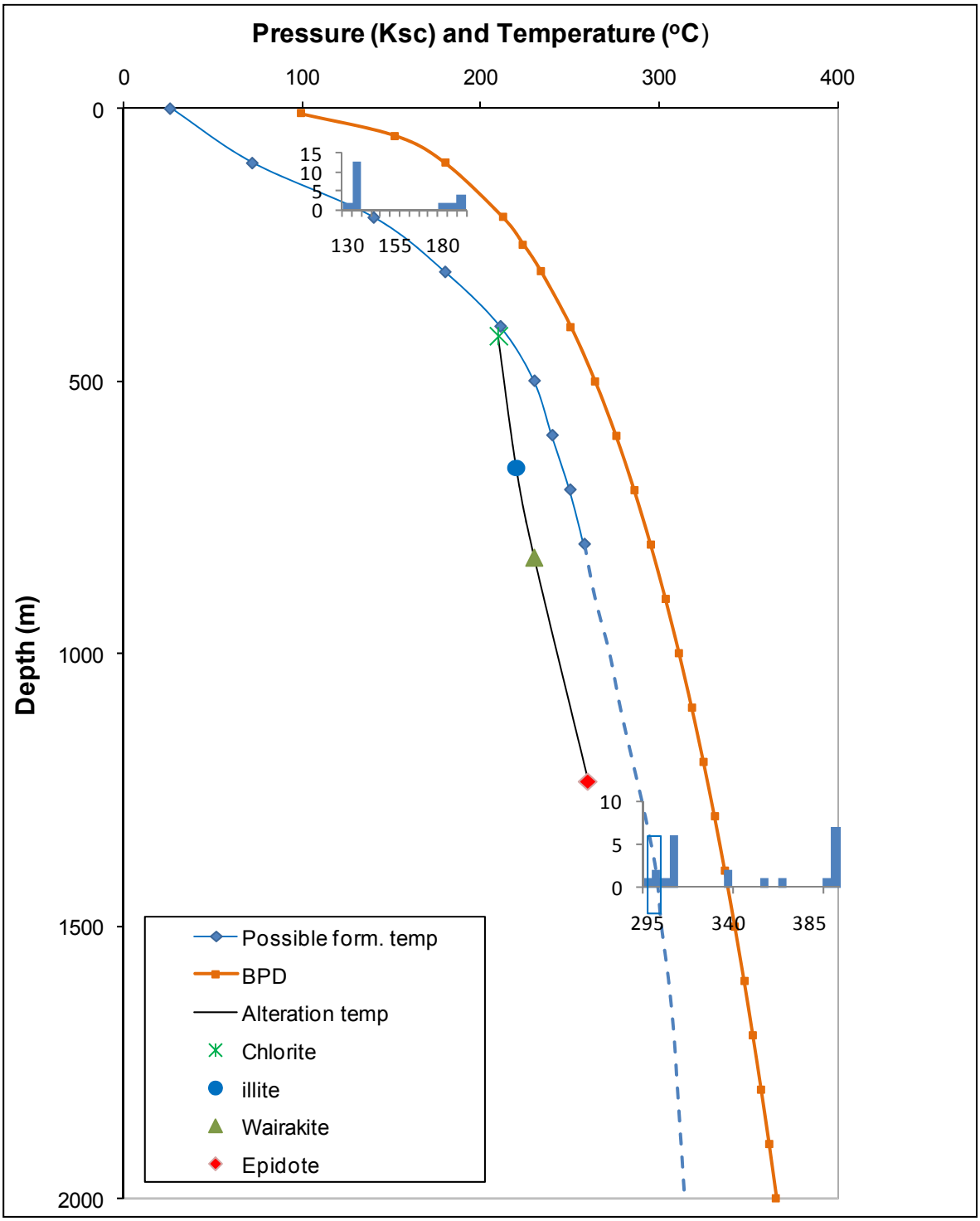

FIGURE 67: Hydrothermal alteration temperatures, homogenization temperatures, fluid inclusions and possible formation temperature of well LHD-23

temperature. However, temperatures at 1700-1800 m depth show very rapid heating, which may reach near to the boiling curve. In addition the pressure curve shows a break at about 1600 m indicating a more vapour rich environment. This would indicate that the aquifer may be in a boiling condition. Later temperature logs failed to reach below the production casing, but showed a gradual heating up of the well above 800 m depth. Probable formation temperature down to that depth may lie slightly higher than the log taken on 13.09.2009, while temperature below is unreliable as mentioned above (Figure 69).

The second temperature curve relates to the minimum formation temperature of chlorite, wairakite, illite and epidote. These temperature estimates are based on experience from geothermal systems in the Philippines (Reyes 1990; Reyes 2000). These appear to be slighlty lower than the expected present

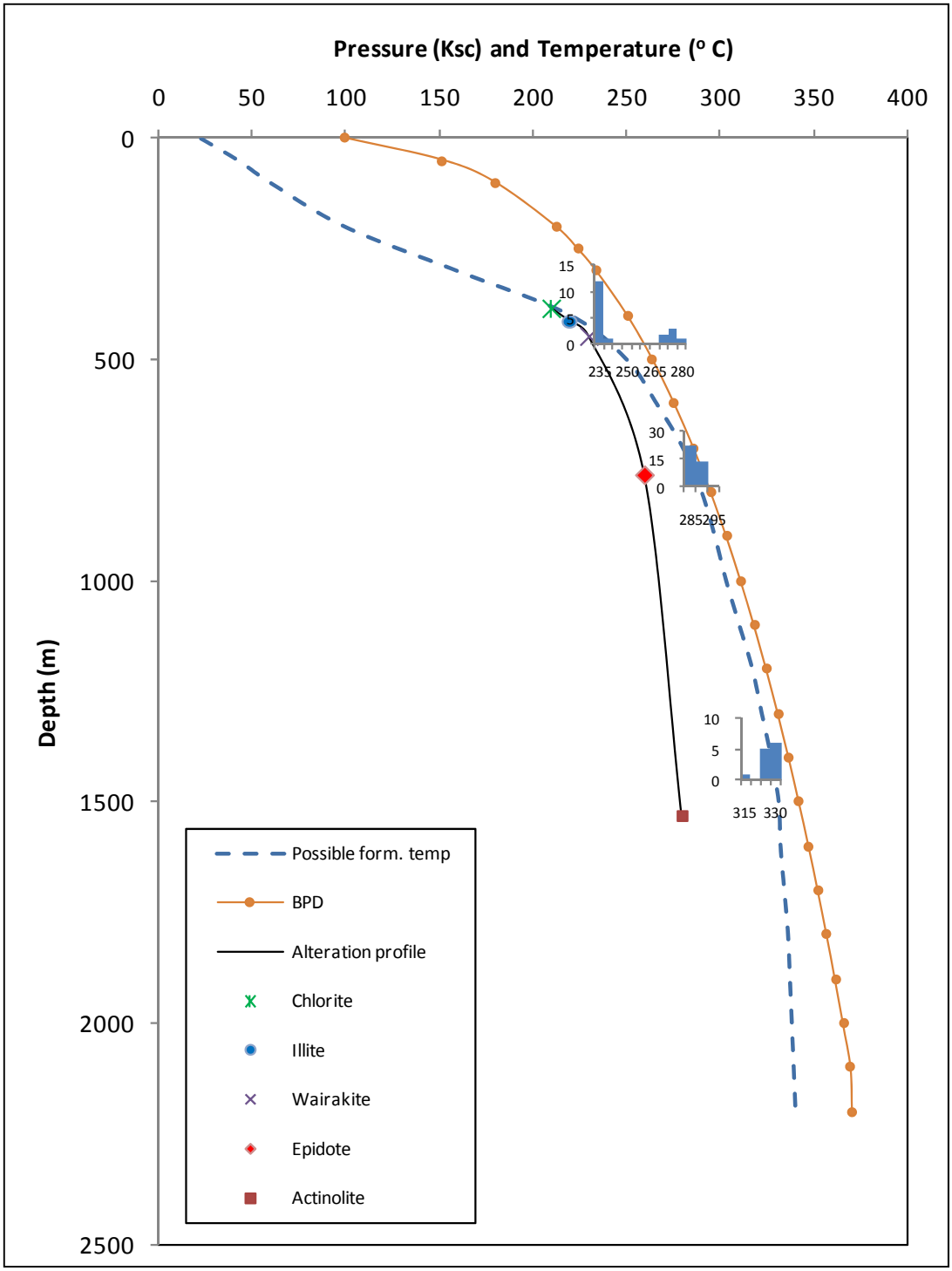

FIGURE 68: Alteration temperatures, fluid inclusion temperatures and possible formation temperature in well LHD-28

formation temperatures, which may either be due to recent heating up of the geothermal system, or that the temperature range of those minerals may be slightly different to the Philippines estimates.

In well LHD-23, a search for fluid inclusions was done at various depths, but only successfully found at two depth intervals; about 195 m and 1421-1481 m depths. Homogenizations temperatures (T_h) are shown in Figure 68. Twenty three inclusions in two quartz crystals from 195 m depth were analyzed and 36 inclusions in two anhydrite crystals taken at 1421-1481 m depth. Two populations of T_h values are evident in the upper location, 130-140°C and then a few that equilibrate at around 180-190°C. The lower one appears to coincide with the last temperature log and may represent the present formation temperature, while the upper one may represent an earlier stage of much higher temperatures in the system or more vapour rich inclusions. The anhydrite inclusions at 1421 m depth (Figure 71) also show two populations. The lower one which is the dominant one ranges from 290-310°C. Traces of higher temperatures, up to 400°C are interpretated as being vapour rich inclusions suggesting vigourous boiling in the system, i.e. temperatures on the boiling point curve.

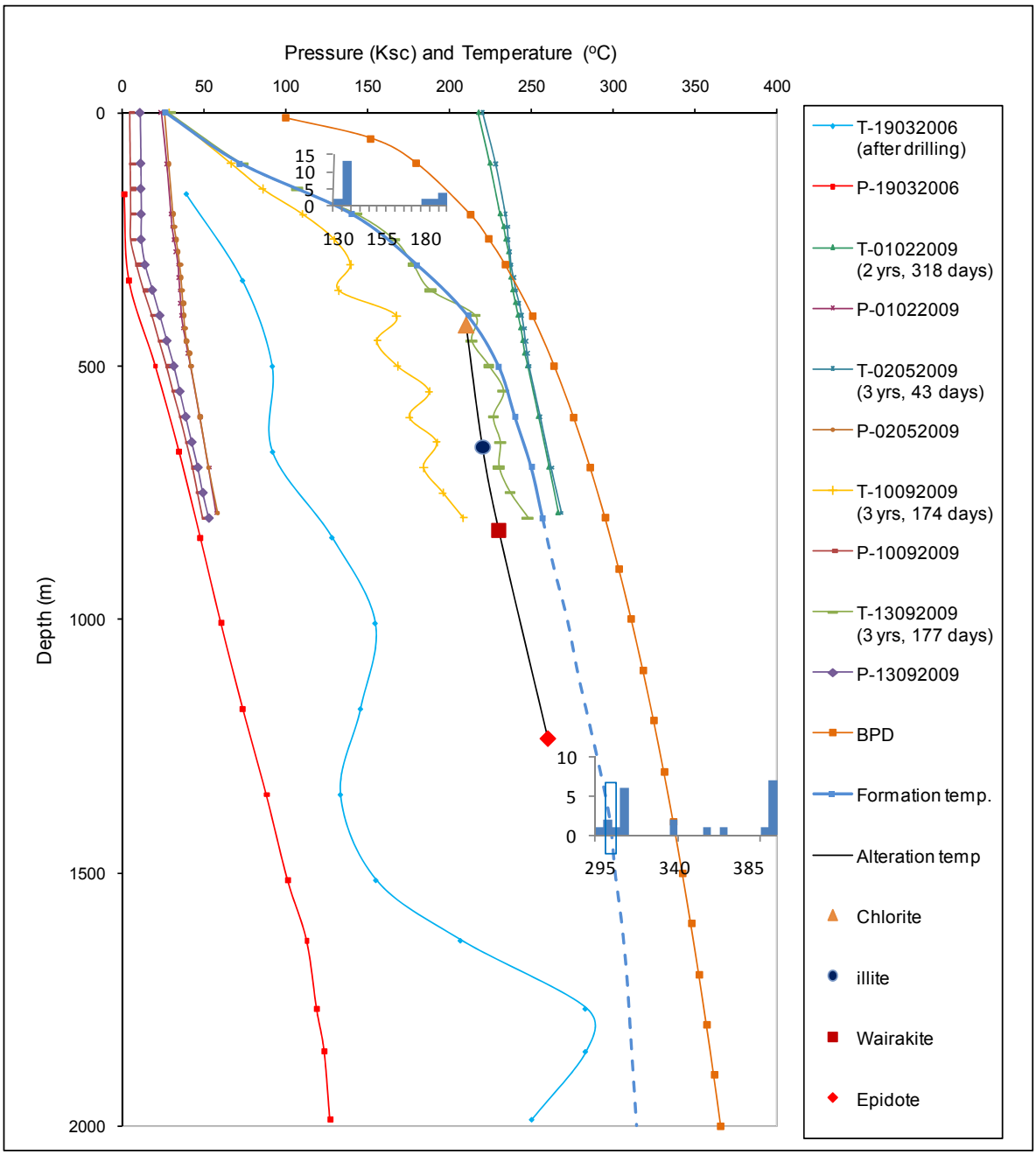

FIGURE 69: Temperature and pressure log, alteration temperatures, fluid inclusion temperatures and possible formation temperature in well LHD-23

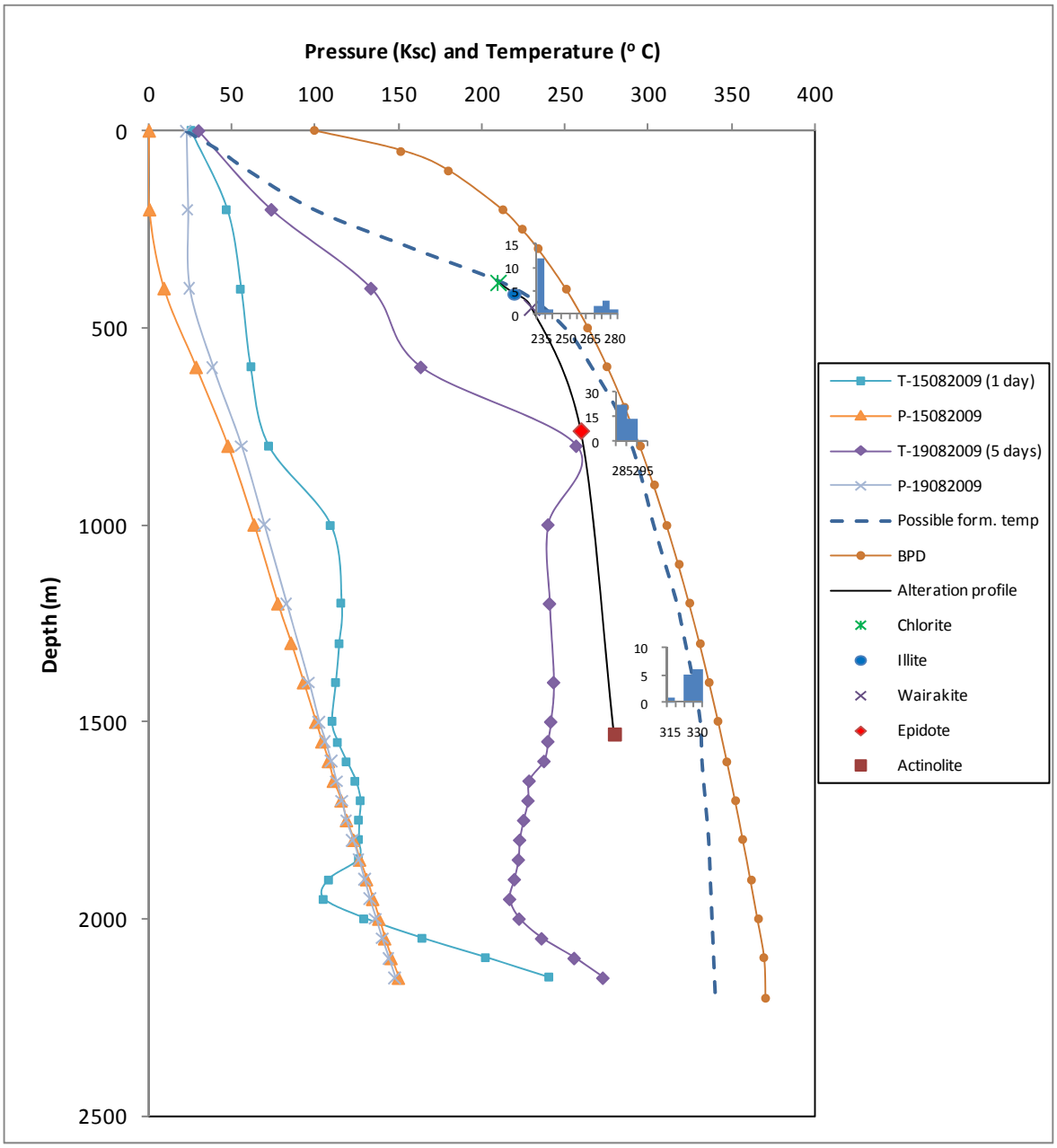

FIGURE 70: Temperature and pressure logs, alteration temperatures and fluid inclusion temperatures in well LHD-28

In the Philippines geothermal systems, drusy quartz, anhydrite and wairakite are sometimes associated with boiling, often corroborated by the presence of some vapor rich fluid inclusions in hydrothermal crystals (Reyes, 1990). In acid alteration zones compared to the adjacent neutral pH alteration minerals high gas fluid inclusions are also more common (Reyes, 1990).

The formation temperature in the reservoir around the well is not well defined, as seen in Figure 67. LHD-23 is a very productive well and important for the power plant, as it produces some 25 MWe. Information on the condition in the well is therefore of importance. Increased effort of fluid inclusion studies is highly recommended as it would constrain better the formation temperature curve and the thermal evolution in that part of the reservoir.

In well LHD-28, temperature logging was done one day after completion and showed slight temperature elevation below the casing point. Five days later logging was repeated showing very rapid heating from the end of the casing, reaching 250°C. The temperature curve shows internal flow of fluid from upper aquifers down to the bottom aquifer at 1900 m depth, explaining the rapid heating

of the well (Figure 70). Temperature logs after discharge are not available, so the formation temperature has not been attained from this kind of logging.

The temperature curve derived from alteration (chlorite, illite, wairakite, epidote and actinolite) is also shown, with temperatures above the last temperature log. Homogenization temperature was measured in quartz crystals at three depths intervals. These show a remarkably narrow temperature range. Temperatures between 235-240°C were found at near 500 m depth. A few values extend to near 280°C, which are interpreted as indicating vapour rich inclusions, thus indicative of boiling. Inclusions at 800 m depth show a range from 285-295°C and 320-330°C near to 1500 m depth. At all depths temperatures tend to lie near the boiling point curve indicating a boiling geothermal system at that location in the geothermal system.

The likely formation temperatures based on the above data are shown in Figures 67-70.

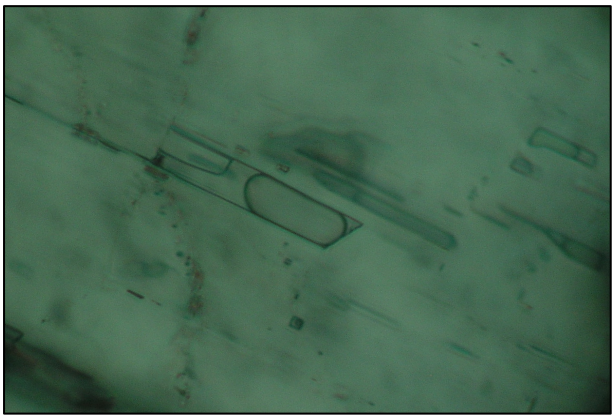

FIGURE 71: Fluid inclusion in anhydrite with a homogenization temperature (T_h) of about 400°C at depth 1421 m, well LHD-23

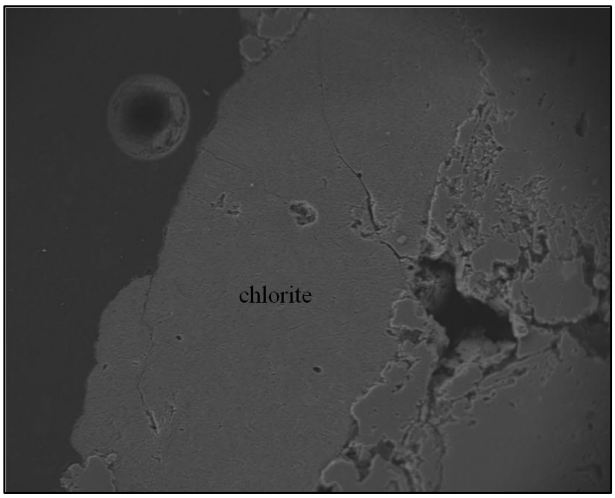

FIGURE 72: Back scatter image of chlorite at a depth of 1463 m, well LHD-23

5.3 Microprobe analysis

Selected samples from wells LHD-23 and LHD-28 were prepared and analyzed using microprobe analysis at the University of Iceland. The analysis was done from selected sample minerals of epidote, chlorite (Figure 72), wollastonite and sulfides (pyrite).

A representative chemical analysis of chlorite is shown in Table 9. A chlorite Fe/(Fe+Mg) ratio has a range of 0.31 to 0.46. Lonker et al., (1993) reported that in well RN-9, higher Fe/(Fe + Mg) ratios and lower Si contents coincided with aquifers and high circulation loss. Four selected samples in well LHD-23 show that the Si content tends to decrease with depth especially near aquifers (Figure 73).

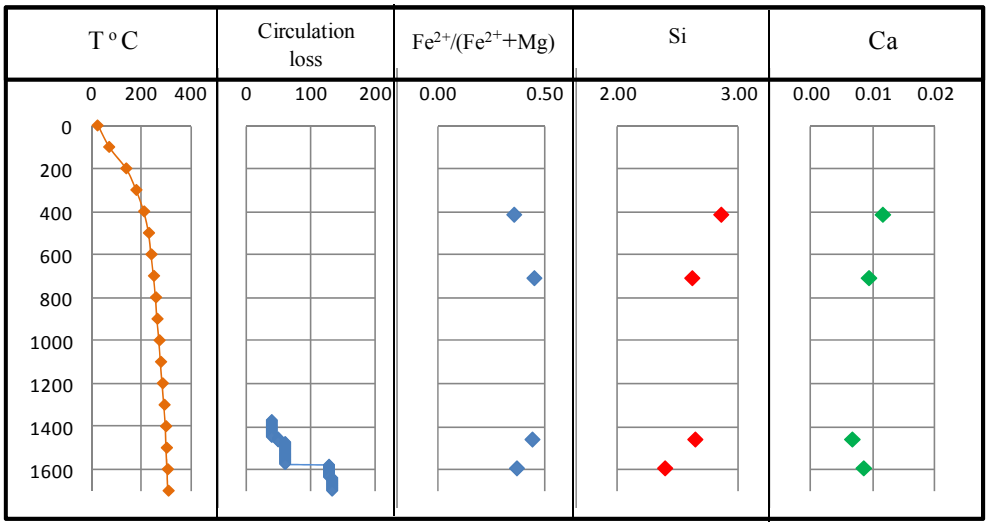

FIGURE 73: Possible formation temperature, loss circulation, and chlorite mineral chemistry against depth in well LHD-23

The analyses therefore show indications of changes in chlorite compositions near permeable zones similar to what Lonker et al. (1993) discovered.

TABLE 9: Representative selected chlorite analysis of well LHD-23 and LHD-28

Well	LHD-23				LHD-28		
Depth (m)	**410**	**707**	**1463**	**1598**	**569**	**825**	**1020**
SiO_2 (wt %)	34.24	28.92	27.31	25.87	36.00	29.44	25.44
Al_2O_3 (wt %)	23.42	20.33	16.58	23.77	13.52	20.90	20.85
TiO_2 (wt %)	0.00	0.00	0.00	0.04	0.00	0.03	0.00
FeO (wt %)	18.26	23.64	18.58	19.60	16.39	23.47	24.53
MnO (wt %)	0.54	0.88	1.24	2.16	1.06	1.81	0.92
MgO (wt %)	22.89	20.27	24.24	20.40	16.01	20.64	16.18
CaO (wt %)	0.13	0.10	0.07	0.09	0.54	0.15	0.17
K_2O (wt %)	0.02	0.00	0.00	1.52	0.47	0.05	0.05
Total	99.51	94.12	88.02	93.44	83.98	96.49	88.15
Formulas based on 14 oxygens							
Si	2.86	2.62	2.65	2.40	3.55	2.61	2.48
Al	2.31	2.17	1.89	2.59	1.57	2.19	2.40
Ti	0.00	0.00	0.00	0.00	0.00	0.00	0.00
Fe	1.28	1.79	1.51	1.52	1.35	1.74	2.00
Mn	0.04	0.07	0.10	0.17	0.09	0.14	0.08
Mg	2.85	2.74	3.50	2.81	2.35	2.73	2.35
Ca	0.01	0.01	0.01	0.01	0.06	0.01	0.02
K	0.00	0.00	0.00	0.09	0.03	0.00	0.00

Epidote is commonly found in wells LHD-23 and LHD-28 as veins and vesicle fillings and as a replacement of phenocysts and groundmass. The major compositional variation in epidotes results from the substitution of Fe^{3+} and Al^{3+} in the octahedral sites (Marks et al., 2009)

TABLE 10: Range and average molar ratio of pistachite (Xps)

Wells	Depth (m)	Molar ratio of pistachite $Fe^{3+}/(Fe^{3+}+Al)$	
		range	average
LHD-23	1337	0.17 - 0.26	0.21
LHD-23	1473	0.21 - 0.28	0.25
LHD-23	1607	0.17 - 0.27	0.23
LHD-28	1566	0.20 - 0.29	0.24
LHD-28	1686	0.22 - 0.26	0.24
LHD-28	1968	0.17 - 0.27	0.22
LHD-28	2085	0.18 - 0.27	0.22

The molar ratio of pistachite in wells LHD-23 and LHD-28 is shown in Table 10 and Figure 74. In well LHD-23, at 1337 m, the molar ratio of pistachite has a range of 0.17 to 0.26 with an average of 0.21. At 1473 m depth there is a slight increase in this ratio to a range of about 0.21 to 0.28 having an average of 0.25. The ratio increases again at 1607 m depth with a range between 0.17 to 0.27 and an average of 0.23. In well LHD-28, epidote samples were analysed at four different depths. At 1566 m, the range of molar ratio of pistachite is from 0.2 to 0.29 with an average of 0.24. A similar average of 0.24 was noticed at 1686 m with this ratio ranging from 0.22 to 0.26 while the average becomes slightly lower at 1968 m depth to 0.22 having a range in this ratio from 0.17 to 0.27. In Reykjanes and Nesjavellir high temperature geothermal systems in Iceland, the decrease in pistachite ratio is observed and interpreted to indicate a decrease in temperature (Hreggvidsdóttir, 1987; Marks et al. 2009). Hence, the lower pistachite ratio at 1337m depth in well LHD-23 and the deeper parts of well LHD-28 might indicate slightly lower temperatures than above. This does, however, not compare well with available data on temperature which indicate temperatures near to boiling at these depths.

Two samples of wollastonite (Figure 5) at 1557 m depth in well LHD-28 were analysed and are presented in the Table 11. Sulfides are abundant at various depths in the wells, and appear to show variable colours and crystal shapes though cubic being most common. They occur as vesicle and vein fillings and disseminated in the groundmass. The analysis of these at variable depths was done to see the variablility of compositions of these minerals. Microprobe analyses of the sulfide minerals from several depths of well LHD-23 and LHD-28 shows that they are only confined to pyrite composition (Figure 76) as shown in the Table 12.

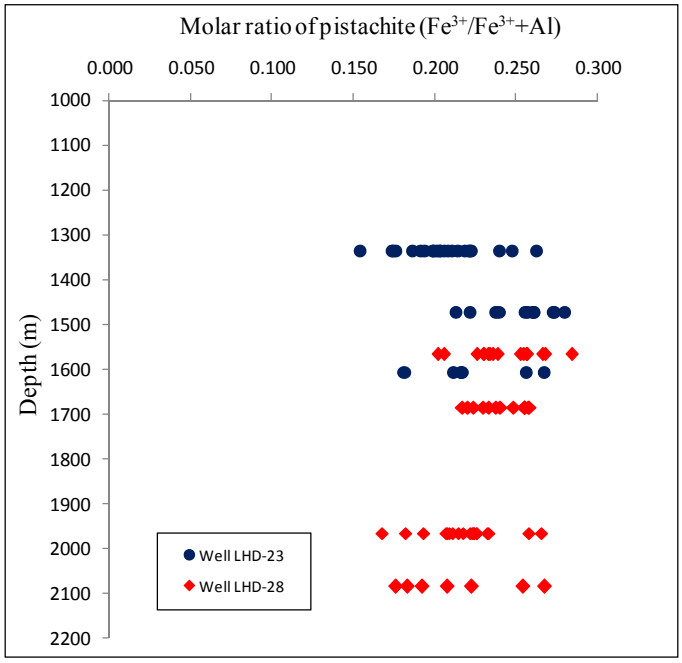

FIGURE 74: Compositions of epidote based on the molar ratio of pistachite at two depths intervals for the two wells of LHD-23 and LHD-28

TABLE 11: Representative wollastonite analyses from depth 1557 m of well LHD-28

Well/depth / Oxide (wt %)	LHD-28 1557 m	
SiO_2	48.49	49.09
TiO_2	0.01	0.00
Al_2O_3	0.15	0.19
FeO	0.06	0.06
MnO	0.43	0.43
MgO	1.73	1.66
CaO	49.49	50.09
K_2O	0.04	0.04
Total	**100.41**	**101.55**

TABLE 12: Representative pyrite analyses from several depths in wells LHD-23 and LHD-28

Well	Depth (m)	Fe	Cu	S	Totals
		(Wt %)			
LHD-23	947	46.91	0.00	52.51	99.42
LHD-23	1412	47.03	0.00	53.22	100.25
LHD-23	1514	44.12	0.00	53.02	97.14
LHD-23	1538	46.19	0.00	53.79	99.98
LHD-23	1574	46.71	0.00	53.27	99.97
LHD-23	1598	44.32	0.00	53.40	97.72
LHD-23	1607	45.86	0.00	53.36	99.23
LHD-28	1026	46.35	0.00	53.13	99.49
LHD-28	1968	48.57	0.00	54.26	102.83
LHD-28	2082	44.14	0.00	54.19	98.33

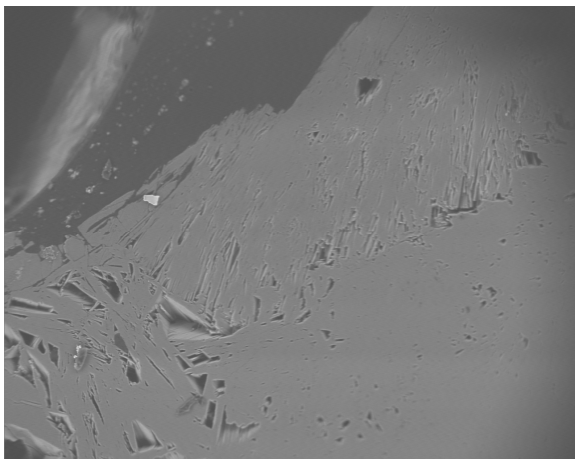

FIGURE 75: Back scatter image of wollastonite from 1557 m depth in well LHD-28

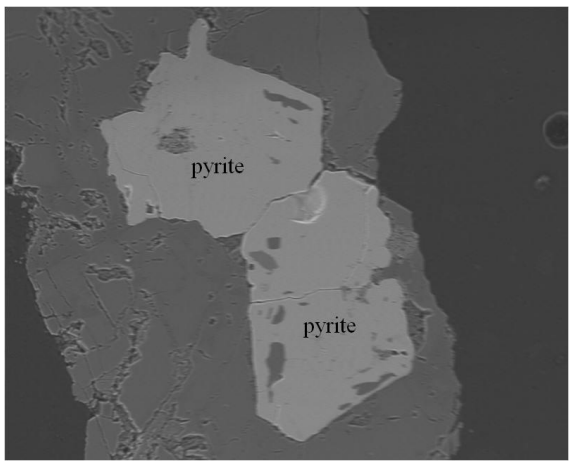

FIGURE 76: Back scatter image of pyrite at 947 m depth, well LHD-23

6. DISCUSSION

The Lahendong geothermal model was first prepared in 1987. Barnet (1987) did the reservoir assessment, and then the geological model based on 7 exploration wells giving emphasis to structure and the lateral and vertical formation temperature distribution by Robert (1987). The combination of the geological data, geophysics and wells data was modeled by Pertamina Geothermal. The model of Azimudin and Hartanto (1997) emphasized the well data after the completion of 14 wells, and then followed by a conceptual model Siahaan (2000), and lastly the 3D inversion Magnetotelluric model by Raharjo et al.,, (2008).

A total of 28 wells have been drilled in Lahendong geothermal field. The highest temperature measured in the system is about 343°C in well LHD-8 and the lowest temperature was measured in the production part of well LHD-7 about 98°C. Well LHD-10 is the deepest well at 2501 m, the shallowest is well LHD-8 at 1506 m deep. The average depth of the wells is about 2000 m.

The stratigraphy observed in wells LHD-23 and LHD-28 show a division of the strata into three parts; Pre-Tondano, which are formed before the large Tondano subsidence, the Tondano Unit that is an extensive pyroclastic layer formed during the subsidence of the huge caldera, and then units that postdate that event. These units have been established in other wells. The chemical analyses of the Pre-Tondano units have, however, shown that they are more acidic in nature than previously believed. Further analysis are recommended to establish the chemical trends in these units, and to constrain better the relation between binocular and petrographic analysis with the chemical composition of the various rocks.

The Tondano Unit is relatively easy to recognize in cutting analysis, and provides therefore a good marker horizon in the area. It has been mapped in most wells. The depth of the layer has been plotted in the Petrel software and its contours are shown in Figure 77. This map shows firstly the sloping surface of the layer which assumedly is due to a regionally tilted succession or its depositional slope. Superimposed on it are irregularities which may indicate a general subsidence of the layer in the area of most wells except for wells LHD-1, LHD-2, LHD-6 and possibly LHD-7. This apparent subsidence which may amount to about 100-200 m may be related to the floor of the Pangolombian caldera. The effect of tectonic faulting in the area cannot be excluded. This has to be studied in future in more detail.

Figure 77 shows how the Tondano unit deposited related to the topography. Based on the figure, the Tondano unit is seems from the east direction, going down to the west. In the middle part, the contour shows irregularities. Generally, this Tondano unit is probably controlled by topography in the east and west direction but structural control of fault and fracture probably control the irregular contour in the middle part of wells LHD-4, LHD-5, LHD-13 and LHD-24 (Figure 77). No wells are located in the western part as there is no prospective geothermal system in the west direction. In well pad LHD-13, the deeper contour of the top of Tondano unit seems to be a match with the contour in the epidote map, showing that the deeper deposition of the Tondano unit related to the geothermal systems in the area. This correlation is also seen, although not clearly in well pada LHD-5, LHD-24 and LHD-4. The irregularities contour in the well pad LHD-4 and well pad LHD-13 is probably also related to the structural pattern of F-1 and F-8.

Only a few aquifers were located in wells LHD-23 and LHD-28. The locations of some of them are tentative as data is limited and includes circulation losses and temperature logs which are mostly Kuster temperature element (KTE) which gives point data at 50-100 m intervals. Only one temperature log is available in the production part of LHD-23. An aquifer is suspected from a temperature log below 1000 m depth. Acid alteration was proposed at 1022-1049 m depth based on the presence of gypsum and sulphur as described in Section 5.1. One assumes that this is an aquifer and that it has an acid fluid composition, one may be tempted to associate that with down flow of condensate water along structure F-6. The major aquifer at the base of the well at about 1800 m depth shows indication of being in boiling condition, judged by the rapid heat-up and steep pressure

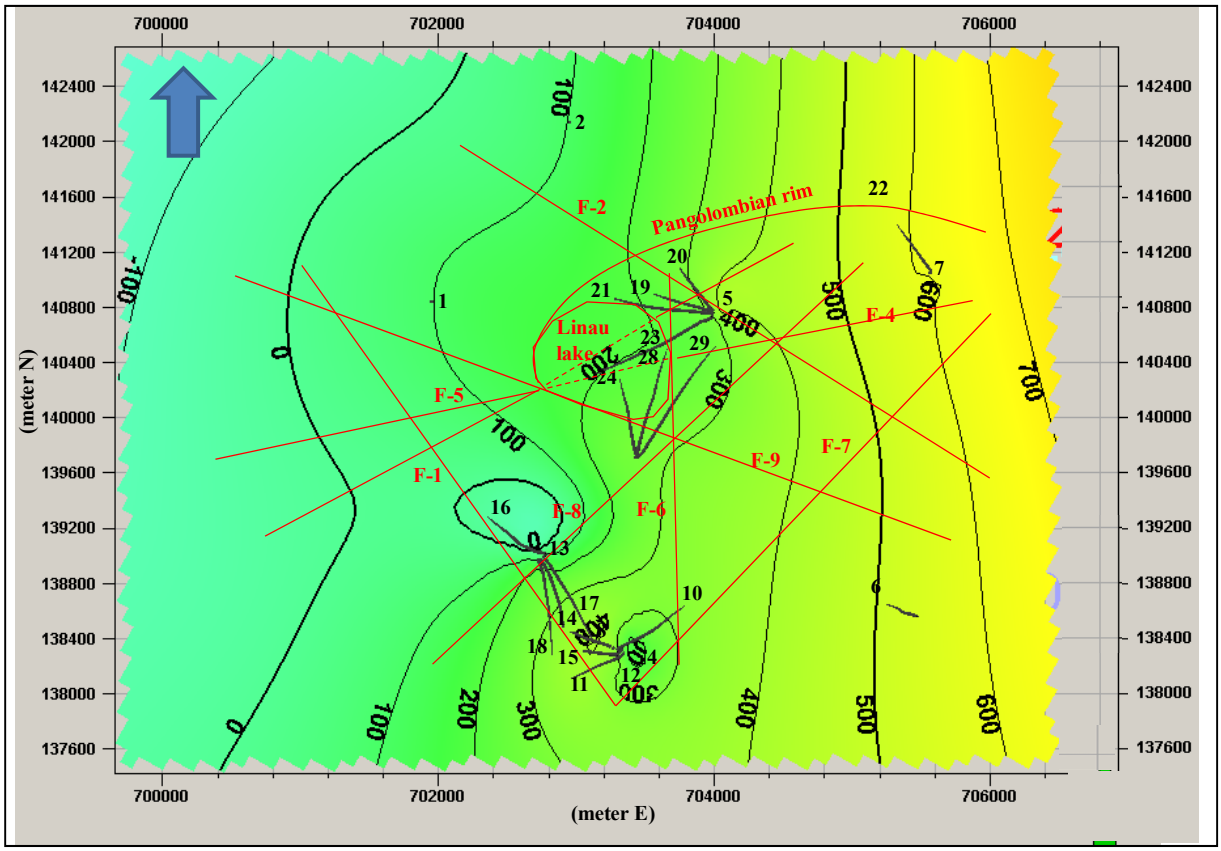

FIGURE 77: Map shows iso-contour elevation (masl) of top Tondano unit in Lahendong

gradient. This aquifer is situated directly below the Linau Lake hydrothermal explosion crater, and one may contemplate that it is related to fractures of that explosive episode.

Aquifers are postulated below 1000 m in well LHD-28, shown in the temperature profile. These shallow aquifers may relate to the structure of F-9 which the well passes around at that depth. The aquifers below 1500 m may coincide with fracture F-4, although it must be mentioned that well LHD-29 did not encounter any aquifer along the same fault trace to the east. The other possibility would be that well LHD-28 is also encountering permeability related to the Linau hydrothermal explosion crater as LHD-23. The Linau Lake hydrothermal explosion crater is believed to have formed as a result of magma entering into a vigorous geothermal system at relatively shallow depth (700 m suggested by Batan, 2005) causing overheating and steam explosive activity and a surface crater formation. The explosion crater is lying adjacent to the Pangolombian caldera margin and may relate to it, e.g. the ascent of magma would follow the caldera margin up to the location of the explosive activity.

Acid aquifers and alteration and are commonly found in Philippines geothermal systems, and these are invariably structurally controlled. These acid fluids are believed to be largely derived from shallow acid condensate zones which percolate down open fault structures to deeper levels. The depths are usually a few hundred meters but may reach as far as 1600 to 1800 m associated with veins and strongly altered formation (Reyes, 2000). Acid and condensate zones are found in Lahendong at depths of about 300 to 600 m (Azimudin and Hartanto, 1997) and are marked by the appearance of kaolinite in the tuff unit there. This acid aquifer has mostly been cased off. Acid grounds are well developed towards west in the direction of well LHD-1. It is proposed by Siahaan (2000) and Azimudin and Hartanto (1997) that the reservoir is moving from the south of well pad LHD-4 to the north, experiencing vigorous boiling (Batan, 2005) and creating acid alteration especially in the location of close to the LHD-1. That is why well LHD-1 is an acid well, probably due to the percolation of acidic fluid along a nearby fault.

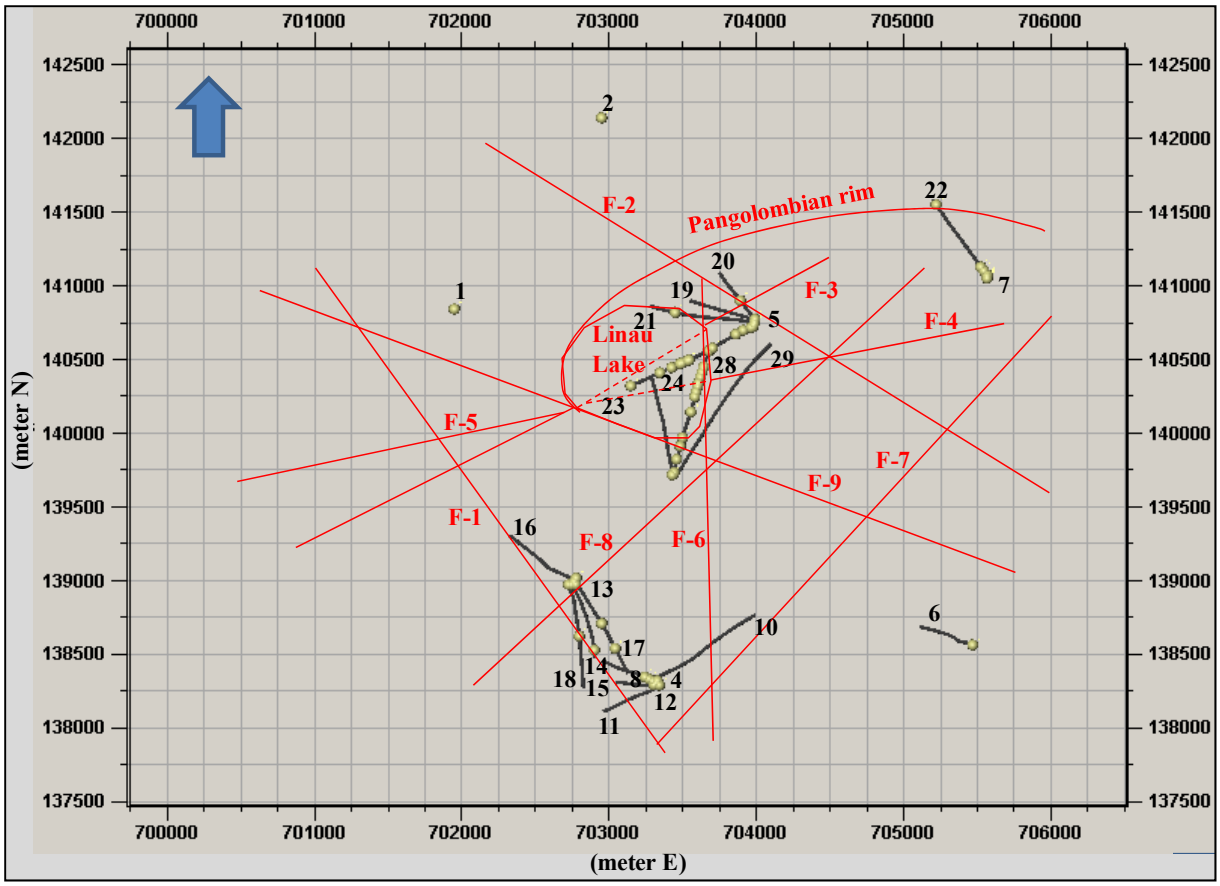

FIGURE 78: The location of aquifers in wells (yellow circle) and the distribution of fault structure in Lahendong field

Figure 78 shows the location of the aquifers and trajectories of the Lahendong wells and their relationship to the fault structures in the area. The following relationships can be discussed here. The probable reason for the greater number of aquifers (feed points) in wells LHD-23 and LHD-28 than in other wells may be due to the integrated search for these using the available data as discussed in Section 4.4, while only the largest aquifers with partial to total circulation losses are emphasized in the other wells. The close correlation between surface geothermal manifestations and fault structures has led to the postulation that geothermal flow is directly related to those features and the best permeability would be found by dissecting those with drill holes. The picture shows that the relationship is not strongly apparent. An assumption is made that these structures are vertical which is certainly an over statement, as they may have a variable inclination depending on their type. It would be an interesting future project to analyze further these relationships using software, such as Petrel, to fit these aquifers with the relevant structures by varying the dips. One must, however, also assume that there would be a number of aquifers that have no relation to surface features, as the latter are only the most recent tectonic events in the area.

Hydrothermal minerals in Lahendong geothermal field are found as replacements of primary minerals and precipitatates in rock voids. Two types of hydrothermal alteration suites are found; neutral pH and acid alteration. Neutral pH alterations are dominant and contain minerals such as quartz, wairakite, albite, epidote, actinolite and wollastonite. The acid alterations on the other hand include minerals such as kaolinite, sulphur, pyrophylite, and diaspore. The distribution of clay minerals and the first appearance of temperature dependent alteration minerals are used to distinguish the different types of zones in the geothermal system, e.g epidote and actinolite. The correlation of the hydrothermal alteration minerals between two wells LHD-23 and LHD-28 show progressive hydrothermal alteration with depth as discussed in detail in Section-5.1.4 and shown in Figure 66.

A comparison between the two wells shows that well LHD-28 has both higher temperature and higher-shallower alteration than well LHD-23, which further is confirmed by the fluid inclusion temperatures in the two wells. This is also seen in the much dryer well LHD-28 compared to well LHD-23.

Epidote is one of the temperature dependent alteration minerals that is easily identifiable in cutting analysis and is reported in most wells in the field. Figure 79 shows the depth of the first appearance of that mineral. Contour map of the first appearance of epidote in wells shows that the epidote is found at the shallowest depth at well pad LHD-24, deeper (-200 masl) in well pads LHD-5 and LHD-4, and still deeper in well pad LHD-13 (-400 masl). Epidote is not reported in well pad LHD-7 and 6 which indicates >-1100 masl. The epidote contour can be looked at as a log term temperature contour, and is therefore shows the landscape of the geothermal system at that depth (Figure 80). The contours outside the outermost wells must be taken with reservations as data is insufficient to project those. The structure of the system shows a definite N-S direction, possibly intersected by a NW-SE (F-2 and F-9) structure around well pads LHD-5 and LHD-24. A rapid deepening of the structures is seen on either side. It seems more localized to the west where well LHD-16 was drilled, and the regional in the east where wells LHD-6 and LHD-7 were drilled. If there is a connection between surface structures and the deep "epidote anomaly", it might may coincide with the northernly F-6 and then between F-2 and F-9. It must, however be born in mind that fault structures not only provide pathways for upflow, they can equally cause down-flow of colder groundwater.

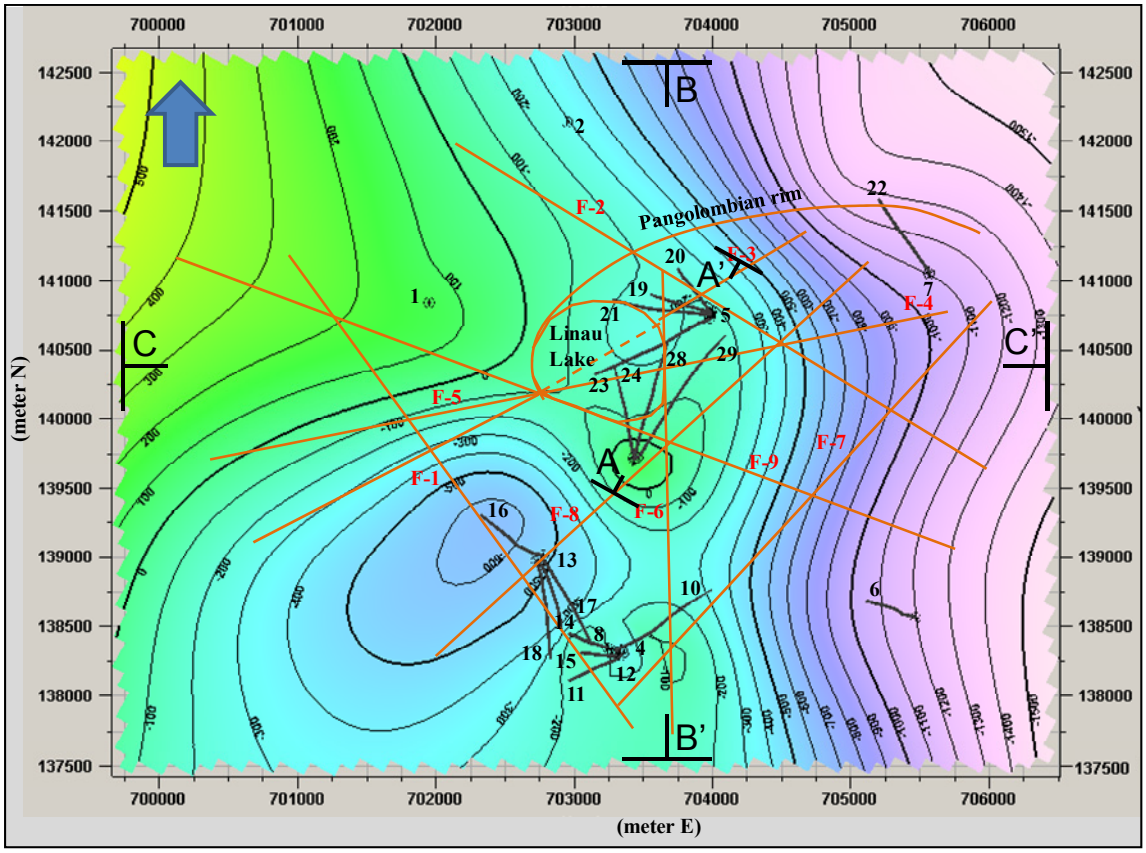

FIGURE 79: Map showing the contour distribution of the first appearance of epidote related to the fault structure in Lahendong field

The likely formation temperature profiles of wells LHD-23 and LHD-28 are shown and discussed in Section 5.2, assembled from temperature logs, alteration and fluid inclusions. The formation temperatures in those wells must, however, be considered to be approximations as the data is not conclusive. The alteration in well LHD-23 is considerably lower than in LHD-28 which to some extent correlates with the fact that the latter is more steam rich than well LHD-23. There may be two reasons for that, one being that the main aquifers at the base of the wells are of different temperatures (only 300-400 m distance beween them), or that aquifers in the upper part of well LHD-28 are steam rich and increase the overall enthalpy of the well relative to well LHD-28. The rapid temperature and

pressure build-up in well LHD-28 as opposed to well LHD-23 may be caused by boiling conditions in the upper aquifers in the former. Another feature is that well LHD-28 was drilled from a location where higher temperatures (and alteration) are found at shallower levels. It has also been suggested that faults F-4/5 may form a boundary between the system to the south and the one that well pad LHD-5 mines.

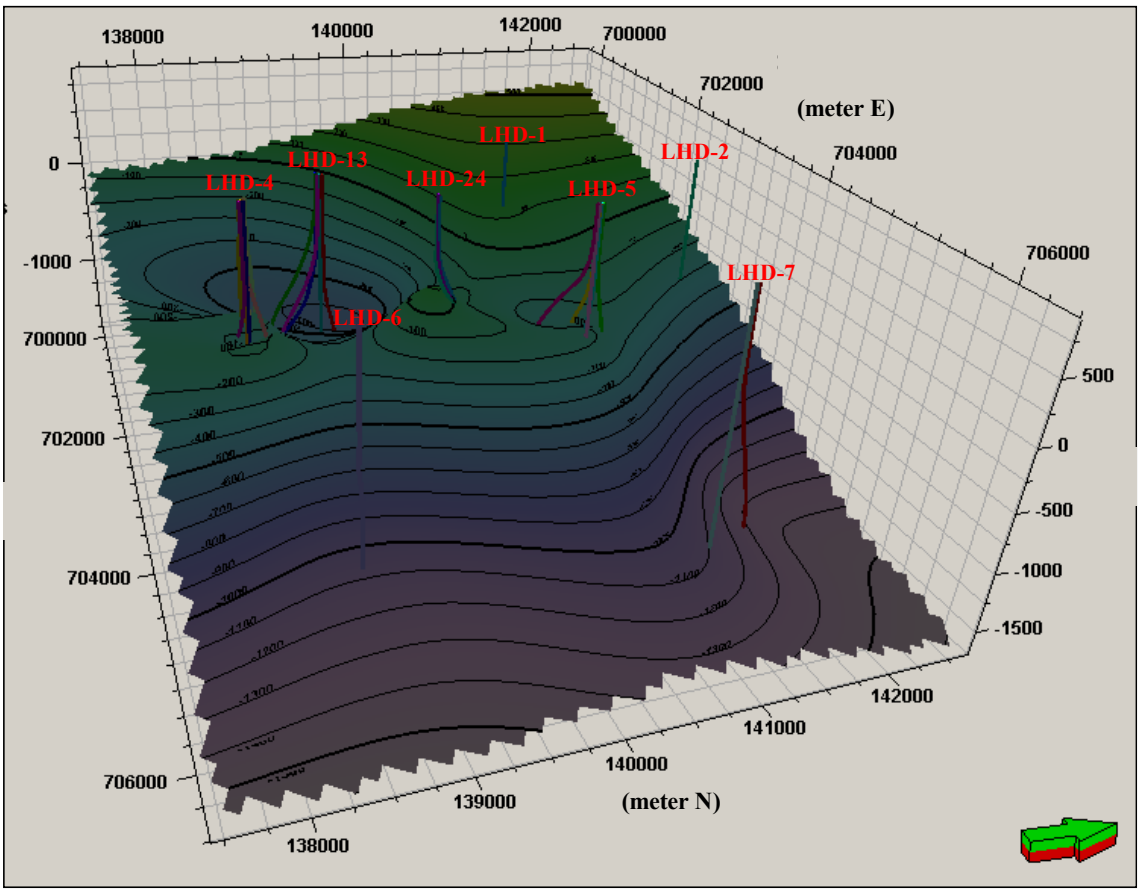

FIGURE 80: 3D profile map showing the contour distribution of the first appearance of epidote in Lahendong field

N-S and E-W temperature profiles are shown in Figures 81 and 82 with a comparison with the depth of the first occurrence of epidote. The temperature distribution shows clearly how the shallow regions of well-pad LHD-24 are much hotter than well pad LHD-5. Epidote occurrence generally shows satisfactory correlation with formation temperatures, except in well-pad LHD-5 (LHD-23 excluded), where temperatures are considerably lower than indicated by epidote. The lower formation temperatures in well pad LHD-5, and especially in wells LHD-19, 20 and 21, may be due to insufficient temperature logs prior to and after discharge. A similar discrepancy appears to be present in well LHD-2. This discrepancy is either explained by "recent" cooling, or perhaps that formation temperatures have not adequately been assessed. It is also interesting to note that well-pad LHD-5 is near to the transition between the colder regions to the east and the thermal anomaly in well-pad LHD-24.

Epidote was neither found in well LHD-7 nor, well LHD-22 which was drilled in the same pad, indicating the absence of a high-temperature resource. It is of interest to note the very low temperatures of around 100°C at more than 2000 m depth. If the temperature logs are correct, it certainly indicates a downward flow of colder groundwater, possibly being the recharge of the system.

This study has focussed on the detailed mapping of the relevant geothermal features of two wells in the Lahendong geothermal field, LHD-23 and LHD-28. A comparison with other wells in the area, as discussed above, has shown a certain relationship between surface features and those in the boreholes.

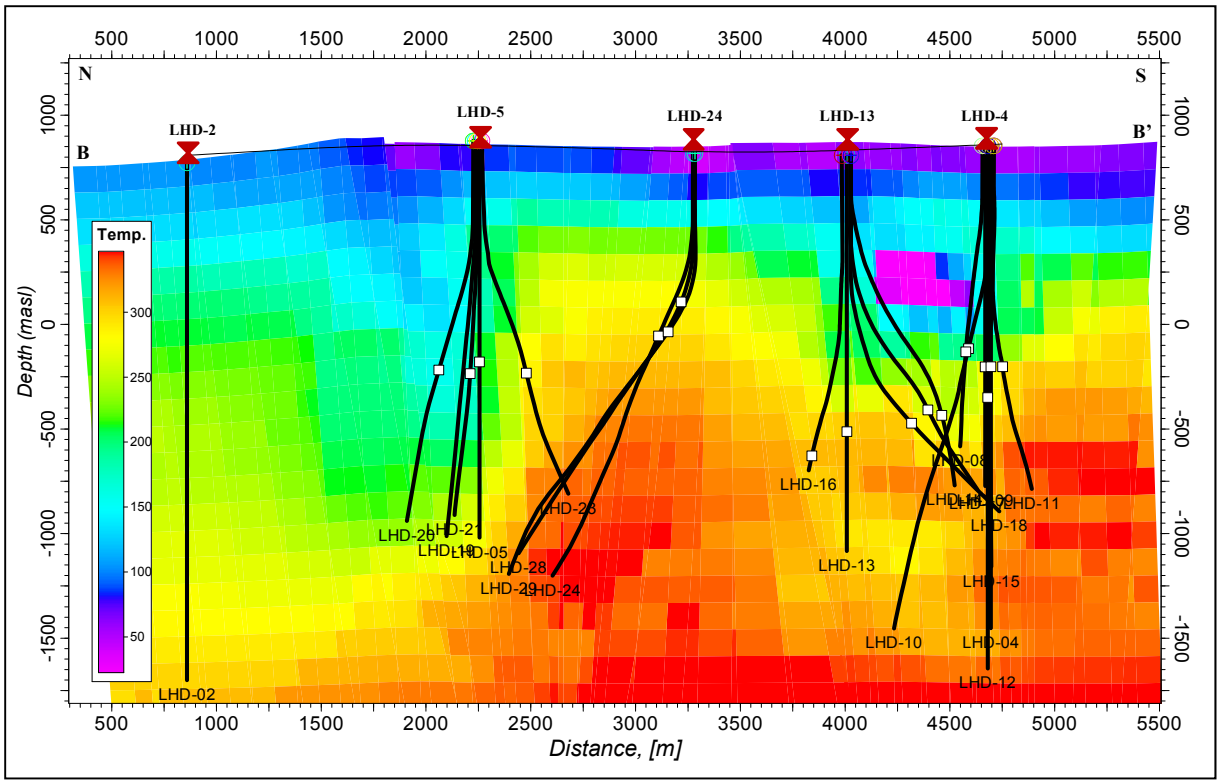

FIGURE 81: N-S cross section showing the distribution temperature of the wells and the first appearance of epidote (white squares)

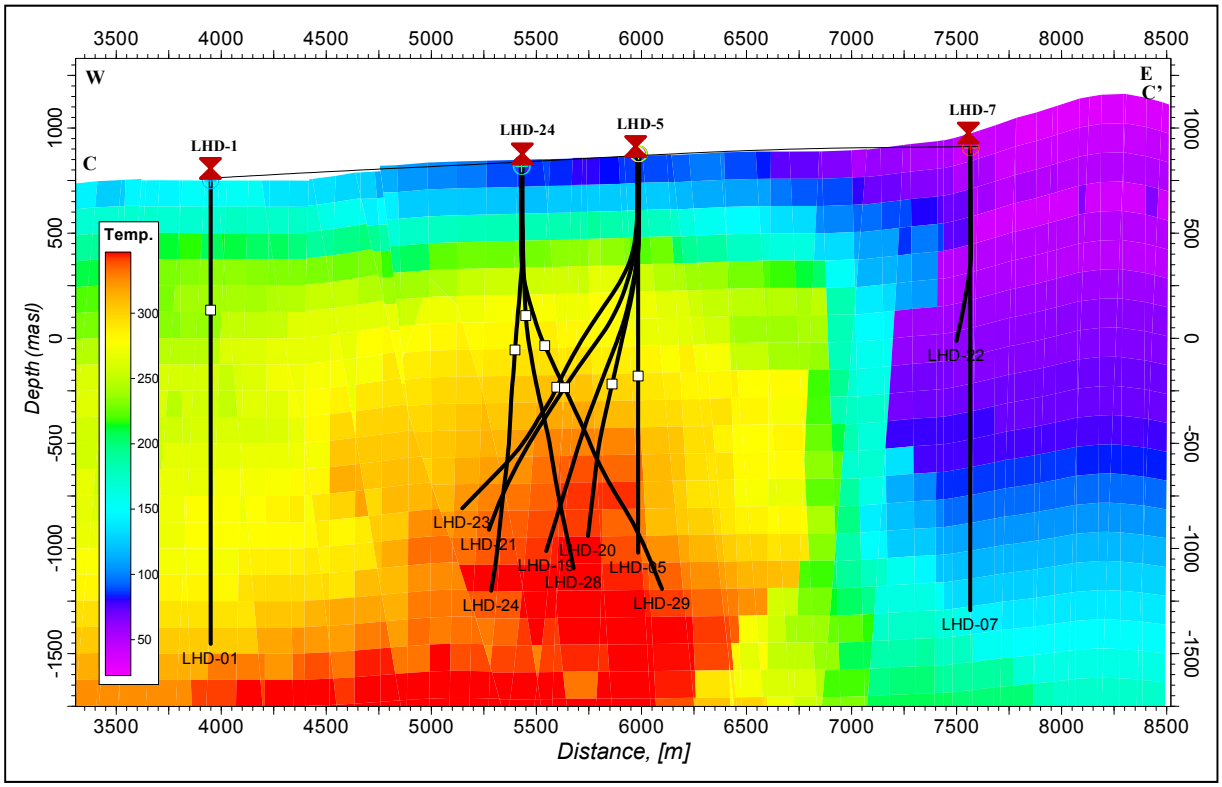

FIGURE 82: E-W cross section showing the temperature distribution and the first appearance of epidote (white squares)

The main ingredients for a high-temperature system are a heat-source and a fracture system that provides the convection route of the groundwater and geothermal system. Figure 83 shows such a summarizing picture. There we have a cold groundwater system to the east of the field in the area where wells LHD-6 and wells LHD-7 and LHD-22 were drilled. The upflow of the system is then

connected to the fault structures shown in Figures 83. The heat-source is magma in some form, and ideas have been forth to connect it to an intermediate diorite, as was encountered in well LHD-5. Figure 84 shows the fault structures in more detail.

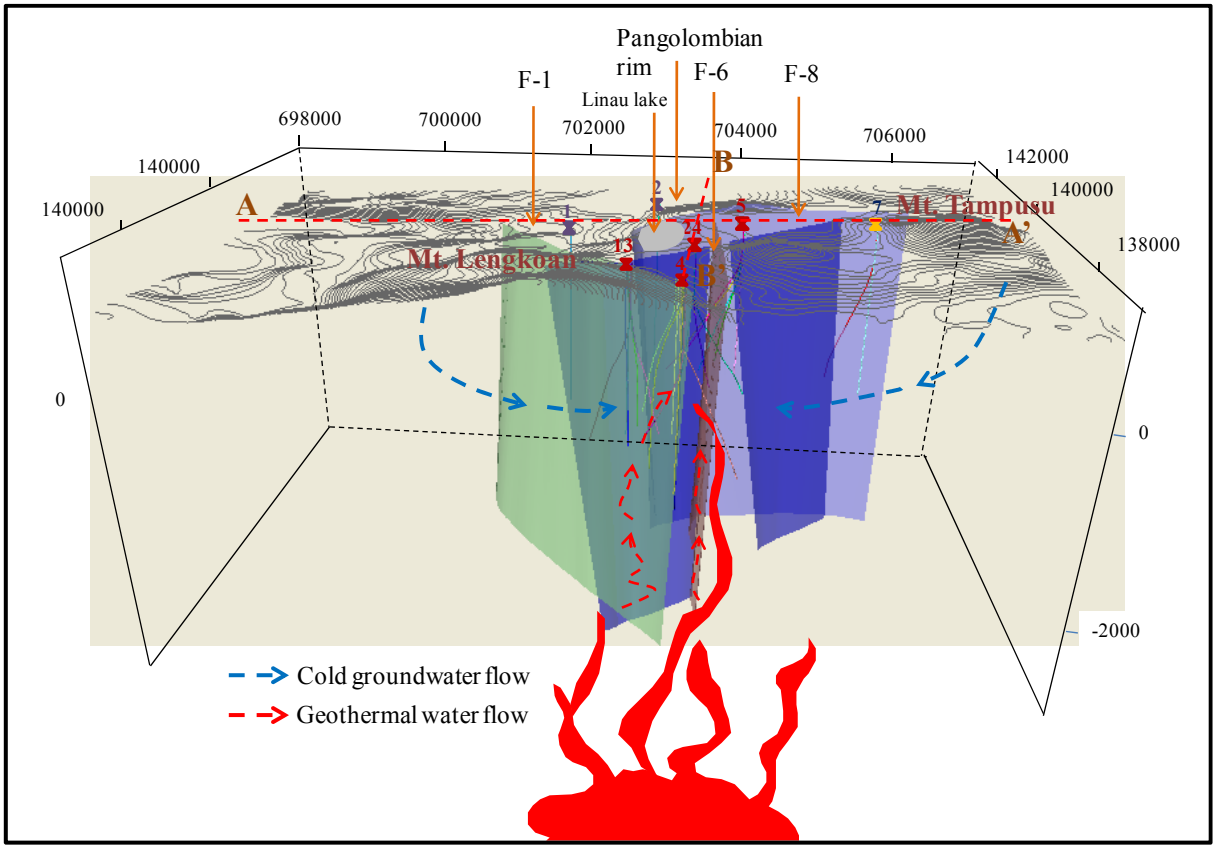

FIGURE 83: The 3 D models of the Lahendong geothermal field

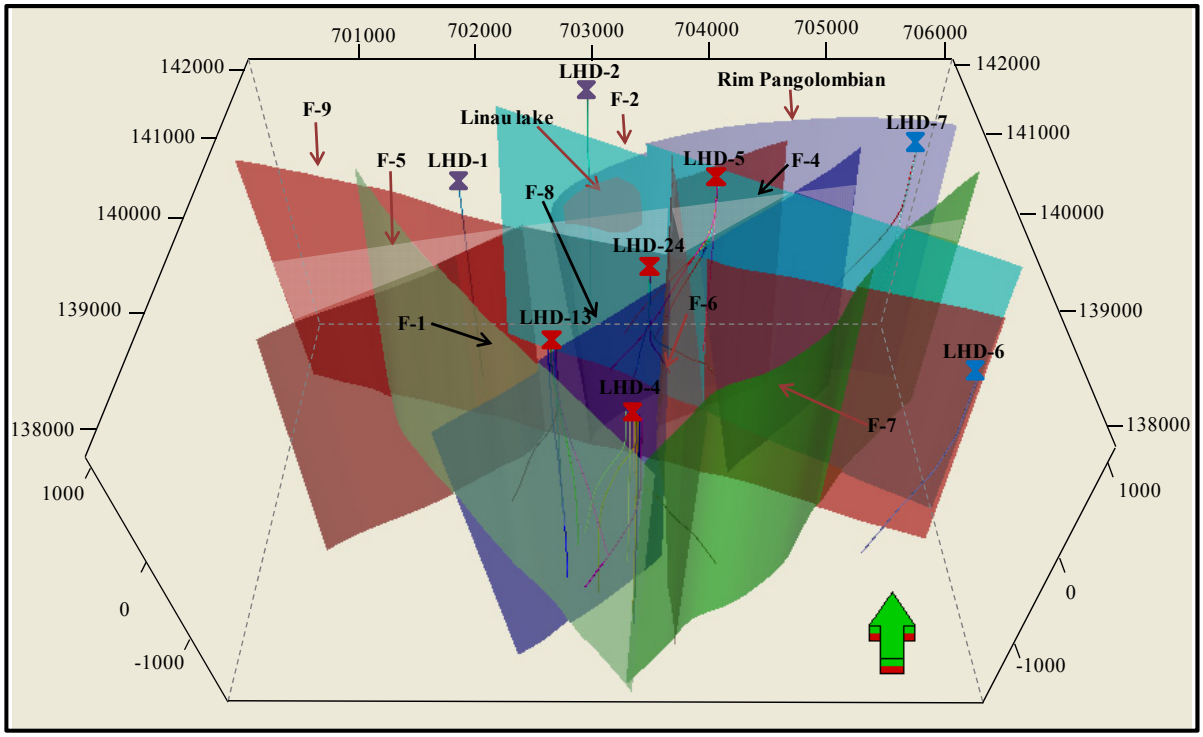

FIGURE 84: The 3 D structural models of the Lahendong geothermal field

7. CONCLUSIONS

1. The strata of Lahendong geothermal field from wells LHD-23 and LHD-28 are divided into two parts: a succession predating the collapse of the Tondano caldera structure and a succession postdating the caldera, and these are separated by pyroclastic units formed during the collapse. The succession is predominantly basaltic andesite lavas, tuffs and breccias, but chemical analyses have shown the older succession to be more rhyolitic than earlier believed.

2. The depth distribution of the Tondano pyroclastite unit shows that the layer has a shallow regional tilt to the west. It lies deeper in many of the wells which may infer a subsidence within the Pangolombian caldera.

3. The hydrothermal alteration minerals in both wells are found as replacement and precipitation in the porosity of veins and vesicles.Two alteration mineral assemblages in wells are neutral pH alteration and acid alteration assemblages. In well LHD-28 higher temperatures (and alteration) are found at shallower levels when compared with well LHD-23.

4. Four hydrothermal alteration zones were found in well LHD-23 and five hydrothermal alteration zones were found in well LHD-28. These are smectite, smectite-chlorite, chlorite-illite, chlorite-illite-epidote, and epidote-actinolite. Two acid alteration zones found in the wells are kaolinite and pyrophyllite-illite zone.

5. A comparison of the depth of first occurrence of epidote in the geothermal field shows that the main geothermal structure is N-S in the central part of the field with a possible NW-SE alignment in the northern part. This conforms to earlier MT geophysical results. A comparison of temperatures with epidote shows a relatively good correlation.

6. Nine aquifers in well LHD-23 and fifteen aquifers in well LHD-28 were recognized above and within the production casing are related to stratigraphy, fracture, fault, secondary porosity and unknown relationship.

7. A comparison of aquifers encountered in the Lahendong wells with known structures on the surface shows only a moderate correlation indicating unknown structural permeability structures at depth.

8. Two populations of T_h values were found in the shallow and deeper part of well LHD-23. In well LHD-28, the two phases of T_h were only found in the upper part and only one population T_h in the lower part. The T_h fluid inclusions showed boiling in both wells.

9. The temperature correlation between the two wells showed that well LHD-28 has higher temperature than well LHD-23.

REFERENCES

Azimudin, T., and Hartanto, D.B., 1997: *Re-evaluation of Lahendong conceptual reservoir models.* Pertamina Internal report (in Indonesian).

Barnet, B., 1987: *Reservoir assessment of Lahendong geothermal field.* GENZL, SMS, report for Pertamina, Jakarta.

Batan, 1991: *Isotope study of Lahendong geothermal field, North Sulawesi*. Report for Pertamina, Jakarta (in Indonesian).

Batan, 2005: *Isotope study and geochemistry of Lahendong geothermal field, North Sulawesi.* Report for Pertamina Geothermal Energy lahendong Field iIn Indonesian).

Batan, 2009: *Water and gas sampling of well LHD-23.* Pertamina, undated internal electronic file.

Browne, P.R.L., 1978: Hydrothermal alteration in active geothermal systems. *Annu. Rev. Earth Planet. Sci., 6*, 229-250.

Browne, P.R.L., 1984: *Lectures on geothermal geology and petrology.* UNU-GTP, Iceland, report 2, 92 pp.

Browne, P.R.L., 1995: *Hydrothermal alteration.* Geothermal Institute, University of Auckland, lecture notes.

Browne, P.R.L., and Ellis, A.J., 1970: The Ohaki-Broadlands hydrothermal area, New Zealand: mineralogy and related geochemistry. Am. J. Sci., 269, 97-131.

Dulce, R.., J.B. Rossel, and M.C. Zaide-Delfin, 1995: Sulfide minerals as indicators of acid Cl-SO_4 Fluids. *Proceedings of the 1996 PNOC-EDC Geothermal Conference*, 137-149.

Fauzi, A., Bahri, S., and Akuanbatin, H., 2000: Geothermal development in Indonesia: An overview of indusrty status and future growth, *Proceedings of the World Geothermal Congress 2000,* Kyushu-Tohoku, Japan, 1109-1114.

Franzson, H., 1983: The Svartsengi high-temperature field, Iceland - subsurface geology and alteration. *Geoth. Res. Council, Transactions*, 7, 141-145.

Franzson, H., 1998: Reservoir geology of the Nesjavellir high-temperature field in SW-Iceland. *Proceedings of the 19th Annual PNOC-EDC Geothermal Conference,* Manila, 13-20.

Franzson, H., 2000: Hydrothermal evolution of the Nesjavellir high-temperature system, Iceland. *Proceedings of the World Geothermal Congress*, Kyushu-Tohoku, Japan, 2075-2080.

Franzson, H., Thordarson, S., Bjornsson, G., Gudlaugsson, S.Th., Richter, B., Friedleifsson, G.O., and Thorhallsson, S., 2002: Reykjanes high temperature field, SW-Iceland, geology and hydrothermal alteration of well RN-10, *Proceedings og the 27th Workshop on Geothermal Reservoir Engineering,* Stanford University, Stanford Ca, SGP-TR-171.

Franzson, H., Zierenberg, R., and Sciffman, P., 2008: Chemical transport in geothermal systems in Iceland Evidence from hydrothermal alteration, *J. Volc. Geoth. Res*., 173, 217-229.

Ganda, S., and Sunaryo, D., 1982: *Preliminary study of the geology of Minahasa Area, North Sulawesi.* Pertamina, internal report (in Indonesian).

Goldstein, R.H., and Reynolds, T.J., 1994: *Systematics of fluid inclusions in diagenetic minerals.* SEPM, Short Course 31, Tulsa, OK, 199 pp.

Gondwana, P.T. 1988: *Magmatic evolution and geochronology of the volcanic activities at the Lahendong area, North Sulawesi.* Report for Pertamina (in Indonesian).

Handoko, B.T., 2009: *Well completion test LHD-28.* Pertamina, undated internal electronic file.

Hemley, J.J., and Jones, W.R., 1964: Chemical aspects of hydrothermal alteration with emphasis on hydrogen metasomatism. *Econ. Geol.,* 59: 538-569.

Henley, R.W., and Ellis, A.J., 1983: Geothermal systems ancient and modern: a geochemical review. *Earth-Sci. Rev.* 19, 1-50.

Hochstein, M.P., and Sudarman, S., 2008: History of geothermal exploration in Indonesia from 1970 to 2000. *Geothermics,* 37-3, 220-266.

Hreggvidsdóttir, H., 1987: *The greenschist to amphibolite facies transition in the Nesjavellir hydrothermal system, southwest Iceland*. Stanford University, MSc thesis, unpublished.

Ibrahim, R.F., Sukhyar R., and Kuncahyo R., 2005: Future of geothermal development in Indonesia, *Proceedings of the World Geothermal Congress 2005*, Antalya, Turkey.

Kristmannsdóttir, H., 1977: Types of clay minerals in altered basaltic rocks, Reykjanes, Iceland. *Jökull*, 26, 3-39.

Kristmannsdóttir, H., 1979: Alteration of basaltic rocks by hydrothermal activity at 100-300°C. In: Mortland, M.M., and Farmer, V.C. (editors), *International Clay Conference* 1978. Elsevier Scientific Publishing Co., Amsterdam, 359-367.

Lonker, S.W., Franzson, H., and Kristmannsdottir, H., 1993: Mineral fluid interactions in the Reykjanes and Svartsengi geothermal systems, Iceland, *American Journal of Science,* 293, 605-670.

Marks, N., Schiffman, P., Zierenberg, R.A., Franzson, H., and Fridleifsson, G.Ó., 2009: Hydrothermal alteration in the Reykjanes geothermal system: Insights from Iceland deep drilling program well RN-17. *J. of Volcanology & Geothermal Research* 189 (2010) 172–190.

Pertamina Drilling Department, 2010: *Drilling report of well LHD-28*. Internal report for Pertamina, (in Indonesian).

Prijanto, Fauzi, A., Lubis, L.I., and Suwana, 1984: Geochemistry of the Minahasa geothermal prospect, North Sulawesi, *Proc. of the 13th Annual Convention of the Indonesian Petroleum Association,* 473-485.

Raharjo, I.B., Wannamaker, P.E., Timisela, D.P., and Arumsari, A.F., 2008: 3D inversion of magnetotellurik, study of the Lahendong geothermal field. *Progress Research, 33th HAGI Annual Meeting*, Indonesia.

Raharjo, I.B., Timisela, D.P., and Arumsari, A.F., 2009: *3D inversion of Lahendong geothermal field.* Pertamina, internal electronic file.

Reyes, A.G., 1979: *The borehole geology and alteration mineralogy of Malitbog-1, Tongonan, Leyte, Philippines.* UNU-GTP, Iceland, report 1, 85 pp.

Reyes, A.G., 1990: Petrology of Philippine geothermal systems and the application of alteration mineralogy to their assessment. *J. Volc. Geoth. Res*., 43, 279-309.

Reyes, A.G., 2000: *Lectures on petrology and mineral alteration in hydrothermal systems: From diagenesis to volcanic catastrophes.* UNU-GTP, Iceland, report 18-1998, 77 pp.

Robert, D., 1987: *Geology model of Lahendong geothermal field: A guide for the development of this field.* Report for Pertamina, Jakarta.

Rollinson, H.R., 1995: Using *geochemical data: Evaluation, presentation, interpretation.* Longman Group Ltd., England.

Saemundsson, K., and Gunnlaugsson, E., 2002: *Icelandic rocks and minerals*. Edda and Media Publishing, Reykjavík, Iceland, 233 pp.

Siahaan, E.E., 2000: *Interpretation of Land-Sat and aerial photos of Lahendong*. Pertamina, internal report, unpublished.

Siahaan, E.E., et al., 2005: *Feasibility study of the Lahendong geothermal field for power plant unit IV and V.* Pertamina, internal report (in Indonesian).

Silaban, M.P., Yani, A., Tesha, Koestono, H., Putra, I.M.K.A, and Nugroho, A.J., 2006*: Drilling report of well LHD-23.* Pertamina Geothermal, Indonesia, internal report.

Silitonga T. H., Siahaan E. E., and Suroso, 2005: A Poisson's ratio distribution from Wadati diagram as indicator of fracturing of Lahendong geothermal field, North Sulawesi, Indonesia. *Proceedings of the World Geothermal Congress 2005,* Antalya, Turkey.

Stefansson, V., and Steingrimsson, B., 1980: *Geothermal logging I: an introduction to techniques and interpretation.* Orkustofnun, Reykjavik, report.

Steiner, A., 1977: The Wairakei geothermal area, North Island, New Zealand: Its subsurface geology and hydrothermal rock alteration. *New Zealand Geological Survey Bulletin,* 90, 136 pp.

Thomson, A.J.B., and Thomson, J.F.H., 1996: *Atlas of alteration: A field and petrographic guide to hydrothermal alteration minerals.* Alphine Press, Ltd., Vancouver, BC, 119 pp.

Utami, P., Browne, P.R.L., Simmons, S.F., and Suroto, 2005: Hydrothermal alteration mineralogy of the Lahendong geothermal system, North Sulawesi: A progress report. *Proceedings 27th New Zealand Geothermal Workshop 2005, Auckland*.

APPENDIX A: Procedure for clay analysis

1. Approximately two tea spoons of drill cuttings is placed into a test tube, cleaned from dust with distilled water. Fill the tube two-thirds full with distilled water and plug.
2. Put the tube in a mechanical shaker for 4 hours.
3. Place about ten drops on a labelled glass slide. Make a duplicate for each sample and let dry at room temperature overnight.
4. Place one set of samples in the desiccator containing Glycole ($C_2H_6O_2$) solution and the other set in a desiccator containing $CaCl_2$ $2H_2O$. Store at room temperature for at least 24 hours.
5. Run both sets of samples from 2-14° on the XRD.
6. Place one set of samples on an asbestos plate and heat in a preheated oven at 500-550°C. Cool the samples.
7. Run the samples from 2-14° on the XRD.

APPENDIX B: Procedure for ICP-OES analysis

Sample preparation.

- Rock sample were weighed in with lithium metaborate and fluxed in graphite crucible for 30 min at 100°C. A constant rock/flux mass ratio of 2 was maintained. Reference samples for instrument calibration were the "in house standards" A-THO, B-ALK and B-HTO (BIR-1).
- Reference samples were made of 250 mg rock powder and 500 mg flux and the unknown samples were made of 100 mg rock powder and 200 mg flux.
- After melting the resulting glass beds were dissolved with continuous agitation in 100 x its weight of acid mixture (75 g for reference samples, 30 g for the unknowns). The acid mixture is made of deionized water with vol 5% nitric acid, 1.33 vol % hydrochloric acid and 1.33 vol% semi-saturated oxalic acid.

Instrument setup and analyses.

- ICP- analyses were made with a cross-flow nebulizer at sample consumption about 2 ml/min. The argon plasma was run at 1200V. Measurements were made in four 25 sec reading sessions after 40 sec flushing of the nebulizer with the sample itself.
- Analytical session starts with running of the three calibration standards. The SpectraVision software is then used to calculate a two or three point calibration line for each element of the analytical routine. Instrumental reference sample (REF) for monitoring eventual fluctuations during analysis was made of equal parts of the three reference samples. This sample was analyzed at the beginning of the session and with ten samples interval through the session. One of the reference samples (B-THO) was analyzed within each batch of 10 samples in order to demonstrate instrument reproducibility in multiple analyses.

Data processing and correction.

- Raw data were processed in the following manner.
- The data is copied and pasted into a correction spreadsheet. All analysis of the batch is normalized to 100% sum.
- The spreadsheet then calculates time dependant variation down each column (element) of the analysis by finding the difference between the first and last readings of the reference sample. The total variation is then divided into ten equal parts. Each line is then corrected by adding the variation-increment which is also added to all subsequent lines of the batch. Then all sums are normalized to 100%.
- After the time dependant variation-correction has been applied to the batch the absolute values of the reference samples at the beginning and at the end are equal. Next, the observed absolute value of the reference sample is recalculated to the nominal values of that sample by a linear correction factor which then is applied to all the unknown samples of the batch.
- Finally, all the unknown samples are normalized to 100% sum.

APPENDIX C: X-ray diffractometer clay results

TABLE 1: X-ray diffractometer clay results of well LHD-23

No.	Depth (m)	Untreated (Å)	Glycolated (Å)	Heated (Å)	Type of clay
1.	45	15.20	15.20	10.20	Smectite
2.	80	12.41	12.43	8.94	Smectite
3.	120	12.86	14.39	9.74	Smectite
4.	190	15.33	15.33	10.27	Smectite
		7.35	7.35	Collapses	
5.	260	13.39	13.77	10.17	Smectite
6.	323	12.25	13.11	10.12	Smectite
		7.17	7.17	Collapses	Kaolinite
7.	329	11.78	12.17	10.12	Smectite
		7.19	7.19	Collapses	Kaolinite
8.	347	11.63	11.90	10.22	Smectite
		7.19	7.19	Collapses	Kaolinite
9.	395	25.21	25.21		MLC
		14.61	14.61	13.79	Smectite
		7.21	7.21	Collapses	Chlorite
		12.11	12.45	9.85	Smectite
10.	419	25.75	25.75		MLC
		14.63	14.63	14.63	Chlorite
		7.22	7.22	Collapses	Chlorite
		12.31	12.31	10.11	Smectite
11.	458	12.91	13.55	9.93	Smectite
12.	509	13.00	13.57	9.93	Smectite
		7.14	7.14	Collapses	Chlorite
13.	533	14.84	14.84	14.84	Chlorite
		7.27	7.27	Collapses	Chlorite
14.	602	12.95	13.54	9.98	Smectite
		7.27	7.27	Collapses	Chlorite
15.	668	14.71	14.71	14.71	Chlorite
		7.22	7.22	Collapses	
		10.27	10.27	10.27	Illite
		7.75	7.75	Collapses	Gypsum
16.	710	14.80	14.80	14.80	Chlorite
		7.24	7.24	Collapses	
		10.27	10.27	10.27	Illite
		7.75	7.75	Collapses	Gypsum
17.	764	14.80	14.80	14.80	Chlorite
		7.24	7.24	Collapses	
		10.27	10.27	10.27	Illite
		7.75	7.75	Collapses	Gypsum
18.	785	7.67	7.67	Collapses	Gypsum
19.	809	14.55	14.55	14.55	Chlorite
		7.18	7.18	Collapses	Chlorite
		7.71	7.71	Collapses	Gypsum
	MIN	7.71	7.71	Collapses	Gypsum
20.	824	25.55	25.55	25.55	MLC
		14.55	14.55	14.55	Chlorite
		7.20	7.20	Collapses	Chlorite
		7.71	7.71	Collapses	Gypsum

No.	Depth (m)	Untreated (Å)	Glycolated (Å)	Heated (Å)	Type of clay
21.	884	14.55	14.55	14.55	Chlorite
		7.20	7.20	Collapses	Chlorite
		6.70	6.70	Collapses	
		8.22	Collapses	Collapses	
22.	911	14.88	14.88	14.88	Chlorite
		7.25	7.25	Collapses	Chlorite
		10.26	10.26	10.26	Illite
23.	959	14.58	14.58	14.58	Chlorite
		7.18	7.18	Collapses	
		10.17	10.17	10.17	Illite
		8.25	Collapses	Collapses	
		7.72	7.72	Collapses	Gypsum
24.	983	14.67	14.67	14.67	Chlorite
		7.19	7.19	Collapses	
		10.32	10.32	10.32	Illite
		7.72	7.72	Collapses	Gypsum
25.	1007	23.96	23.96		MLC
		14.58	14.58	14.58	Chlorite
		7.19	7.19	Collapses	
		11.52	11.52	11.52	Illite
		7.72	7.72	Collapses	Gypsum
26.	1052	14.58	14.58	14.58	Chlorite
		7.19	7.19	Collapses	
		10.15	10.15	10.15	Illite
		7.71	7.71	Collapses	Gypsum
27	1091	14.60	14.60	14.60	Chlorite
		7.22	7.22	Collapses	Chlorite
		8.24	8.24	Collapses	
		7.71	7.71	Collapses	Gypsum
28.	1118	14.60	14.60	14.60	Chlorite
		7.22	7.22	Collapses	Chlorite
		7.71	7.71	Collapses	Gypsum
		8.24	Collapses	Collapses	
29.	1157	14.56	14.56	14.56	Chlorite
		7.71	7.71	Collapses	Gypsum
		10.07	10.07	10.07	Illite
		8.20	Collapses	Collapses	
		7.15	7.15	Collapses	
30.	1178	14.56	14.56	14.56	Chlorite
		7.13	7.13	Collapses	
		10.06	10.06	10.06	Illite
		9.09	Collapses	Collapses	
		8.43	Collapses	Collapses	
		8.16	Collapses	Collapses	
		7.69	7.69	Collapses	Gypsum
31.	1196	8.38	Collapses	Collapses	
32.	1226	14.58	14.58	14.58	Chlorite
		7.18	7.18	Collapses	
		10.19	10.19	10.19	Illite
		8.43	Collapses	Collapses	
		8.27	Collapses	Collapses	
		7.72	7.72	Collapses	Gypsum

No.	Depth (m)	Untreated (Å)	Glycolated (Å)	Heated (Å)	Type of clay
33.	1271	14.58	14.58	14.58	Chlorite
		7.19	7.19	Collapses	
		7.75	7.75	Collapses	Gypsum
		10.19	10.19	10.19	Illite
34.	1316	25.28	25.28	25.28	MLC
		14.71	14.71	14.71	Chlorite
		7.21	7.21	Collapses	
		10.33	10.33	10.33	Illite
35.	1355	7.75	7.75	Collapses	Gypsum
		10.30	10.30	10.30	Illite
		8.30	Collapses	Collapses	
36.	1379	10.24	10.24	10.24	Illite
		7.74	7.74	Collapses	Gypsum
37.	1466	14.72	14.72	14.72	Chlorite
		7.23	7.23	Collapses	
		7.77	7.77	Collapses	Gypsum
		10.24	10.24	10.24	Illite
38.	1559	14.52	14.52	14.52	Chlorite
		7.16	7.16	Collapses	
		7.68	7.68	Collapses	Gypsum
		10.20	10.20	10.20	Illite
		9.33	9.33	9.33	Pyrophyllite
39.	1625	14.52	14.52	14.52	Chlorite
		7.16	7.16	Collapses	
		7.70	7.70	Collapses	Gypsum
		10.13	10.13	10.13	Illite
				8.98	

TABLE 2: X-ray diffractometer clay results of well LHD-28

No.	Depth (m)	Untreated (Å)	Glycolated (Å)	Heated (Å)	Type of clay
1.	249	14.87	13.12	10.26	Smectite
		7.31	7.31	Collapses	Chlorite
2.	385	14.97	14.97	10.26	Smectite
		7.26	7.26	Collapses	Chlorite
3.	4 414	14.62	14.62	14.62	Chlorite
		7.18	7.18	7.18	Kaolinite
		10.16	10.16	10.16	Illite
		7.68	7.68	Collapses	Gypsum
4.	555	15.22	15.22	10.41	Smectite
		7.86	7.86	Collapses	Gypsum
		7.33	7.33	Collapses	Chlorite
5.	642	14.75	14.75	14.75	Chlorite
		7.26	7.26	Collapses	Chlorite
		10.25	10.25	10.25	Illite
		7.74	7.74	Collapses	Chlorite
6.	768	14.75	14.75	14.75	Chlorite
		7.26	7.26	7.26	

No.	Depth (m)	Untreated (Å)	Glycolated (Å)	Heated (Å)	Type of clay
		10.25	10.25	10.25	Illite
		7.74	7.74	Collapses	Gypsum
7.	882	14.62	14.62	14.62	Chlorite
		7.21	7.21	7.21	
		10.25	10.25	10.25	Illite
		7.74	7.74	7.74	Gypsum
8.	969	14.62	14.62	14.62	Chlorite
		7.21	7.21	7.21	
		10.25	10.25	10.25	Illite
		7.72	7.72	Collapses	Gypsum
9.	1065	14.59	14.59	14.59	Chlorite
		7.21	7.21	Collapses	
		7.72	7.72	Collapses	Gypsum
10.	1158	14.81	14.81	14.81	Chlorite
		7.25	7.25	Collapses	Chlorite
		7.87	7.87	Collapses	Gypsum
11.	1224	14.41	14.41	14.41	Chlorite
		7.15	7.15	Collapses	
		7.66	7.66	Collapses	Gypsum
12.	1356	14.46	14.46	14.46	Chlorite
		7.15	7.15	Collapses	
13.	1467	15.02	15.02	15.02	Chlorite
		7.28	7.28	Collapses	Chlorite
14.	1587	14.57	14.57	14.57	Chlorite
		7.17	7.17	Collapses	Chlorite
		10.23	10.23	10.23	Illite
		9.35	9.35	Collapses	Pyrophyllite
15.	1674	14.93	14.93	14.93	Chlorite
		7.26	7.26	Collapses	Chlorite
		7.83	7.83	Collapses	Chlorite
		6.52	6.52	6.52	
16.	1776	14.84	14.84	14.84	Chlorite
		7.26	7.26	Collapses	Chlorite
		10.27	10.27	10.27	Illite
		7.81	7.81	Collapses	Gypsum
17.	1866	17.90	17.90		Swelling-
		14.63	14.63	14.63	Chlorite
		7.23	7.23	Collapses	Chlorite
		10.24	10.24	10.24	Illite
		7.75	7.75	Collapses	Gypsum
18.	1956	14.63	14.63	14.63	Chlorite
		7.21	7.21	Collapses	Chlorite
		10.22	10.22	10.22	Illite
19.	2064	14.62	14.62	14.62	Chlorite
		7.23	7.23	Collapses	Chlorite
		10.22	10.22	10.22	Ilite

APPENDIX D: Chemistry analysis from surface samples

Table chemistry analysis from surface samples in Lahendong Field (Gondwana, 1988).

Code sample	**L-07**	**L-41**	**L-05**	**L-08**	**L-10**	**L-26b**	**L-12**	**L-01**	**L-02**	**L-29**	**L-34**	**L-17**	**L-04**	**L-14**	**L-21**	**L-09**
Depth (m)	**Surface**	**Surface**	**Surface**	**Surface**	**Surface**	**Surface**	**Surface**	**Surface**	**Surface**	**Surface**	**Surface**	**Surface**	**Surface**	**Surface**	**Surface**	**Surface**
SiO_2	71.92	66.52	63.09	57.9	55.11	53.78	52.62	51.83	50.71	49.96	49.23	47.66	47.44	57.17	54.91	54.73
TiO_2	0.16	0.53	0.6	0.75	0.76	0.9	0.81	0.95	0.93	0.77	0.91	0.83	0.71	0.66	0.84	0.8
Al_2O_3	14.77	15.51	18.21	18.63	18.19	17.89	18.93	19.49	20.2	19.97	19.77	19.57	19.19	17.14	17.86	18.95
Fe_2O_3	0.23	1.04	1.15	1.38	1.98	1.31	2.08	4.07	3.08	2.49	2.9	3.28	2.7	2.06	4.45	1.98
FeO	2.66	3.55	4.79	6.21	6.21	8.52	6.39	5.68	6.74	7.28	7.81	6.39	7.45	5.15	4.61	6.57
MnO	0.06	0.1	0.15	0.17	0.17	0.25	0.17	0.19	0.21	0.17	0.2	0.16	0.19	0.15	0.15	0.17
MgO	1.04	1.74	2.38	3.67	3.82	3.6	3.87	4.46	4.61	5.27	5.11	5.26	6.6	3.67	3.87	3.87
CaO	3.01	4.44	5.15	7.44	7.9	7.73	8.59	9.45	10.02	9.65	9.48	12.45	12.88	7.59	7.2	8.16
Na_2O	2.64	3.29	1.6	1.45	2.58	3.12	2.75	1.45	1.6	1.69	2.2	1.6	1.45	3	2	1.6
K_2O	2.57	2	1.94	1.5	1.35	0.8	1.41	0.8	0.8	0.55	0.65	0.8	0.3	2	2.11	1.71
P_2O_5	0.03	0.1	0.05	0.06	0.03	0.02	0.04	0.06	0.05	0.07	0.08	0.03	0.06	0.04	0.05	0.06
SO_3	0.03	0.07	0.05	0.04	0.04	0.05	0.06	0.05	0.03	0.05	0.04	0.05	0.03	0.05	0.08	0.07
H_2O^+	0.08	0.12	0.12	0.11	0.34	0.1	0.17	0.08	0.13	0.19	0.1	0.19	0.18	0.04	0.23	0.12
H_2O^-	0.13	0.14	0.17	0.1	0.24	0.33	0.54	0.69	0.22	0.63	0.5	0.96	0.19	0.74	0.88	0.17
H.D	0.54	0.64	0.72	0.86	1.68	1.56	1.61	1.43	0.95	1.74	1.48	1.83	1.04	1.2	1.77	1.02
Total	99.87	99.79	100.17	100.27	100.4	99.96	100.04	100.68	100.28	99.99	100.46	101.06	100.41	100.66	101.01	99.98

APPENDIX E: Lithological description and hydrothermal alteration minerals of drill cuttings

Well LHD-23: Lithological description and hydrothermal alteration minerals of drill cuttings

The description is a combination of binocular and petrographic analysis. Hydrothermal alteration minerals given for each rock type is based on binocular and petrographic microscopes, X-ray diffraction and electron microprobe analysis.

15-25 m (15-25 mTVD) (875 – 860 masl) Tuff breccia
Tuff breccia, a mixture of tuff and crystallized andesite, slightly altered, grayish white to white in the upper part and becomes more yellowish in the deeper part, pyrite disseminated in the rock and fracture fillings.
Alteration minerals: calcite, pyrite, sulphur (?).

25-35 m (25-35 mTVD) (860 – 775 masl) Basaltic andesite
Crystallized basaltic andesite, predominantly darkish grey, slightly altered, plagioclase and pyroxene porphyritic in a microcrystalline groundmass, and becomes slightly mixed with tuff in the lower part. The rock is oxidized in some locations.
Alteration minerals: calcite, pyrite, oxides.

35-50 m (35-50 mTVD) (775 - 835 masl) Tuff breccia
Tuff breccia, made up of a mixture of dominant tuff and crystallized andesite, slightly to moderately altered, showing open vesicles and some vesicles filled by calcite and pyrite. Intense oxidation appears almost in the whole rock.
Alteration minerals: calcite, pyrite, oxidation.

50 – 110 m (50 – 110 mTVD) (835 - 775 masl) Basaltic Andesite
Plagioclase-pyroxene porphyritic basaltic andesite is slightly altered in the bottom and upper part but more fresh in the middle, opaque minerals common in the groundmass. Clay is starting to alter the groundmass and plagioclase alters to clay and calcite as observed in thin section.
Alteration minerals: pyrite, iron oxide, calcite

115 – 130 m (115 – 130 mTVD) (775 – 755 masl) Tuff
Tuff is white, yellowish green to grey in colour, fragmental. The tuff is highly altered mainly to clay with small evenly distributed pyrite. Crystallized andesite is more common in the upper part but tuff dominates below.
Alteration minerals: smectite, pyrite.

130 – 175 m (130 – 175 mTVD) (755 - 685 masl) Basaltic andesite
Basaltic andesite, greyish to darkish grey, slightly altered, plagioclase-pyroxene porphyritic set in the microcrystalline groundmass. The rock shows slight oxidation, and has some veins filled by calcite, quartz and pyrite.
Alteration minerals: smectite, calcite, pyrite, quartz.

175 – 200 m (175 – 200 mTVD) (710 – 685 masl) Tuff breccia
Tuff breccia, greyish green to whitish, highly altered, a mixture with crystallized basaltic andesite, predominantly tuff, pyrite dominant vesicles are often open but also, as the veins, filled with calcite, quartz, and pyrite. Thin section at 185 m depth shows that the primary rock of plagioclase and pyroxene phenocrysts is slightly altered to calcite and clay.
Alteration minerals: smectite, calcite, quartz, pyrite.

200 – 220 m (200 – 220 mTVD) (685 – 665 masl) Basaltic andesite lava
Basaltic andesite lava, porphyritic texture of plagioclase and pyroxene in a plagioclase and pyroxene groundmass, some oxidation in the upper part but decreases downward, greyish to reddish coloured alteration but the rock is overall fresh to slightly altered.
Alteration minerals: smectite, calcite, quartz, pyrite, oxidation.

220 – 320 m (220 – 320 mTVD) (665 – 565 masl) Basaltic andesite lava
Basaltic andesite lava, predominantly blackish grey, highly plagioclase-pyroxene porphyritic, relatively fresh to weakly altered, microcrystalline groundmass that contains opaque minerals, plagioclase and pyroxene. Rare calcite and pyrite, found a few veins with calcite and pyrite. Only minor increase in alteration compared to the unit above.
Alteration minerals: smectite, calcite, pyrite, quartz.

320 – 408 m (320 – 408 mTVD) (565 – 477 masl) Tuff
Tuff, whitish, greenish and grayish in colour, very soft and highly altered to clay. The tuff seems to have two textures (fine grain light colour and course grained darker colour). Minor amount of crystallized fresh looking plagioclase-pyroxene porphyritic andesite fragments. Yellow coloured probable sulphur is found in the middle part, at 338 and 389 m depth. Veins and vesicles are filled by quartz, calcite and pyrite. The first appearance of chlorite is identified based on XRD analysis at depth 395 m.
Alteration minerals: smectite, calcite, pyrite, quartz, kaolinite, chlorite, sulphur.

408 - 423 m (408 - 423 mTVD) (477 – 462 masl) Tuff
Tuff, whitish to greenish white, clear fragmental texture, intermediate to highly altered. It is dominantly glassy material mixed up with lithic vesiculer fragments. Veins filled by quartz, calcite and pyrite. Chlorite is recognized from XRD at depth of 419 m.
Alteration minerals: smectite, calcite, pyrite, quartz, chlorite

423 – 659 m (423 – 637 mTVD) (462 - 247 masl) Basaltic andesite lava
Basaltic andesite is dark grey, plagioclase-pyroxene porphyritic in a microcrystalline groundmass of pyroxene, plagioclase and opaques. Alteration increases between 530 m and 545 m seen by the alteration of the phenocrysts. In this depth range, minor tuff appears mixed with the basaltic andesite. Alteration decreases again below 545 m thin section at 425 and 536 m depths showing that plagioclase and pyroxene become altered to smectite, calcite, chlorite and illite.
Alteration minerals: smectite, calcite, pyrite, quartz, chlorite, chalcedony, illite.

659 – 692 m (637 – 663 mTVD) (247 – 221 masl) Tuff breccia
Tuff breccia, predominantly whitish grey and greenish grey, consists of vitric tuff and vitric crystal tuff of plagioclase fragments and crystallized basaltic andesite. The rock is moderately altered. Local choritisation and silicification occur in some samples, glass is altered mostly to chlorite. Anhydrite, illite, calcite and quartz replace plagioclase. The rocks mixed with a minor amount of porphyritic basaltic andesite, slightly altered, probably derived from the formation above. Thin section at 659 m depth shows that glass alters to clay, plagioclase is replaced by quartz, calcite and illite, pyroxene altered to illite and opaque is altered to sphene.
Alteration minerals: smectite, calcite, pyrite, quartz, chlorite, illite.

692 – 830 m (663 – 771 mTVD) (247 – 114 masl) Breccia
Breccia, whitish green to darkish grey, consists of a mixture of basaltic andesite and vitric tuff. Basaltic andesite is plagioclase and pyroxene porphyritic in the groundmass of microcrystalline plagioclase and pyroxene. Tuff is altered. Veins are filled by quartz, pyrite and calcite and may indicate a fracture system at that depth. Plagioclase phenocrysts are altered to calcite, quartz, anhydrite, and illite, while pyroxene only seems to alter to illite. Some opaque minerals are starting to alter to sphene and glass is altered to chlorite. Illite was also recognized from XRD at that depth range. At depth 752 m to 767 m, the rock is basaltic andesite, darkish grey, plagioclase and phenocryst porphyritic, consisting of a small fracture that was filled by pyrite and quartz. Slight number of iron oxide is found in the above and below parts.
Alteration minerals: calcite, pyrite, quartz, illite, chlorite, sphene, wairakite.

830 – 863 m (771 – 797 mTVD) (114 – 88 masl) Basaltic andesite lava
Basaltic andesite lava, darkish grey, the texture is plagioclase-pyroxene porphyritic,in the aphanitic groundmass. Pyroxene fenocrysts are slightly altered. Oxidation is found at the top, middle and in the

bottom part of the layer. A number of voids are found in the lower part mostly filled by clay (smectite-chlorite) and veins filled by quartz, calcite and pyrite.
Alteration minerals: calcite, pyrite, quartz, chlorite, sphene, wairakite, anhydrite, illite.

863 – 911 m (797 – 835 mTVD) (88 – 51 masl) Basaltic andesite lava
Compact basaltic andesite lava is darkish grey, plagioclase and pyroxene porphyritic texture, in the groundmass of microporphyritic material. The rock is slightly altered with some fine sized disseminated pyrite in the groundmass of the rock along with some oxidation. Below 890 m to 899 m the rock is more compact and fresh to slightly altered looking, some moderately altered tuff is found at 863 m - 869 m (88-83 masl) and 902 - 911 m (56-51 masl). The tuff may indicate division between individual lava flows. Thin section analysis from depth of 869 m shows plagioclase altered to calcite, illite and chlorite. Anhydrite and quartz also replace plagioclase, whereas pyroxene is mostly altered to calcite and chlorite.
Alteration minerals: calcite, pyrite, quartz, chlorite, anhydrite, illite, sphene

911 – 923 m (835 – 845 mTVD) (51 – 39 masl) Basaltic andesite lava
Basaltic andesite lava is plagioclase and pyroxene porphyritic. Pyroxene is more common than in the formation above. It is grayish in colour and is fresher than units above and below. Rare pyrite embedded in the groundmass. The rock is a possible intrusion.
Alteration minerals: calcite, pyrite, quartz, smectite

923 – 956 m (845 – 872 mTVD) (39 – 13 masl) Basaltic andesite lava
Basaltic andesite lava is plagioclase and pyroxene porphyritic in the microporphyritic plagioclase and pyroxene groundmass. The alteration increases below 947 m where the colour changes to more greyish green Minor amount of veins are filled by quartz, calcite and pyrite. Thin section at 956 m depth shows that the rock is altered, common hydrothermal alteration minerals especially as replacements of primary minerals, glass is highly altered, plagioclase is altered to calcite, anhydrite, chlorite, quartz, sphene, epidote, albite and illite, pyroxene is altered to chlorite and calcite. The paragenetic sequence in vesicles shows that anhydrite and epidote form early followed by wairakite and quartz.
Alteration minerals: calcite, pyrite, quartz, chlorite, illite, wairakite, anhydrite, albite, sphene, epidote.

956 – 980 m (872 – 891 mTVD) (13 to -7 masl) Tuff breccia
Tuff breccia, whitish to greenish white, fragmental, consisting of lithic fragments of andesite in the groundmass of volcanic glass. Veins are filled by pyrite, calcite and quartz, small cubic pyrite, quartz and intermittent epidote.
Alteration minerals: sphene, calcite, pyrite, quartz, chlorite, illite, wairakte, trace of epidote.

980 – 983 m (891 – 894 mTVD) (-7 to -9 masl) Basaltic andesite intrusion
Basaltic andesite, predominantly greenish, plagioclase-pyroxene porphyritic in an aphanitic groundmass. It is slightly alteredIt is considered to be a possible intrusion.
Alteration minerals: calcite, pyrite, quartz, chlorite.

983 – 1019 m (894 – 924 mTVD) (-9 to -39 masl) Breccia
Plagioclase porphyritic basaltic andesite breccia may be a continuation of the one above the intrusion. It is predominantly whitish grey to greyish green and consists of a mixture of crystallized basaltic andesite and glass tuff. The rock is highly altered with veins and vesicles mostly filled by calcite, pyrite, epidote, anhydrite and quartz. Fine crystals of pyrite are found disseminated in the rock, a trace of anhedral epidote is found intermittently below this depth. Under thin section at depth 956 m, the primary minerals of plagioclase are altered to calcite, anhydrite, chlorite, quartz, epidote, albite and illite. Pyroxene is altered to calcite and chlorite while opaques are altered to sphene. Paragenesis mineral sequence in voids shows anhydrite > epidote > wairakite.
Alteration minerals: calcite, pyrite and quartz, epidote, albite, sphene, illite, chlorite.

1019-1040 m (924 – 941 mTVD) (-39 to -57 masl) Breccia
Plagioclase-pyroxene porphyritic in a microcrystalline groundmass, it is a mixture of crystallized rock and tuff. The rock is yellowish in colour which may infer sulphur addition. The alteration of the primary minerals show plagioclase altered to calcite, anhydrite, quartz, illite, chlorite, wairakite, albite and illite. Pyroxene is altered to calcite, chlorite and intensively by anhydrite. Some of the fragments undergo silicification and pervasive calcification.
Alteration minerals: Sphene, calcite, pyrite, quartz, chlorite, illite, wairakite.

1040 – 1079 m (941 – 974 mTVD) (-57 to -89 masl) Breccias
Porphyritic basaltic andesite breccia, predominantly greenish grey, and consists of a mixture of crystallized rock and tuff. Small amount of pyrite is observed. The yellow colour of probable sulphur is drastically decreased compared to the formation below and above.
Alteration minerals: calcite, pyrite, quartz, chlorite, epidote.

1079 – 1088 m (974 – 982 mTVD) (-89 to -97 masl) Breccias
Plagioclase-pyroxene porphyritic basaltic andesite breccia, consisting of crystallized rock and tuff. It is brownish grey to greenish grey. Crystallized andesite becomes more common with depth. Under thin section at depth 1085 m, it shows that the primary mineral of plagioclase is altered to calcite, epidote, chlorite and illite, anhydrite replaces pyroxene, and commonly sphene alters opaque minerals. Some parts of the rock show illitisation and silicification.
Alteration minerals: sphene, calcite, pyrite, quartz, epidote, chlorite, illite.

1088 – 1148 m (982 – 1033 mTVD) (-97 to -148 masl) Basaltic andesite lava
Basaltic andesite is darkish grey to darkish green, pyroxene and plagioclase porphyritic with an aphanitic groundmass. The degree of alteration increases slightly with depth. The rock shows oxidation at the top and bottom of the sequence which may infer it as being an intrusion. The rock becomes more altered below 1115 m and becomes more greenish in colour possibly due to increasing chloritisation. Pyrite and quartz are found in vein fillings Thin section at depth 1109 to 1118 m shows that plagioclase is replaced by calcite, epidote, chlorite, anhydrite, albite and quartz, and illite and some epidote are also seen precipitating in the veins and vesicles. Illite is also a common replacement of the groundmass.
Alteration minerals: sphene, calcite, pyrite, quartz, chlorite, illite, wairakite, epidote, anhydrite.

1148 – 1169 m (1033 – 1051 mTVD) (-148 to -167 masl) Breccia
Plagioclase-pyroxene porphyritic basaltic andesite breccia, highly altered, greenish grey, fragmental texture, consists of a mixture between crystallized rock and tuff. It has undergone strong chloritisation, veins are filled by quartz, calcite, pyrite and oxides. Under thin section at depth 1157 m, it shows that calcite, chlorite, illite, albite, quartz and wairakite replace plagioclase and calcite also replaces pyroxene. Quartz and pyrite are seen deposited in veins. Sphene is abundant as a replacement of groundmass and opaques
Alteration minerals: sphene, calcite, pyrite, quartz, chlorite, illite, anhydrite, wairakite.

1169 – 1196 m (1051 – 1075 mTVD) (-167 to 190 masl) Tuff breccia
Tuff breccia, white to greenish white in colour, the white colour of tuff is dominant in the upper part and then decreases in the lower part. A porphyritic basaltic andesite that is possibly an intrusion, dark grey in colour and relatively fresh-slightly altered is found at 1187-1190 m depth. Probable rhyolite is found at 1193 m and 1196 m depths with pyrite and opaque mineral disseminated in the groundmass.
Alteration minerals: sphene, calcite, pyrite, quartz, chlorite, illite, epidote.

1196 – 1307 m (1075 – 1173 mTVD) (-190 to -288 masl) Basaltic Andesite lava
Porphyritic basaltic andesite, light to dark grey, to greenish grey, highly altered. Anhedral epidote found at 1235 m depth and becomes subhedral-euhedral crystals below 1274 m depth. Crystallized rock is dominant (90%) compared to tuff (< 10%) at depth below 1256 m. Under thin section at depth 1220 m shows that the primary minerals of plagioclase are intensively altered to chlorite, albite, epidote, illite, and quartz and pyroxene is altered to chlorite and calcite.
Alteration minerals: sphene, calcite, pyrite, quartz, chlorite, illite, wairakite, epidote.

1307 – 1316 m (1173 – 1180 mTVD) (-288 to -296 masl) Basaltic Andesite lava
Plagioclase-pyroxene porphyritic basaltic andesite with microcrystalline groundmass, highly altered. Pyrite disseminated in the rock and is sometimes associated with chlorite and quartz. Thin section at 1310 m depth shows that primary plagioclase is altered to epidote, calcite, albite, chlorite, illite and wairakite, and pyroxene is altered to chlorite, and opaques minerals altered to sphene.
Alteration minerals: sphene, calcite, pyrite, quartz, chlorite, illite, trace epidote.

1316 – 1352 m (1180 – 1212 mTVD) (-296 to -328 masl) Breccias
Breccia, highly altered, consist predominantly of crystallized rock relic texture of plagioclase and pyroxene phenocrysts in the afanitic groundmass of basaltic andesite. Epidote and quartz are found in the vesicles and the number of minerals increase with depth, pyrite is embedded in the rock and is sometimes associated with quartz.
Alteration minerals: sphene, calcite, pyrite, quartz, chlorite, illite, wairakite, epidote.

1352 – 1442 m (1212 – 1290 mTVD) (-328 to -405 masl) Rhyolite
Rhyolite, white coloured, the rock is very dominant in the sample between 90% to more than 95% and slightly mixed with a few number of altered andesite at about 5 to 10%. The rock is sparsely feldspar porphyritic, and seems to undergo high silicification in the groundmass. Sperulitic texture is commonly recognized in thin section at 1355 m.

At 1367 to 1373 m and 1409 to 1418 m depth, the rock changes pre dominantly to light greenish coloured andesite, , highly altered, feldspar porphyritic, where the phenocrysts are altered mostly to epidote and chlorite. At 1433 m the chlorite increases slightly and shows minor epidote. ICP analysis from depth 1421 m shows that SiO_2 content of the rock is about 78.78 wt% which is well within the rhyolite field. Thin section at depth 1355 m shows that primary minerals of feldspar altered to quartz, anhydrite, epidote, chlorite, and calcite. Calcite is commonly replacing the groundmass. A few veins were seen filled by epidote and quartz.
Alteration minerals: sphene, calcite, pyrite, quartz, chlorite, illite, anhydrite, epidote.

1442 – 1460 m (1290 – 1305 mTVD) (-405 to -420 masl) Rhyolite
Rhyolite, light green and highly altered, relict texture of feldspar phenocrysts being replace by epidote, in a much more dominating way compared to chlorite. ICP analysis at depth 1457 m shows that the rock has about 77.68 wt% of SiO_2 content in the sample.
Alteration minerals: sphene, calcite, pyrite, quartz, chlorite, illite, epidote.

1460 - 1472 m (1305 – 1314 mTVD) (-420 to -430 masl) Rhyolite
Andesite, highly altered, the colour of the rock is more greenish, predominantly feldspar porphyritic. Epidote and chlorite have become abundant. Thin section at 1466 m depth shows that the primary mineral of feldspar is altered to epidote, quartz and albite.
Alteration minerals: sphene, calcite, pyrite, quartz, chlorite, illite, epidote, albite.

1472 – 1499 m (1305 – 1337 mTVD) (-430 to -452 masl) Rhyolite
Rhyolite, slightly feldspar porphyritic, white and very altered. The amount of epidote decreases dramatically, the rock is obviously very siliceous, epidote becomes rarer below 1480 m depth.
Alteration minerals: sphene, pyrite, chalcopyrite, quartz, chlorite, illite, epidote.

1499 – 1655 m (1337 – 1456 mTVD) (-452 to -572 masl) Rhyolite
Rhyolite, light grey coloured, and strongly altered, it is plagioclase porphyritic in a groundmass of feldspar, quartz and opaque minerals. The opaques are mostly altered to sphene. Veins and vesicles are mostly filled by quartz, epidote and pyrite. Thin section analysis shows abundant anhydrite at 1514 m depth. Epidote is common at 1625 and 1640 m depths., At 1562 m depth a high refractive index mineral was found with parallel extinction and has one main cleavage direction and a relief higher than anhydrite. This mineral is proposed to be diaspore. At 1523 and 1586 m depths, ICP analysis of rocks shows composition 75.01 wt% and 74.52 wt%, respectively. This renders them as rhyolite rather than andesite.

Alteration minerals: sphene, pyrite, chalcopyrite, quartz, albite, anhydrite, chlorite, illite, epidote, diaspore.

1655-1658 m (1456 – 1458 mTVD) (-572 to -574 masl) Rhyolite
Rhyolite, whitish colour, highly altered. The colour of the rocks changes at this depth. The rock become much whiter in colour and the appearance of chlorite and epidote decrease a lot and becomes rare.
Alteration minerals: sphene, pyrite, quartz, chlorite, illite, epidote.

1658-1703 m (1458 – 1490 mTVD) (-574 to -606 masl) Rhyolite
Rhyolite, light grey, whitish grey, highly altered. It is feldspar porphyritic and set in a feldspar and quartz groundmass. Most of the groundmass is very silicieous. Thin section analysis petrographic at 1676 and 1691 m depths shows that the feldspar is altered to epidote, calcite, chlorite, illite, anhydrite and quartz. Opaques are altered to sphene.
Alteration minerals: sphene, calcite, pyrite, quartz, chlorite, illite, epidote.

1703-2000 m (1490 – 1693 mTVD) (-606 to -808 masl) No cuttings (Total circulation loss)

Well LHD-28: Lithologic description and hydrothermal alteration minerals of drill cuttings

The description is combined with the description from the thin section petrographic analysis. The list of hydrothermal alteration minerals given for each rock type is based on binocular, petrographic, X-ray diffraction and electron microprobe analyses (The cutting analyses above 300 m are partly based on Pertamina internal report).

35-66 m (35-66 mTVD) (796 – 763 masl) Andesite pyroclastics
Unconsolidated soft volcanic pyroclastic material, the rock is brownish to dark grey, with lithic fragments of andesite, pumice and glass. Some of the fragments have undergone surface oxidation and weathering.

66-114 m (66-114 mTVD) (763 - 717 masl) Breccia
Breccia, brownish to dark grey, fresh, consists of crystallized basaltic andesitic fragments, about 80% and tuff about 20%, some of the fragments have undergone oxidation and weathering.

114 -180 m (114 -180 mTVD) (717 - 651 masl) Breccia
Breccia, dark to brownish grey, consisting of crystallized fragments between 70-90% and tuff between 10-30%. The rock shows slight to intermediate alteration, some contain veins filled by quartz and pyrite. The basaltic andesite is pyroxene-plagioclase porphyritic in a groundmass of volcanic glass. The rock shows smectite and chlorite alteration. Plagioclase is predominantly slightly altered, mainly at the margin and along cleavage planes; pyroxene is altered to clay at the rim of the crystals.
Alteration minerals: smectite, pyrite, quartz, calcite

180-207 m (180-207 mTVD) (651 - 624 masl) Tuff breccia
Tuff breccia, grayish white, has a fragmental texture with a few fragments of crystallized rock but it is predominantly tuff, alteration intermediate showing smectite, calcite, quartz and pyrite. Few veins are filled with iron oxide.
Alteration minerals: smectite, calcite, pyrite and quartz

207-216 m (207-216 mTVD) (624 - 615 masl) Basaltic andesite lava
Basaltic andesite lava is dark grey, grey, plagioclase-pyroxene porphyritic in aphanitic groundmass, slightly altered to smectite, calcite and pyrite.
Alteration minerals: smectite, calcite, pyrite

216-225 m (216-225 mTVD) (615 - 606 masl) Breccia
Breccia, light grey, consist of 60% crystallized fragments and 40% tuff, moderately to highly altered, some of the veins are filled with quartz and pyrite.
Alteration minerals: smectite, calcite, pyrite, quartz.

225-261 m (225-261 mTVD) (606-570 m) Basaltic andesite lava
Basaltic andesite lava is dark-greyish to greenish, pyroxene-plagioclase porphyritic in a microcrystalline groundmass. Intermediate alteration, veins filled by quartz and smectite. Calcite alters the groundmass and also the plagioclase and pyroxene phenocrysts. Sphene is commonly replacing opaque minerals.
Alteration minerals: smectite, pyrite, quartz, calcite.

261-285 m (261-285 mTVD) (570-546 masl) Breccia
Breccia, greenish grey to, grey, the rock consists of crystallized fragments embedded in moderately to strongly altered tuff.
Alteration minerals: smectite, pyrite, quartz.

285-297 m (285-297 mTVD) (546-534 masl) Tuff breccia
Tuff breccia, light grey, predominantly made up of tuff with minor crystallized fragments. The rock shows intermediate to high alteration with dominant smectite, calcite, pyrite and quartz.
Alteration mineral: smectite, calcite, pyrite, quartz.

297-309 m (297-309mTVD) (534-522 masl) Breccia
Breccia, grey, greenish grey, porphyritic, consists predominantly of crystallized fragments in a tuff matrix. The rock is intermediately to strongly altered, veins and vesicles are filled by pyrite, quartz and calcite.
Alteration minerals: calcite, pyrite and quartz

309 – 402 m (309 – 402 mTVD) (522-429 masl) Tuff
The unit is dominantly tuff with minor crystallized fragments. Crystallized fragment is plagioclase and pyroxene porphyritic, the rock is greyish to white but becomes greenish in the middle part. Oxidation is observed; especially at about 384 m. Veins are notable in the middle part mostly filled by chalcedony quartz, calcite and pyrite. Thin section from 332 m shows calcite and smectite partially altering plagioclase and pyroxene, quartz also starts to replace plagioclase. Disseminated pyrite is also common in the tuff part of the rock.
Alteration mineral: pyrite, quartz, calcite, sphene, chalcedony, and chlorite.

402 – 459 m (402 – 459 mTVD) (429-372 masl) Basaltic andesite lava
Basaltic andesite, light to dark grey, the unit is predominantly porphyritic (plagioclase-pyroxene), basaltic andesite becoming more crystalline in the lower part. It is moderately altered, mostly to chlorite in the groundmass and the phenocrysts. Veins are common and filled by pyrite, calcite, quartz and chalcedony. Thin section from depth 434 m shows that the plagioclase phenocrysts are are only slightly altered to smectite, chlorite, calcite, quartz and pyrite. Pyroxene is dominantly altered to calcite at margin and along cleavage planes.
Alteration minerals: pyrite, quartz, calcite, sphene, chalcedony, and chlorite.

459 – 549 m (459 – 549 mTVD) (372-282 masl) Basaltic andesite lava
Basaltic andesite, dark greenish, dominantly pyroxene and plagioclase porphyritic in a microcrystalline groundmass.Thin section from depth 533 m shows that plagioclase has altered to different type of secondary minerals such as calcite, smectite, quartz, pyrite, epidote and illite, while pyroxene is largely fresh.
Alteration mineral: pyrite, quartz, calcite, chalcedony, sphene, anhedral epidote.

549 – 573 m (549 – 572 mTVD) (282-259 masl) Tuff breccia
Tuff breccia, greyish white, fragmental, consists of mixture of tuff and crystallized fragments, small pyrite crystals very abundant with small size, some cubically big sized, euhedral and filling in the

veins, few number of phenocryst of plagioclase and pyroxene altered to green clay. Starting at 558 m, the colour of the rock change to predominantly greyish green, chlorite clay starts to appear commonly. Trace of anhedral epidote is appearing in this unit.
Alteration minerals: sphene, calcite, quartz, chalcedony, pyrite, chlorite.

573 – 654 m (572 – 651 mTVD) (259-180 masl) Breccia
The rock consists of a mixture of greenish crystallized andesite and tuff in various proportions with the tuff becoming more dominant at deeper levels. Some of the basaltic andesite has porphyritic and vesicular texture. Pyrite, quartz, anhedral epidote and calcite fill the veins and vesicles. Chlorite also precipitates and fills in the vesicles commonly preceeded by chalcedony. Thin section at 632 m shows that glass alters to smectite, chlorite and illite and calcite. Chlorite, calcite, quartz, wairakite and illite commonly replace plagioclase; pyroxene is altered to chlorite and opaques replaced by sphene.
Alteration minerals: sphene, calcite, pyrite, quartz, chlorite, chalcedony, epidote.

654 – 662 m (651-658 mTVD) (180-173 masl) Basaltic andesite lava
Basaltic andesite is plagioclase and pyroxene porphyritic. The rock shows some oxidation. The rock is looks fresh to slightly altered.
Alteration minerals: sphene, smectite, calcite, pyrite, quartz, chlorite.

662 – 729 m (658-721 mTVD) (173-110 masl) Breccia
Breccia, consisting of a mixture of crystallized basaltic andesite and tuff with various ratios between 60 to 90 % crystallized. Basaltic andesite is pyroxene-plagioclase porphyritic in the aphanitic groundmass. The rock is greyish white to green, highly altered and shows some vesicular texture, which is filled by chlorite and epidote. Pyrite is common in the ground mass and some veins and vesicles. Subhedral epidote starts to form both as vesicular fillings and replacing plagioclase.
Alteration mineral: sphene, calcite, pyrite, quartz, chlorite, chalcedony, epidote.

729 – 741 m (721-732 mTVD) (110-99 masl) Breccia
Breccia, consisting of a mixture of plagioclase-pyroxene porphyritic crystallized fragments and tuff. The rock is dark - greyish green coloured. Veins are filled with pyrite, quartz and chalcedony. Hematite may appear at depth 741 m. Thin section shows that the rock has a porphyritic texture and is vesicular. Glass is altered to clay and calcite. Primary minerals of plagioclase commonly altered to pyrite, chlorite, quartz, calcite, albite, anhydrite and a few of them to epidote and wairakite. Pyroxene is altered to chlorite and illite, and opaques to sphene. Vesicles are commonly filled by chalcedony and chlorite as the earlier stage of paragenesis and followed by wairakite at the later stage.
Alteration minerals: sphene, calcite, pyrite, quartz, chlorite, chalcedony, epidote.

741 – 879 m (732-855 mTVD) (99 to -24 masl) Basaltic andesite lava
Basaltic andesite, greyish green, altered, porphyritic, phenocryst of plagioclase is sometimes altered to epidote, and pyroxene to chlorite. The vesicular texture of basaltic andesite is predominantly filled by chlorite but also some by epidote and chlorite. Anhydrite appears intermittently in the some depth. Wairakite is also commonly found precipitating in the vesicles. Thin section at 834 m shows that some of the rock shows a common precipitation of quartz. Plagioclase is altered to calcite, albite, chlorite, quartz, anhydrite and illite. Pyroxene is completely altered to chlorite, while opaques are altered to sphene. Mineral sequence shows that chalcedony > chlorite deposition is earlier than epidote > quartz.
Alteration minerals: sphene, quartz, chlorite, epidote, calcite, chalcedony, pyrite, illite, wairakite, and anhydrite.

879 – 950 m (855-915 mTVD) (-24 to -84 masl) Breccia
Breccia, greyish green, grey, strongly altered, predominantly made up of crystallized plagioclase-pyroxene porphyritic basaltic andesite and vesicular pyroclastic tuff. The rock is locally intensely chloritized. Vesicles are mainly filled with chalcedony, chlorite and epidote. The feldspar phenocrysts are often altered to epidote. Thin sections at depth 882 m and 933 m, shows that glass is altered to clay and quartz, plagioclase is altered to quartz, epidote, calcite, albite and chlorite,

pyroxene is altered to calcite, epidote, quartz and chlorite. Commonly sphene alters opaques minerals. In these thin sections, common epidote also forms in the vesicles. The depositional sequence at this depth is generally chalcedony > chlorite and at the later stage one may see quartz > epidote > calcite.
Alteration minerals: sphene, quartz, chlorite, epidote, calcite, chalcedony, wairakite, pyrite, and illite.

950 – 1014 m (915-967 mTVD) (-84 to -216 masl) Basaltic andesite lava
This rock is predominantly greyish green in colour, pyroxene-plagioclase porphyritic and vesicular texture. It is highly altered, almost all the vesicles are filled by chlorite and epidote. At 1008 to 1014 m, the well intersects a fresh looking andesite which due to its relative freshness is interpreted as an intrusion into the altered basaltic andesite. Thin section at depth 963 m and 1005 m shows that porphyritic texture of basaltic andesite becomes more dominant with depth and less vesicular. Plagioclase is altered to albite, epidote, illite, quartz, calcite, chlorite and anhydrite, while pyroxene is altered to chlorite and calcite. Sphene commonly alters opaque minerals. Vesicles are mostly filled by chalcedony and chlorite as the common paragenesis sequence in the early stage and epidote+quartz or quartz+calcite at a later stage. Veins are filled by epidote and quartz. Sphene and silicification are commonly found in the section.
Alteration minerals: sphene, quartz, chlorite, epidote, albite, calcite, chalcedony, pyrite, illite and anhydrite.

1014 – 1050 m (967-996 mTVD) (-105 to -165 masl) Basaltic Andesite lava
The rock is greyish green to reddish brown in colour, plagioclase and pyroxene porphyritic in a microcrystalline groundmass, the rock is quite vesicular mostly filled by chalcedony and chlorite and some filled by epidote. Epidote is also seen altering the plagioclase. Chalcedony also forms in the veins and is usually associated with quartz and pyrite. Thin section from depth 1032 m shows that the rock is altered; plagioclase is altered to illite, calcite, epidote, anhydrite, chlorite, albite and wairakite, while pyroxene may have altered to calcite and chlorite. Calcification in the rock is notable. The unit is a part of the top unit of basaltic andesite.
Alteration minerals: sphene, pyrirte, quartz, calcite, epidote, illite, chalcedony, and chlorite.

1050 – 1101 m (996-1037 mTVD) (-165 to -206 masl) Basaltic andesite lava
Basaltic andesite is greyish green, plagioclase-pyroxene porphyritic and somewhat vesicular. The porphyritic texture becomes dominant with depth. Vesicles are predominantly filled by chlorite.
Alteration minerals: sphene, pyrirte, quartz, calcite, epidote and chlorite.

1101 – 1152 m (1037-1077 mTVD) (-206 to 246 masl) Basaltic andesite lava
This basaltic andesite is grey to greenish coloured. It is plagioclase and pyroxene porphyritic in the microcrystalline groundmass of plagioclase and pyroxene, moderately altered. Chalcedony forms in the veins and is usually associated with quartz and pyrite. The rock shows oxidation in some parts. Thin section at depth 1132 m shows that plagioclase alters to albite, chlorite, anhydrite, calcite and epidote, while pyroxene is altered to chlorite and epidote. A few veins and vesicles are filled by anhydrite.
Alteration minerals: sphene, pyrite, quartz, epidote, chlorite, chalcedony, and calcite.

1152 – 1179 m (1077-1099 mTVD) (-246 to -268 masl) Breccia
Breccia, grey to greenish grey, consist of predominantly plagioclase and pyroxene porphyritic basaltic andesite in a microcrystalline plagioclase and pyroxene groundmass and tuff especially in the upper and bottom part of the layer. The layer is particularly silicic in the central part. Euhedral epidote is found in the lower part of the layer, especially as a replacement of the feldspar phenocrysts and vesicle and deposition. Thin section at depth 1173 m shows that calcification occurs in the groundmass and phenocryst of plagioclase. The glassy tuff is altered to illite, plagioclase altered to epidote, chlorite, calcite, quartz, albite and illite, while pyroxene and opaque minerals are altered to chlorite and sphene, respectively. The depositional sequence found in the veins and vesicles are chalcedony > chlorite+calcite and in the later stage may precipitate epidote and quartz.
Alteration mineral: sphene, pyrite, quartz, epidote, chlorite, chalcedony, illite, albite and calcite.

1179 – 1218 m (1099-1130 mTVD)(-268 to -300 masl) Basaltic andesite lava
Basaltic andesite is greenish grey to reddish brown, plagioclase and pyroxene porphyritic in the groundmass of microcrystalline plagioclase and pyroxene. The rock is highly altered. The rock is variably oxidized, highest in the middle but diminishing to top and bottom.
Alteration minerals: sphene, pyrite, quartz, epidote, chlorite, chalcedony and calcite.

1218 – 1245 m (1130-1153 mTVD) (-300 to -319 masl) Breccia
Breccia, greenish grey, highly altered in the upper part but less below. Variable mixture of crystallized versus tuff, though is dominant in the upper part. The rock is plagioclase and pyroxene porphyritic of basaltic andesite set in the microcrystalline groundmass. Thin section at 1233 m shows that illite, albite and quartz predominantly replace plagioclase, pyroxene is altered to illite and chlorite, opaque minerals are altered to sphene. Pyrite is relatively rare.
Alteration minerals: sphene, pyrite, quartz, epidote, chlorite, illite and calcite, albite.

1245 – 1269 m (1153-1172 mTVD) (-319 to -341 masl) Basaltic andesite lava
Basaltic andesite is darkish grey, plagioclase-pyroxene porphyritic, compact, and relatively fresh looking. The rock is considered to be an intrusion. Oxidation is notable around this rock which may be due to heating from the intrusion. A few vesicle near the bottom are filled with epidote,.
Alteration minerals: sphene, pyrite, quartz, epidote, chlorite, illite and calcite.

1269 – 1293 m (1172-1191 mTVD) (-341 to -360 masl) Breccia
Breccia, grey, greenish grey, very altered, consisting of a mixture of crysallized basaltic andesite and tuff. The crystallized fragments are more dominant (70%) than tuff (30%). A dramatic increase occurs here in alteration. Thin section at depth 1293 m shows that the glass tuff is mostly altered to clay, calcite is altering the groundmass and phenocryst of plagioclase. Other secondary minerals including epidote, albite, quartz and chlorite are also seen altering plagioclase. Pyroxene is commonly altered to chlorite and quartz, while opaque minerals are altered to sphene.
Alteration minerals: sphene, pyrite, quartz, epidote, chlorite, illite and calcite.

1293 – 1305 m (1191-1200 mTVD) (-360 to -369 masl) Rhyolite
Rhyolite is predominantly greyish to white coloured, highly altered, sparsely plagioclase porphyritic. The phenocrysts are completely altered to clay. A few veins are found with chlorite filling in the veins.
Alteration minerals: sphene, pyrite, calcite, quartz, epidote, chlorite.

1305 – 1335 m (1200-1225 mTVD) (-369 to -394 masl) Breccia
Breccia is greyish green to reddish brown. The rock is a mixture of crystallized basaltic andesite and tuff, where the crystallized part is dominant within a range of 70% to 90%. The rock is plagioclase and pyroxene porphyritic. Epidote replaces plagioclase and deposits in the vesicles. Under petrographic thin section at depth 1335 m, epidote is very abundant; the abundant quartz may indicate secondary silification. Plagioclase is altered to chlorite, epidote, wairakite and albite, pyroxene may alter to chlorite and opaques are altered to sphene.
Alteration mineral: sphene, pyrite, calcite, quartz, epidote, wairakite, albite, chlorite.

1335 – 1371 m (1225-1256 mTVD) (-394 to 425 masl) Basaltic andesite lava
Sparsely porphyritic basaltic andesite, light green coloured. Most of the plagioclase is altered to epidote and quartz, and some epidote also forms in the veins and vesicles.
Alteration minerals: sphene, pyrite, calcite, quartz, epidote, chlorite.

1371 – 1392 m (1256-1273 mTVD) (-425 to -439 masl) Breccia
Breccia is greyish green to greenish white coloured. Crystallized fragments are dominant (70-90%). A fraction of the cuttings are mildly altered plagioclase-pyroxene porphyritic basaltic andesite at 1380-1398 m which may indicate a minor intrusion there. Chlorite mostly forms in the vesicles. Under thin section at depth 1386 m, plagioclase is altered to epidote, quartz, albite and chlorite. Opaques are altered to sphene. Epidote is abundant at this depth as vein and vesicle fillings and also replacing plagioclase.

Alteration minerals: albite, sphene, pyrite, calcite, quartz, epidote, chlorite.

1392 – 1400 m (1273-1280 mTVD) (-439 to -449 masl) Basaltic andesite lava
Basaltic andesite, dark grey to greenish, highly altered. Most of the rock is massive. The rock has the green colour of chlorite, and epidote replaces plagioclase.
Alteration minerals: sphene, pyrite, calcite, quartz, epidote, chlorite.

1400 – 1434 m(1280-1307 mTVD) (-449 to -476 masl) Breccia
Breccia is whitish to greenish grey. It is a basaltic andesite plagioclase-pyroxene porphyritic rock and a mixture of crystallized and tuffaceous fraction. It is highly altered. Quartz, pyrite chlorite and epidote form in veins and vesicles. Under thin section at depth 1431 m, the rock seems to be silicified, all the phenocrysts are completely altered, plagioclase altered to epidote, calcite, chlorite, quartz and albite, while pyroxene is altered to chlorite and illite and opaque minerals are altered to sphene. Euhedral epidote also forms in the vesicles. A simple depositional sequence of epidote>quartz is found at this depth.
Alteration minerals: sphene, pyrite, calcite, quartz, epidote, chlorite, illite, albite.

1434 – 1473 m (1307-1339 mTVD) (-476 to -508 masl) Basaltic andesite lava
Basaltic andesite is greyish green to reddish in colour. It is predominantly feldspar porphyritic and highly altered. The colour becomes lighter below 1452 m and epidote increases. Vesicles are filled by chlorite, quartz, pyrite and euhedral epidote. A portion of the samples from **1449-1455** m are relatively fresh and may indicate the presence of an intrusion there.
Alteration minerals: sphene, pyrite, calcite, quartz, epidote, chlorite, illite, anhydrite.

1473 – 1515 m (1339-1372 mTVD) (-508 to -541 masl) Basaltic andesite lava
Basaltic andesite is grayish to greenish in colour. It is porphyritic in texture the rock is highly altered, mostly to chlorite, pyrite, epidote and quartz. Some fractures are filled with quartz, pyrite and chlorite. Relatively fresh compact andesite is found at **1476-1479** m depth and may be a minor intrusion.
Alteration minerals: sphene, pyrite, calcite, quartz, epidote, chlorite, anhydrite.

1515 – 1554 m (1372-1396 mTVD) (-541 to -573 masl) Basaltic andesite lava
Basaltic andesite, greenish, greenish grey, highly altered, plagioclase and pyroxene porphyrtic in amicrocrystalline groundmass. The rock shows also vesicular texture, and most of the vesicles are filled by chlorite. The vesicular texture decreases with depth and crystallized rocks becomes more dominant. Euhedral epidote is very abundant in this sequence associated with quartz. Under thin section at depth 1533 m and 1542 m the rock is highly altered, spherulitic texture appears and tuff fragments, which may indicate rhyolitic composition. Epidote is very abundant, calcite rare. Epidote, quartz and chlorite fill the vesicles; common euhedral crystals of epidote are associated with quartz. Plagioclase is commonly altered to epidote, albite, chlorite and quartz. Pyroxene is altered to epidote, chlorite and actinolite, while opaques alter to sphene. Paragenesis sequence of wollastonite>epidote and epidote>calcite is found in the depth.
Alteration minerals: sphene, pyrite, calcite, quartz, epidote, chlorite, albite, anhydrite, actinolite, wollastonite.

1554 – 1578 m (1372-1425 mTVD) (-573 to -594 masl) Breccia
Breccia, predominantly greenish to greenish grey coloured. The rock is porphyritic andesite, a mixture of tuff, and vesicular crystallized fragments. The rock is getting more compact with depth. Most of the vesicles are filled by chlorite.
Alteration minerals: sphene, pyrite, calcite, quartz, epidote, chlorite.

1578 – 1599 m (1425-1442 mTVD) (-594 to 611 masl) Rhyolite
Rhyolite is whitish coloured, highly altered. In this feldspar porphyritic, rhyolite is dominant. Epidote becomes much less abundant at this depth. Only a few examples of epidote replacements of feldspar are observed. Sulfides minerals are disseminated in the groundmass.
Alteration minerals: sphene, pyrite, calcite, quartz, epidote, chlorite.

1599 – 1731 m (1442-1550 mTVD) (-611 to 719 masl) Rhyolite lava
Rhyolite is greenish coloured, highly altered. It has a sparsely plagioclase porphyritic texture. At depths of 1689 m and 1692 m the greenish colour of alteration in the groundmass changes to more brownish gray. Some epidote forms in veins and vesicles and is there associated with quartz. Thin section analysis shows that plagioclase is replaced by epidote, chlorite, albite, quartz and illite. Common euhedral crystal of epidote appears, an abundance of quartz crystals as may an indication of silicification. Under thin section at depth 1632 m and 1692 m shows that the rock contain phenocryst that already altered to epidote and chlorite, some of the grain probably rhyolite marked by spherulitic texture, shows crystalline euhedral epidote, abundance of quartz probably an indication of silcification. Plagioclase commonly altered to illite, epidote, quartz, chlorite, anhydrite, albite, and pyroxene is altered to chlorite and epidote, and opaques to sphene.
Alteration minerals: sphene, albite, pyrite, calcite, quartz, epidote, chlorite, illite, ahydrite.

1731 – 1749 m (1550-1565 mTVD) (-719 to -734 msal) Breccia
Breccia, grey to greyish green, highly altered. A mixture of relatively fresh basaltic andesite is seen in the upper part of the depth interval suggesting a minor intrusion cutting through the breccias. Thin section shows that vesicles are filled by epidote and quartz, plagioclase is replaced by albite, illite, epidote, pyrite, quartz and few anhydrites. Under thin section petrography at depth 1732 m, primary minerals of plagioclase are altered to albite, illite, epidote, pyrite, quartz, anhydrite, pyroxene is altered to illite and chlorite, and opaques are altered to sphene. Illite is abundant, some epidote and quartz are also found filling the vesicles.
Alteration minerals: sphene, albite, pyrite, albite, calcite, quartz, epidote, chlorite, illite, anhydrite.

1749 – 1785 m (1565-1595 mTVD) (-734 to -764 masl) Rhyolite lava
Rhyolite, greyish green, highly altered (90%), feldspar porphyritic in a groundmass of feldspar, quartz and opaque minerals. The unit shows some indication of a little moderately altered andesite lava in the samples. Calcite is absent and different types of sulfides are seen but are not abundant. Under thin section at depth 1770 m, the rock seems siliceous; plagioclase is altered to illite, albite, epidote, quartz, and anhydrite, while opaques are altered to sphene.
Alteration mineral: sphene, pyrite, quartz, epidote, chlorite, illite, anhydrite, albite.

1785 – 1803 m (1595-1610 mTVD) (-764 to -779 masl) Rhyolite
Rhyolite, white to greenish white, highly altered, a few of opaque minerals are in the groundmass many of which are altered to sphene. The rock shows a small quantity of pyrite minerals disseminated in the groundmass.
Alteration minerals: sphene, pyrite, calcite, quartz, epidote, chlorite, illite.

1803 – 1902 m (1610-1692 mTVD) (-779 to -861 masl) Rhyolite lava
Rhyolite, white to greenish white, highly altered. This is a thick sequence of rhyolite, sparsely feldspar porphyritic, most of the phenocrysts have altered to epidote and some to chlorite. In thin section analysis, the rock shows that plagioclase is partly replaced by epidote, illite, quartz and albite. Some of the epidote is forms in the vesicles associated with quartz and sulfides. Some illite also alters the groundmass of the rock. Under thin section at depths 1833 and 1884 m, rock shows patches of feldspar porphyritic, some shows siliceous. Illite is altering the groundmass, some epidote forms in the vesicles of possibly secondary porosity. Plagioclase is to a minor extent altered to epidote, illite, quartz and albite, most of opaques are already altered to sphene. Common strongly fibrous minerals (illite) are sometimes associated with anhydrite,
Alteration minerals: sphene, pyrite, quartz, epidote, chlorite, illite, anhydrite, albite.

1902 – 1980 m (1692-1756 mTVD)(-866 to 925 masl) Rhyolite lava
Rhyolite, the rock is predominantly feldspar porphyritic, slightly mixed with tuff, greenish grey, highly altered to chlorite, epidote, illite, sphene, pyrite and quartz. The rock exhibits very siliceous as shown from thin section. The rock shows pervasive illitisation attacking the rock, some completely altering the rock phenocrysts. Albite, illite and quartz are common as alterations of plagioclase. Under thin section at depth 1932 m, plagioclase is altered to albite, illite, epidote, anhydrite and opaques are altered to sphene.

Alteration minerals: sphene, albite, pyrite, quartz, epidote, chlorite, illite, anhydrite.

1980 – 2007 m (1756-1779 mTVD) (-925 to -943 masl) No cuttings Total circulation loss

2007 – 2010 m (1779-1781 mTVD) (-943 to -948 masl) Rhyolite lava
Rhyolite, slightly mixed up with white rock fragments of probable tuff, greenish to whitish grey feldspar porphyritic, highly altered to chlorite, epidote, illite, sphene, pyrite and quartz.
Alteration minerals: sphene, pyrite, quartz, epidote, chlorite, illite.

2010 – 2025 m (1781-1794 mTVD)(-948 to -963 masl) No cuttings Total circulation loss

2025 – 2043 m (1794-1809 mTVD) (-963 to -978 masl) Rhyolite lava
Rhyolite, greenish grey, porphyritic, highly altered to chlorite, epidote, illite, sphene, pyrite and quartz. Under thin section at depth of 2031 m, the rock consists of feldspar porphyritic in a feldspar and quartz groundmass, opaque minerals common in the groundmass, the phenocrysts of the rock are highly altered, primary minerals of plagioclase is altered to albite with or without twinning, calcite, quartz, illite and epidote, illite and anhydrite, and opaque minerals are altered to sphene. Illite commonly alters groundmass and phenocryst.
Alteration minerals: sphene, albite, pyrite, quartz, epidote, chlorite, illite, anhydrite.

2043 – 2058 m (1809-1821 mTVD) (-978 to -990 masl) No cuttings Total circulation loss

2058 – 2070 m (1821-1831 mTVD) (-990 to -1000 masl) Rhyolite lava
Rhyolite lava, greenish grey, porphyritic, highly altered to chlorite, epidote, illite, sphene, pyrite and quartz. The rock shows oxidation. Thin section analysis at depth 2064 m shows that the feldpar porphyritic is very dominant, the primary minerals of plagioclase are altered to epidote, quartz, albite and chlorite. Illitisation is commonly found in the rocks. Veins filled by anhydrite, quartz and adularia, also show that vesicles are filled by quartz and coarse grained and high birefringence clay which may be illite. The rock also shows spherulitic texture which may be an indication of more rhyolitic composition
Alteration minerals: sphene, pyrite, quartz, epidote, chlorite, illite, albite, adularia.

2070 – 2082 m (1831-1841 mTVD) (-1000 to -1008 masl) No cuttings Total circulation loss

2082 – 2085 m (1841-1844 mTVD) (-1008 to -1013 masl) Rhyolite lava
Rhyolite lava, the cuttings appear to be highly mixed but feldspar porphyritic is dominant, greenish grey to grey in colour. It is highly altered to chlorite, epidote, illite, sphene, pyrite and quartz. Under thin section petrographic at depth 2084 m, the primary plagioclase is altered to albite without twinning, epidote, anhydrite and illite.
Alteration mineral: sphene, pyrite, quartz, epidote, chlorite, illite, albite, anhydrite.

2085-2181 m (1844-1924 mTVD) (-1013 to -1093 masl) No cuttings Total circulation loss

APPENDIX F: Proceedings of World Geothermal Congress 2010

Proceedings World Geothermal Congress 2010,
Bali, Indonesia, 25-29 April 2010

Geothermal Model of the Lahendong Geothermal Field, Indonesia

Hary Koestono[1], Eben Ezer Siahaan[1], Marihot Silaban[1], Hjalti Franzson[2]
[1]Pertamina Geothermal Energy, Jakarta, Indonesia
[2]Iceland GeoSurvey, Reykjavik, Iceland

hary_ka@pertamina.com, eesiahaan@pgeindonesia.com, marihots@plasa.com, hf@isor.is

Keywords: Lahendong geothermal field, reservoir permeability, hydrothermal alteration, temperature.

ABSTRACT

Lahendong Geothermal Field is tectonically located in the northern neck arm of Sulawesi Island. The field is part of the depression of the Pangolombian caldera with clear structures in the eastern part but relatively open to the west. The depression of the Pangolombian caldera is being one of the most important with respect to the geothermal system in Lahendong. Thermal structures on surface are mostly fault controlled with a dominant NW-SE and NE-SW directions, and are believed to control the permeability of the Lahendong system. The Lahendong geothermal field is hot water dominated system divided into two reservoirs, the Southern and Northern one. A total of twenty three wells have been drilled into these reservoirs. The Southern one has temperatures of 300 to 350°C with about 80% dryness, and the northern one has lower temperatures between 250 to 280°C with around 30% dryness. Three main alteration zones are encountered in this field namely smectite, smectite-chlorite and illite-prehnite-epidote zones. The smectite zone is mainly characterized by the appearance of low temperature clay and a layer with resistivity <10 ohmm. The smectite-illite-chlorite zone is characterized by the appearance of an acid layer and illite-prehnite-epidote zone is characterized by the appearance of chlorite, epidote, prehnite, and secondary quartz. The temperature distribution shows that the interesting site for geothermal resource utilization in the field is located in the NW, W, and SW direction of well pad LHD-4 and W and SW direction of well pad LHD-5.

1. INTRODUCTION

Lahendong geothermal field is located about 30 km south of Manado, in the northern arm of Sulawesi Island (Figure 1). Sulawesi Island is formed due to an active subduction in the south eastern part (Mollusca sea) and northern part (Celebes sea).

Regionally, this field is located in the west margin of the Tondano Depression which extends about 20 km in north-south direction and opens to the west. Within this depression is the Pangolombian rim circular in shape and is an important structure in Lahendong geothermal system.

This geothermal field was discovered in 1982 and geological, geochemical and geophysical works has been conducted since that time. Three shallow wells were drilled around Linau Lake in the same year. From 1982 to 1987, Pertamina drilled 7 exploration wells LHD-1 and LHD-5 in the northern reservoir system, LHD-4 in the southern reservoir system and LHD-3, LHD-6 and LHD-7 in the boundary margin of the prospect area (Robert, 1987; Siahaan, 2005).

The development wells LHD-8 to LHD-16 in Lahendong geothermal field were drilled from 1991 to 1998 and the first 20MW power plant commenced in 2001. The development stage continued from 2005 to 2007; 7 production wells were drilled which generated 2 X 20 MW electricity for power plant Unit II and III and which commenced in 2007 and 2008.

The paper will discuss about the tectonic structure, hydrothermal alteration, reservoir, temperature, and the geothermal model of the system based on data from 23 wells. The geological data is mostly based on the cutting analysis of samples taken at 3 m interval. There are 7 production wells in well pad LHD-4 and LHD-13 are located in the southern block and 5 wells on pad LHD-5 in the northern block, whereas well pad LHD-7 in the eastern part is reinjection wells.

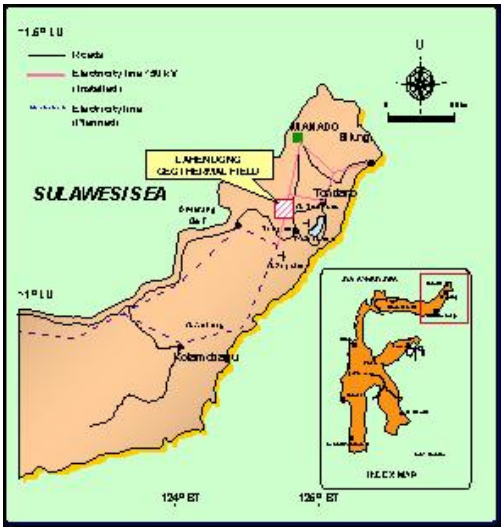

Figure 1. Location map of Lahendong Geothermal Field

2. GEOLOGICAL OUTLINE

2.1. Regional Geology

The geology of Lahendong consists of hyaloclastites and lava flows intercalated with sediment formation formed during Miocene time. The Tondano depression is the important structure in the area and formed due to the big eruption which occured in the Late Miocene or Early Pliocene time.

The stratigraphy of Lahendong geothermal field can be divided into 3 lithological units i.e. Pre-Tondano, Tondano and Post Tondano Units.

Post Tondano Unit is commonly found covering the upper part of the stratigraphy and comprises pumice, tuff and volcanic breccia in the upper part and basaltic andesite in the lower part.

The Post-Tondano unit consists of 2 sub-units, the Pra-Pangalombian and Post-Pangalombian Sub-units. The Pra-Pangalombian sub-unit mainly consists of basaltic andesite lava deposited in the northern and southern part of Pangalombian depression. The second sub-unit, the Post-Pangalombian, is composed of eruptions located in the central and peripheral of the depression. The chronological sequence from early to late deposition is described as basaltic andesite lava of Kasuratan, Linau breccia consisting of volcanic breccia and pyroclastic rock, Tampusu basaltic andesite lava and pyroclastic rock, product of Mt. Lengkoan andesitic lava, obsidian and tuff breccia, an altered ground located in the northern side of Kasuratan village extending to Pangalombian rim, in Leilem creek and in the eastern side of Lahendong village (Figure 2). Lake Linau and its crater rim were formed due to the hydrothermal eruption activities and is believed to be the centre of surface thermal manifestations in the field. (Siahaan, 2000).

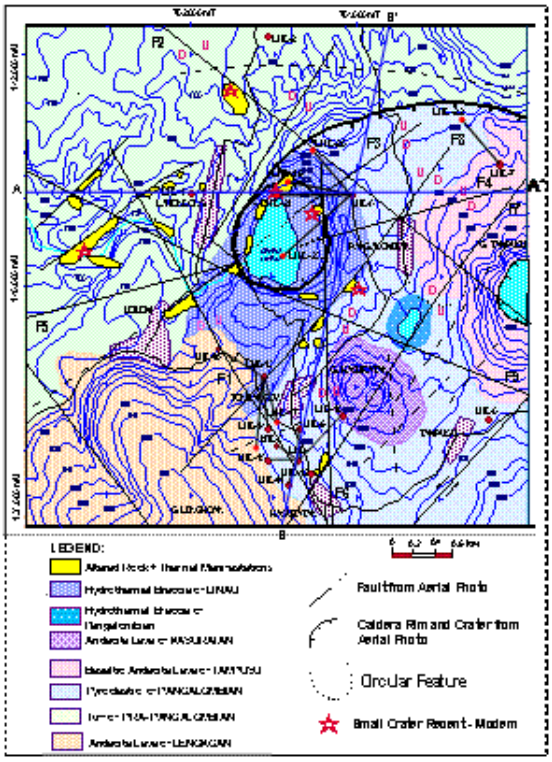

Figure 2. Geological and structural map of Lahendong geothermal field (Siahaan, 2000).

Tondano unit consist of rhyo-dacitic pumice rich ignimbrites in the upper part, whereas the influence of micro dioritic intrusion in the lower part makes it difficult to determined its true lithological character.

The last unit, the Pre-Tondano, consists of series of basaltic andesite, andesites, volcanic breccia, hyaloclastites and pyroclastic products.

The sedimentary formation includes limestone and silty marl with foraminifera identified on wells LHD-1, LHD-2 and LHD-3 (Robert, 1987).

2.2. Geochemistry

The surface manifestations that indicate a geothermal system in this field are such as hot springs, mud pools, fumaroles, and altered rock (Figure 3).

The Lahendong geothermal area can be divided into two groups of hot water based on their chemical characteristics of the Cl-B ratio as Lokon-Mahawu group and Lahendong-Tompaso group.

Lokon-Mahawu group is located in the Northern part and is characterized by low silica content and low temperature while the concentration of Ca, Mg and SO_4^{2-} is relatively high. The ratio of Cl/B in this group is higher than the second group. The second group is Lahendong-Tompaso group. This group is located in the middle and southern part of the field. The temperature estimation based on the gas geothermometry is around 322°C.

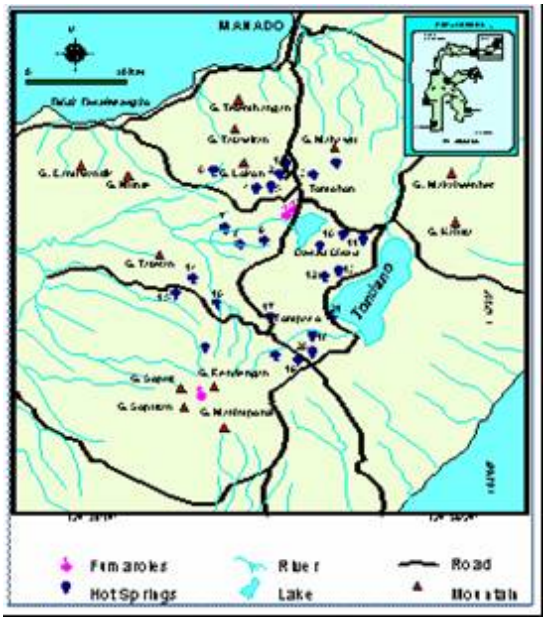

Figure 3. Map showing the distribution of surface manifestation in the field (Siahaan, 2000).

2.3. Geophysics

The geophysical methods used to assess the geothermal system are resistivity, MT and gravity and were conducted in this field since its discovery 1982.

The results of Schlumberger resistivity (AB/2=1000 m) and magnetotelluric (MT-5 EX) showed that the width of the geothermal prospect area identified by low resistivity anomaly (<10 ohmm) is around 15 to 25 km^2. This prospect area is centred around Linau Lake (Figure 5).

A detailed MT survey was done in 2008 by modelling of 3D MT inversion and showed an updome resistivity structure at around Linau Lake. The updome resistivity structure is characterized by the resistivity value of 20-60 ohmm which is interpreted as the propilitic zone. This zone is covered by the conductor resistivity structure with value <10 ohmm as the clay cap and part of the argillic zone (Raharjo, et.al, 2008).

3. TECTONIC STRUCTURE

The study on the distribution of the geological structure of the Lahendong Geothermal Field has been carried out by Pertamina since 1982. Ganda and Sunaryo (1982) mapped the geology of the area. Later in 1987, Geoservice studied the geology and structure of the field based on aerial photographs. Robert (1987) compiled the data of Geoservice together with the well data. Head on resistivity Survey was carried out by Pertamina in 1988. Aerial photograph, landsat interpretation and surface manifestation evaluation was done by Siahaan (2000).

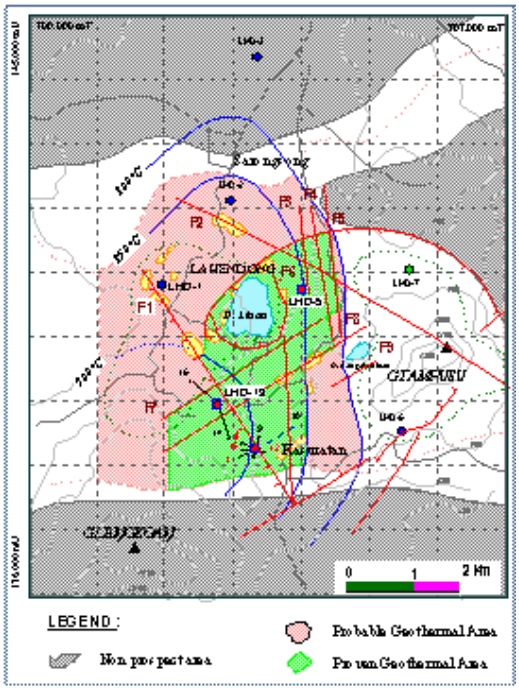

Figure 5. Geophysical map of the Lahendong prospect area (Siahaan, 2000)

Tectonically, five main structures were encountered in the Lahendong geothermal field. The structures are rim Pangolombian, faults striking NE-SW, E-W, NW-SE and N-S.

The Pangolombian structure is a caldera rim that is interpreted to provide good permeability in the field. The NE-SW fault structure is normal and lateral fault, acting as the major volcanic axis. The E-W fault structure is lateral and a transcurrent fault. The NW-SE fault and N-S faults are normal faults which are interpreted to provide good permeability to the geothermal system (Robert, 1987). The important faults structure controlling the geothermal systems in the field are F-1 in well pad LHD-4 and 13 and F-2 and Pangolombian rim for well pad LHD-5. These three well pads are production site, whereas well pad LHD-7 in the western part has the reinjection wells.

The geological structure and a cross section are shown in the Figure 2 and 6. Well LHD-1 and 2 intersects NW-SE fault and dipping SW at depths of 350 m and 650 m, respectively, but do not intersect the main structure at depth. No productive structure was intersected by well LHD-3. Well LHD-4 intersects the main F-1 structure at depth 2200-2250 m and well LHD-5 intersects the F-2 structure at 1170-1220 m (Figure 6). LHD-6 intersects a NW-SE F-9 fault at depth of 780 m but failed to intersect a permeable structure in the production part. Well LHD-7 intersects the Pangolombian Rim at depth 1950 m. No open fault structure is intersected by wells LHD-8, 11 and 12.

These are show low to no permeability due to silicification in the well fractures. Well LHD-10 intersects the F-6 fault and Well LHD-13 intersect F-1 fault (Azimudin and Hartanto, 1997). Well LHD-14 intersects F-1 fault at 1470 m. Well LHD-17 intersect F-8 fault at close to the surface. Well LHD-18 intersect F-1 fault at 1468 m. No circulation loss is found in well LHD-19. Well LHD-20 and 21 intersects F-2 fault at 1048 and 1355 m, respectively. Well LHD-22 intersects Pangolombian rim at 2107. Well LHD-23 intersects the Pangolombian rim at 1703-2000 m as indicated by total loss circulation and is an interesting target structure for northern part of the reservoir system in this field (Figure-6).

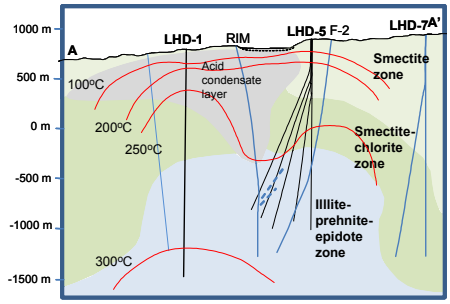

Figure 6. Cross section A-A' showing the wells, geological structures, temperature and alteration zones.

4. ALTERATIONS MINERALOGY

Hydrothermal minerals in Lahendong occur as replacements of primary minerals, replacement and deposition in vein and cavities. The replacement hydrothermal records the interactions between the wall rocks and the hydrothermal fluids, while space-filled minerals reflect the processes that affected the circulating fluid (Browne, 1988).

The subsurface lithology of the Lahendong Geothermal field is dominated by andesitic rocks except on the Tondano Unit that mostly comprises of rhyolitic type (Utami et al.,, 2005).

The alteration minerals at shallow depth are dominated by calcite, quartz, hematite and iron oxide. Anhydrite is formed by the partial replacement of plagioclase and pyroxene. Clay minerals commonly found are smectite and interlayered smectite-chlorite at shallow level. Chlorite relatively more common found than illite (Utami, et. al, 2005).

In the depths of the reservoir, epidote appears at depth around 133 mbsl in well LHD-1, 115 to 200 mbsl in the pad LHD-4, 120 to 240 mbsl at pad LHD-5 and deeper towards the pad of LHD-13 where epidote is found at depth of about 400 to 500 mbsl (Figure 7), indicating an underlying hot propylitic zone. Epidote is found at temperature more than 240°C-250°C (Browne, 1978). Deeper down in the wells LHD-4, 10, 12 and 13, silicification occurs that probably results in sealing the permeability marked by the low permeability in these wells.

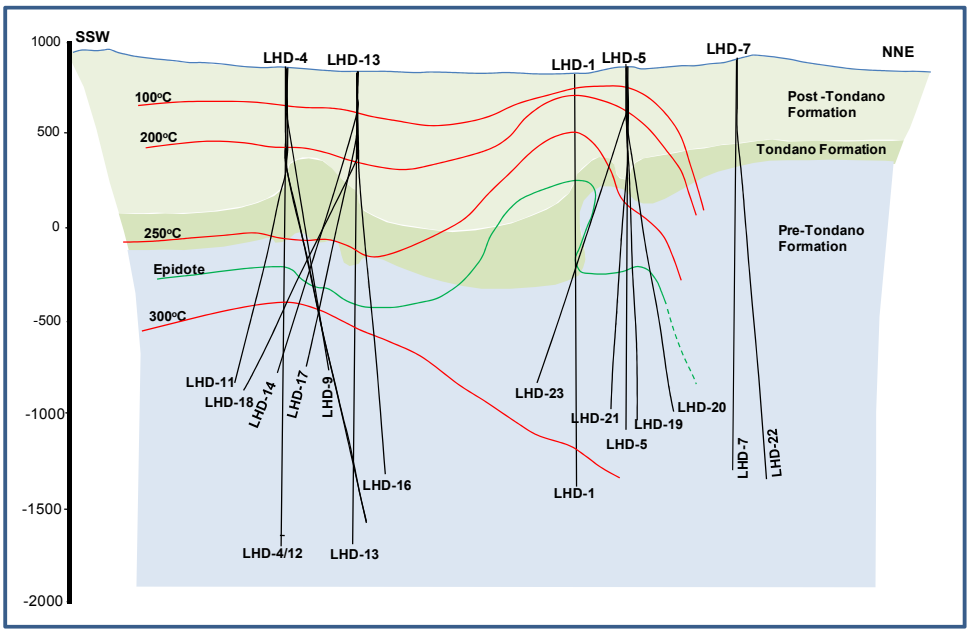

Figure 7. Cross section along B-B' showing the different formation, temperature distribution and depth of the the first appearance of epidote.

5. RESERVOIR

The important factor in the reservoir of a geothermal system is the permeability and this is controlled by the faults system. The reservoir rock found in the Lahendong geothermal system is mostly andesite, a part of the unit of Pre-Tondano.

The reservoir system of the Lahendong geothermal field is divided into two systems, the Southern and Northern one. The Southern one has temperatures of 300 to 350°C with dryness about 80%, and the northern one has lower temperatures between 250 to 280°C with dryness around 30%. These two blocks are separated by a structure trending N-S and interpreted to be acting as the pressure barrier.

Some of the well data shows the existence of a shallow reservoir. The shallow reservoir in this field is encountered at a depth about 400 to 700 m. A shallow reservoir is found at a depth of about 650 m in well LHD-1, LHD-2, pad LHD-4 and 5 indicating lateral outflow from a shallow aquifer (Robert, 1987, Siahaan, 2003; Siahaan, 2005).

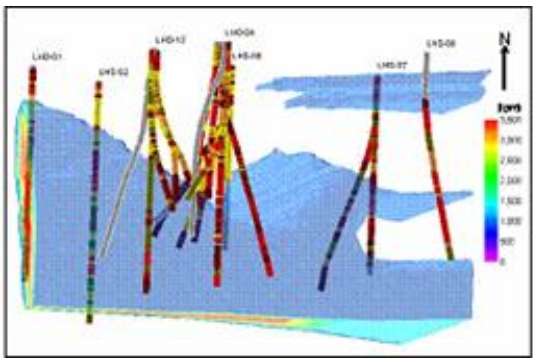

Figure 8. Section E-W showing the depth of circulation loss during drilling in the each well

The deep reservoirs are located at depths below 1000 meter characterized by the appearance of epidote and usually correspond to circulation losses during drilling. Total circulation loss occurs at different depth in several wells especially in LHD-5, LHD-7 and LHD-23. The depth of circulation loss in the different wells is shown in Figure 8.

6. TEMPERATURE DISTRIBUTION

The formation temperature in the Lahendong geothermal field was measured during the heating-up period. Most of the wells in the Lahendong geothermal field have temperature ranging from 250°C to 350°C except wells LHD-3, 6 and well pad LHD-7 having temperatures below 150°C (Figure 9). These wells are located at the boundary of the geothermal system.

Generally, temperature distribution correlation between well pad LHD-5 in the northern part and LHD-4 and 13 in the southern part shows a temperature increase (Figure 9).

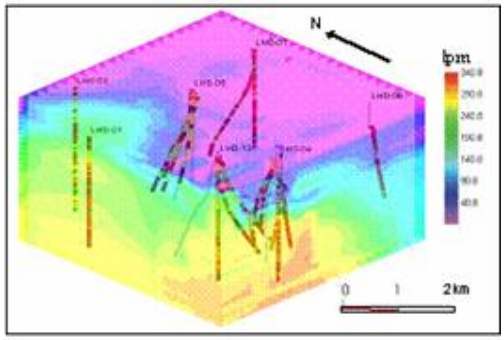

Figure 9. 3D view of temperature distribution in Lahendong geothermal field

In well pad LHD-4 higher temperature distribution is observed in the W, NW and SW part of the well pad towards Mt. Lengkoan as compared to the eastern part. Well pad LHD-5 also shows the same trend in W and SW direction of the well pad. This increase in

temperature distribution is evidenced by an increase in maximum temperature from 250°C in well LHD-5 to 280°C in well LHD-23. This site which shows an increase in temperature distribution occurs below Linau Lake which is believed be the center of the upflow zone having temperature >300°C. These higher temperature distributions in both well pads make it an interesting site for geothermal resource utilization in the future.

High temperature minerals such as epidote, albite, wairakite and prehnite are especially found in wells LHD-4 and 5 and corresponds to the measured temperature from the near neutral pH alkali chloride water at temperature around 250 to 350°C. Fluid inclusions study at well LHD-5 shows that the homogenization temperature is around 227 to 269°C (Utami et al., 2005).

7. GEOTHERMAL MODEL OF LAHENDONG

The Lahendong geothermal model was first prepared in 1987. Barnet (1987) did the reservoir assessment, and then the geological model based on 7 exploration wells giving emphasis to structure and the lateral and vertical formation temperature distribution by Robert (1987). The combination of the geological data, geophysics and wells data was modeled by Pertamina Geothermal. The model of Azimudin and Hartanto (1997) emphasized the well data after completion of 14 wells, conceptual model by Siahaan (2000), and the 3D inversion Magnetotelluric model by Raharjo et al.,, (2008).

Based on the geological analysis the subsurface condition of the Lahendong Geothermal Field can be divided into three main layers namely: smectite zone, smectite-chlorite zone and illite-prehnite-epidote zone (Figure 10).

The smectite zone is mainly characterized by the appearance of the low temperature clay mineral formed at temperatures between 100 to 150°C. This zone is dominated by basaltic andesite and tuff ignimbrite from the Post Tondano and Tondano Units respectively. In the Lahendong field, this zone behaves as the caprock and especially found throughout wells LHD-3, LHD-6 and LHD-7 (Siahaan, 2005). This layer is characterized by a conductive layer having resistivity <10 ohmm (Raharjo, et. al., 2008).

The smectite-illite-chlorite zone is characterized by the appearance of chlorite in general and an acid layer with the presence of kaolinite in particular in wells LHD-1 and 5. This acid layer observed in wells LHD-1 and 5 occurs from the surface to 1000 m depth in the former and at shallow depth in the latter. This zone is located in the Tondano and Pra-Tondano Units.

The illite-prehnite-epidote zone is characterized by the appearance of prehnite, epidote, and secondary quartz at depths of about 700 m in well LHD-1 and 2 and at around 1000 to 1300 m in the well pads LHD-4, 5, and 13. This zone is dominated by the Pra-Tondano Unit and marked by resistivity value of 20 to 60 ohm m (Siahaan, 2005; Raharjo, et. al., 2008).

The reservoir fluid of the wells in the Lahendong geothermal fluid is mainly dominated by the neutral chloride water except the wells LHD-1, 3 and 7. In the western part, the shallow reservoir is associated with an acid fluid and several wells indicate a vapor dominated zone. The reservoir system is believed to center at around Lahendong-Kasuratan-Linau and is characterized by the distribution of surface thermal manifestation.

The temperature profile shows different characteristics. Wells LHD-1, 2 and 5 in the northern part exhibit a sharp change in temperature gradient at about 350 m depth that stable at 250 to 280°C, whereas, most of the temperature profile of well pad LHD-4 and 13 in the southern part show a change in the temperature gradient at depth 650 m where the gradient is stable at about 320-340°C.

The heat source for the geothermal system in this field is believed to be magma cooling beneath Mt. Lengkoan and Mt. Kasuratan (Siahaan, 2005).

One of the important aspects for sustaining a geothermal system is the recharge from the surrounding system. The recharge area of the system is from Mt. Tampusu in the east and Mt. Lengkoan in the SW at an elevation of about 800-900 masl (Batan, 1991).

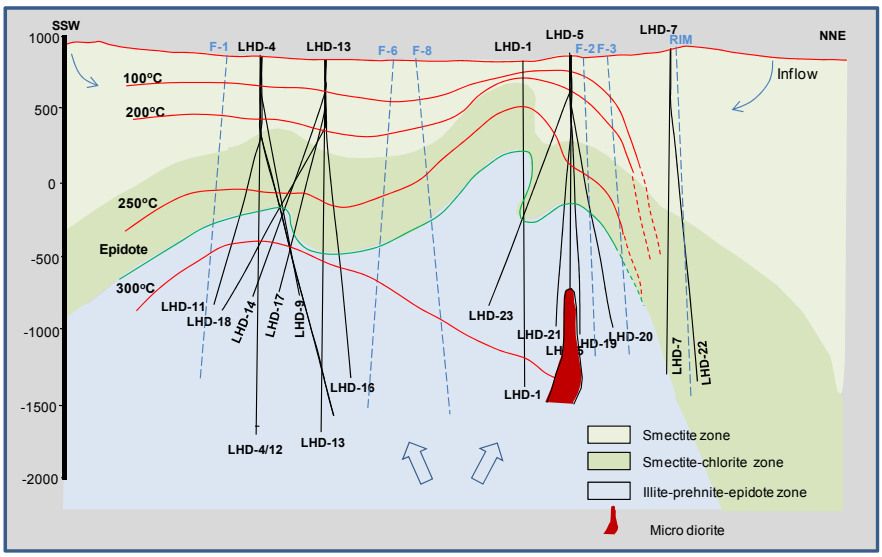

Figure 10. Geothermal model of Lahendong geothermal field (Modified from Siahaan, 2000).

8. CONCLUSION

The stratigraphy of Lahendong geothermal field can be divided into 3 lithological units i.e. Pre-Tondano, Tondano and Post Tondano Units.

Five main structures were encountered in the Lahendong geothermal field. The structures are Pangolombian rim, and faults striking NE-SW, E-W, NW-SE and N-S.

The reservoir system in the Lahendong geothermal field is divided into two reservoirs, the southern part has temperatures of 300 to 350°C with dryness about 80%, and the northern one has lower temperatures between 250 to 280°C with dryness around 30%.

Based on the temperature distribution, the interesting site for geothermal resource utilization are located in NW, W, and SW direction from well pad LHD-4 and W and SW direction of well pad LHD-5.

Three main alteration zone encountered in this field: smectite, smectite-chlorite and illite-prehnite-epidote zone.

The recharge area of the system is from the drainage system of Mt. Tampusu and Mt. Lengkoan

REFERENCES

Azimudin, T., Hartanto, D.B., 1997: *Reevaluation of Lahendong conceptual reservoir models.* Pertamina Internal report (in Indonesian).

Barnet, B., 1987.: *Reservoir assessment of Lahendong Geothermal Field, GENZL, SMS,* Report for Pertamina, Jakarta.

Batan, 1991: *Isotope study of Lahendong geothermal field, North Sulawesi,* Report for Pertamina, Jakarta (In Indonesian)

Browne, P.R.L., 1978: Hydrothermal alteration in active geothermal systems. *Annu. Rev. Earth Planet. Sci*., *6*, 229-250

Ganda, S., and Sunaryo, D., 1982: *Preliminary study of the Geology of Minahasa Area, North Sulawesi*. Pertamina Internal Report (in Indonesian).

Geoservice, 1987: *Aerial photograph study of the Lahendong, North Sulawesi,* Report for Pertamina, Jakarta (in Indonesian).

Raharjo, I.B., Wannamaker, P.E., Timisela, D.P., Arumsari, A.F., 2008: 3 D inversion of Magnetotellurik, Study of the Lehendong Gedothermal Field, Progress research, *33th HAGI Annual meeting, Indonesia*.

Robert, D., 1987: *Geology Model of Lahendong Geothermal Field: A guide for the development of this field,* Report for Pertamina, Jakarta.

Siahaan E.E., 2000, Interpretation of Land sat and Aerial Photo of Lahendong, *Pertamina internal report-unpublished.*

Siahaan, E.E., 2000: *Mineral alteration study in Lahendong Geothermal Field,* Pertamina Internal Report (in Indonesian).

Siahaan, E.E., 2003: *Development Plan of Lahendong and Tompaso Geothermal Field,* Pertamina Internal Report (in Indonesian)..

Siahaan, E.E., 2005: Feasibility study of the Lahendong Geothermal Field for Power Plant Unit IV and V, *Pertamina Internal Report* (In Indonesian).

Utami, P., Browne, P.R.L., Simmons, S.F., Suroto, 2005: Hydrothermal alteration mineralogy of the Lahendong Geothermal System, North Sulawesi: A progress report, *Proceedings 27th NZ Geothermal Workshop 2005*.